

ผลของปริมาณนาโนเคลย์ต่อความสามารถในการย่อยสลายได้ทางชีวภาพ
ของนาโนคอมพอสิตของเมทิลเซลลูโลส/มอนต์มอริลโลไนต์



นางสาวโสธรา จริงจิตร

สถาบันวิทยบริการ

จุฬาลงกรณ์มหาวิทยาลัย

วิทยานิพนธ์นี้เป็นส่วนหนึ่งของการศึกษาตามหลักสูตรปริญญาวิศวกรรมศาสตรมหาบัณฑิต

สาขาวิชาวิศวกรรมเคมี ภาควิชาวิศวกรรมเคมี

คณะวิศวกรรมศาสตร์ จุฬาลงกรณ์มหาวิทยาลัย

ปีการศึกษา 2549

ISBN 974-14-3007-8

ลิขสิทธิ์ของจุฬาลงกรณ์มหาวิทยาลัย

EFFECT OF NANOCLAY COMPOSITIONS ON BIODEGRADABILITY
OF METHYL CELLULOSE/MONTMORILLONITE NANOCOMPOSITES



Miss Sorada Jingjid

สถาบันวิทยบริการ
A Thesis Submitted in Partial Fulfillment of the Requirements
for the Degree of Master of Engineering Program in Chemical Engineering

Department of Chemical Engineering

Faculty of Engineering

Chulalongkorn University

Academic Year 2006

ISBN 974-14-3007-8

Copyright of Chulalongkorn University

Thesis Title EFFECT OF NANOCLAY COMPOSITIONS ON BIODEGRADABILITY OF METHYL
CELLULOSE/MONTMORILLONITE NANOCOMPOSITES


By Miss Sorada Jingjid

Field of Study Chemical Engineering

Thesis Advisor Assistant Professor Sarawut Rimdusit, Ph.D.


Thesis Co-advisor Associate Professor Siriporn Damrongsakkul, Ph.D.

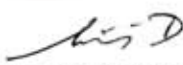
Accepted by the Faculty of Engineering, Chulalongkorn University in Partial
Fulfillment of the Requirements for the Master's Degree


 Dean of the Faculty of Engineering
(Professor Direk Lavansiri, Ph.D.)

THESIS COMMITTEE

 Chairman
(Associate Professor Chirakorn Muangnapoh, Dr. Ing.)

 Thesis Advisor
(Assistant Professor Sarawut Rimdusit, Ph.D.)

 Thesis Co-advisor
(Associate Professor Siriporn Damrongsakkul, Ph.D.)

 Member
(Assistant Professor Muenduen Phisalaphong, Ph.D.)

 Member
(Assistant Professor Varong Pavarajarn, Ph.D.)

โสธรา จริ่งจิตร : ผลของปริมาณนาโนเคลย์ต่อความสามารถในการย่อยสลายได้ทางชีวภาพของนาโนคอมพอสิตของเมทิลเซลลูโลส/มอนต์มอริลโลไนต์ (EFFECT OF NANOCLAY COMPOSITIONS ON BIODEGRADABILITY OF METHYL CELLULOSE/MONTMORILLONITE NANOCOMPOSITES) อ. ที่ปรึกษา: ผศ. ดร. สราวุธ ริมคุสิต, อ. ที่ปรึกษาร่วม: รศ. ดร. ศิริพร คำรงค์ศักดิ์กุล 89 หน้า. ISBN 974-14-3007-8.

งานวิจัยนี้มีจุดประสงค์เพื่อที่จะพัฒนาเมทิลเซลลูโลสซึ่งเป็นพอลิเมอร์ที่ย่อยสลายได้ทางชีวภาพ โดยมีแนวทางในการพัฒนา 2 วิธีคือ การเติมสารเสริมแรงระดับนาโนชนิดมอนต์มอริลโลไนต์เพื่อเตรียมนาโนคอมพอสิต และการเติมสารเชื่อมโยงชนิดกลูตาไรต์ไฮดริด์ เพื่อทำให้เกิดการเชื่อมโยงกันระหว่างสายโซ่โมเลกุลของเมทิลเซลลูโลส และทำการเปรียบเทียบสมบัติต่างๆ ของแผ่นฟิล์มนาโนคอมพอสิตและฟิล์มเมทิลเซลลูโลสที่เกิด โครงสร้างตาข่ายกับเมทิลเซลลูโลสบริสุทธิ์ ทางด้าน สัณฐานวิทยา ความร้อนพลศาสตร์ ทางกล การดูดซับความชื้น การละลายน้ำ และความสามารถในการย่อยสลายได้ทางชีวภาพ ผลการทดลองพบว่า ด้วยเทคนิค X-Ray Diffractometry (XRD) และTransmission Electron Microscope (TEM) พิสูจน์ว่าฟิล์มนาโนคอมพอสิตที่เตรียมจากสารแขวนลอยมอนต์มอริลโลไนต์ผสมกับสารละลายเมทิลเซลลูโลสนั้น จัดอยู่ในประเภท exfoliate และในระบบของการเกิดพันธะเชื่อมโยงของเมทิลเซลลูโลส เทคนิค Fourier-Transform Infrared Spectroscopy (FTIR) พิสูจน์ว่าความหนาแน่นของการเกิดโครงร่างตาข่ายเป็นสัดส่วนโดยตรงกับปริมาณกลูตาไรต์ไฮดริด์ โดยที่ความเข้มข้น 4.5 เปอร์เซ็นต์โดยน้ำหนักเป็นความเข้มข้นที่ทำให้มีการเชื่อมโยงพันธะหนาแน่นที่สุด ยิ่งไปกว่านั้นเมทิลเซลลูโลสคอมพอสิตที่เตรียมด้วยวิธีทั้งสองจะมีจุดเด่นในการพัฒนาสมบัติที่ต่างกัน โดยในกลุ่มนาโนคอมพอสิตจะช่วยเพิ่มสมบัติทางแรงดึงเป็นอย่างมาก (มอดูลัสและความทนแรงดึงเพิ่มขึ้น 65 และ 35 เปอร์เซ็นต์ตามลำดับ) ในขณะที่การเกิด โครงร่างตาข่ายช่วยเพิ่มสมบัติทางความร้อน(อุณหภูมิเปลี่ยนสถานะคล้ายแก้วเพิ่มขึ้น 15 เปอร์เซ็นต์) เพิ่มความสามารถในการต้านทานดูดซับความชื้นและเพิ่มความสามารถในการต้านทานการละลายของฟิล์มเมทิลเซลลูโลส การทดสอบการย่อยสลายทางชีวภาพของแผ่นฟิล์มที่เตรียมจากทั้งสองวิธีนั้น พบว่าฟิล์มที่ทำให้เกิด โครงร่างตาข่ายมีศักยภาพในการต้านทานการย่อยสลายได้ดีกว่า โดยในช่วงเวลาในการทดสอบ 6 สัปดาห์พบว่าปริมาณก๊าซคาร์บอนไดออกไซด์ที่ปลดปล่อยออกมาจะลดลง 80 เปอร์เซ็นต์เมื่อเทียบกับฟิล์มเมทิลเซลลูโลสที่ไม่ได้เติมสารใดเลย

ภาควิชา....วิศวกรรมเคมี.....
สาขาวิชา....วิศวกรรมเคมี.....
ปีการศึกษา....2549.....

ลายมือชื่อนิสิต.....โสธรา จริ่งจิตร.....
ลายมือชื่ออาจารย์ที่ปรึกษา.....
ลายมือชื่ออาจารย์ที่ปรึกษาร่วม.....

4770522521 : MAJOR CHEMICAL ENGINEERING

KEY WORD: BIODEGRADABILITY / METHYL CELLULOSE / MONTMORILLONITE /
NANOCOMPOSITE / CROSSLINKED / GLUTARALDEHYDE

SORADA JINGJID: EFFECT OF NANOCLAY COMPOSITIONS ON BIODEGRADABILITY OF METHYL CELLULOSE/MONTMORILLONITE NANOCOMPOSITES.
THESIS ADVISOR: ASST. PROF. SARAWUT RIMDUSIT, Ph.D., THESIS COADVISOR:
ASSOC. PROF. SIRIPORN DAMRONGSAKKUL, Ph.D., 89 pp. ISBN 974-14-3007-8.

This research aims to develop methyl cellulose (MC), a biodegradable polymer by using two methods. The first method is the use of montmorillonite (MMT) as nanoreinforcement for preparation of nanocomposites. The second one is the use of glutaraldehyde (GA) to promote covalent linkages between MC polymer chains. In comparison of the rendered films from two methods with pure MC, some characterizations such as the analysis of morphology, thermal properties, dynamic mechanical properties, tensile properties, moisture absorption, water solubility, and biodegradability were determined. MC/MMT nanocomposite films prepared by MMT suspension was exfoliated nanocomposite which was confirmed by XRD and TEM results. In the crosslinked system, the FTIR spectra revealed the crosslink density between MC and GA. This value was proportional to the GA content, and optimum GA content was 4.5wt%. In addition, MC prepared from both methods was capable to enhance different properties. The MC/MMT nanocomposites could significantly improve tensile properties (65% for tensile modulus and 35% for tensile strength), while MC crosslinked film could outstandingly increase thermal properties (15% for T_g) and water solubility properties. The crosslinkage technique had more potential to hinder the biodegradation process. In 6 weeks, the CO_2 emission of crosslinked films was reduced around 80% in comparison with that of pure MC.

Department...Chemical Engineering...

Field of Study Chemical Engineering...

Academic Year.....2006.....

Student's Signature.....*โสธร อธิวิจิตร*.....

Advisor's Signature.....*Sarawut Rimdusit*.....

Co-advisor's Signature.....*Siriporn Damrongsakkul*.....

ACKNOWLEDGMENTS

I wish to express my sincerest gratitude and deep appreciation to my advisor, Asst. Prof. Dr. Sarawut Rimdusit, and my co-advisor, Assoc. Prof. Dr. Siriporn Damrongsakkul, for their kindness, invaluable supervision, invaluable guidance, advice, and encouragement throughout the course of this study and editing of this thesis.

Gratefully thanks to Assoc. Prof. Chirakarn Muangnapoh, Asst. Prof. Dr. Muenduen Phisalaphong, and Asst. Prof. Dr. Varong Pavarajarn for their substantial advice as thesis committee.

This research is supported by the Affair of Commission for Higher Education Chulalongkorn University Graduate Thesis Grant (2005) and the National Nanotechnology Center (2006-2007). My advisor also gratefully acknowledges the additional financial support from the Research Grant for Mid-Career University Faculty of the Ministry of Education and the Thailand Research Fund 2005-2007.

The Physics Department and the Center of Nanoimaging (CNI) of Mahidol University are also acknowledged for the XRD and TEM experiments. I wish to thank Asst. Prof. Toemsak Srihirin for his helpful and good advice on XRD and TEM analysis.

Many thanks to my senior colleagues especially Mr. Sunan Tiptipakorn and Mr. Varurit Jiraprawatthagool for his edit in the writing of my work and everyone in the Polymer Engineering Laboratory, Chulalongkorn University, for their discussion and friendly encouragement. Moreover, I would like to thank everyone here. I feel so fortunate having a chance to learn here.

Finally, I would like to affectionately give all gratitude to the members of my family for their wholehearted understanding, encouragement, and patient support throughout my entire study.

CONTENTS

	PAGE
ABSTRACT (THAI)	iv
ABSTRACT (ENGLISH)	v
ACKNOWLEDGEMENTS	vi
TABLE OF CONTENTS	vii
LIST OF TABLE	x
LIST OF S FIGURES	xi
 CHAPTER	
I INTRODUCTION	1
II THEORY	5
2.1 Biodegradable Polymers	5
2.2 Cellulose and Methyl Cellulose (MC)	6
2.2.1 Cellulose	6
2.2.2 Methyl cellulose	6
2.3 Polymer/clay Nanocomposites.....	7
2.3.1 Structure and properties of Montmorillonite (MMT).....	7
2.3.2 Types of polymer nanocomposites	8
2.3.3 Techniques used for the characterization of nanocomposites	9
2.3.4 Preparative techniques of nanocomposites.....	11
2.4 Crosslinking of Methyl Cellulose.....	11
2.4.1 Crosslinking reaction of methyl cellulose with glutaraldehyde.....	12
2.4.2 Crosslinking procedure of methyl cellulose with glutaraldehyde.....	13
2.4.3 Techniques used for the characterization of crosslinked methyl cellulose.....	13
III LITERATURE REVIEWS	15

	PAGE
IV EXPERIMENT	21
4.1 Material	21
4.2 Preparation of Nanocomposite Films.....	21
4.2.1 Preparation of montmorillonite suspension	21
4.2.2 Preparation of methyl cellulose nanocomposite films.....	22
4.3 Preparation of Crosslinked Methyl Cellulose Films	22
4.4 Specimen Characterization	23
4.4.1 Viscosity	23
4.4.2 X-ray diffraction	23
4.4.3 Transmission electron microscope	23
4.4.4 Differential scanning calorimetry	24
4.4.5 Thermogravimetric analysis	24
4.4.6 Dynamic mechanical analysis	24
4.4.7 Universal testing machine.....	25
4.4.8 Fourier transform infrared spectroscopy	25
4.4.9 Moisture absorption	25
4.4.10 Degree of biodegradation.....	26
4.4.11 Composing degradation	27
V RESULTS AND DISCUSSION	28
5.1 Suitable Conditions for MMT Suspension Preparation.....	28
5.1.1 Effect of pre-swelling times on viscosity of MMT suspension.....	28
5.1.2 Effect of MMT contents on viscosity of MMT suspension.....	29
5.1.3 Effect of mixing speeds on viscosity of MMT suspension.....	30
5.1.4 Effect of mixing times on viscosity of MMT suspension.....	30
5.2 Characterization of MC/MMT Nanocomposites.	31
5.2.1 Morphology of nanocomposite films.....	32
5.2.2 Thermal properties of nanocomposite films	34
5.2.3 Dynamic mechanical analysis of nanocomposite films	36
5.2.4 Tensile properties of nanocomposite Films.	37
5.2.5 Moisture absorption of nanocomposite Films.....	37
5.3 Characterization of Crosslinked MC.	38

	PAGE
5.3.1 FTIR spectroscopy investigation of the crosslinked reaction.....	38
5.3.2 Moisture absorption of crosslinked MC	39
5.3.3 Tensile properties of crosslinked MC.....	39
5.3.4 Dynamic mechanical analysis of crosslinked MC.....	40
5.4 Biodegradability of MC/MMT Nanocomposite and Crosslinked MC Films	41
VI CONCLUSIONS	74
REFERENCES	76
APPENDICES	82
Appendix A Viscosity of MMT suspension at various compositions.....	83
Appendix B d-spacing calculation.....	84
Appendix C Tensile properties of MC nanocomposites and crosslinked films.....	85
Appendix D Net CO ₂ evaluation of MC nanocomposites and .crosslinked films.....	86
Appendix E Calibration curve.....	87
Appendix F Comparison on properties of nanocomposites and crosslinked MC.....	88
VITA	89

LIST OF TABLES

TABLE	PAGE
2.1 Peak assignments of IR spectra of glutaraldehyde, methyl cellulose, and crosslinked methyl cellulose.....	14
2.2 Lists of parameters studied in this work.....	21
2.3 Viscosity of MMT suspension at various mixing conditions.....	48



สถาบันวิทยบริการ
จุฬาลงกรณ์มหาวิทยาลัย

LIST OF FIGURES

FIGURE	PAGE
2.1 Biodegradation by surface of biodegradable material: action of exo-and endo-enzymes.....	5
2.2 Methyl cellulose.....	6
2.3 Structure of 2:1 phyllosilicates.....	8
2.4 SEM micrograph of montmorillonite.....	8
2.5 Schematic illustration of two different types of thermodynamically achievable polymer/layered silicate nanocomposites.....	9
2.6 The state of intercalation and exfoliation of nanoparticles has typically been established using XRD analysis and TEM.....	10
2.7 Aldehyde-mediated crosslinking of polymers containing hydroxyl groups.....	12
3.1 XRD patterns of APES/Cloisite 30 and APES/Cloisite 10A with various contents of Cloisite 30B, 10A.....	16
3.2 Biodegradability of APES/Cloisite 30B and APES/Cloisite 10A nanocomposites with different contents of Cloisite 30B, 10A.....	17
3.3 Percentage in the compost media at 60°C and 90% relative humidity as a function of exposure time.....	18
3.4 Degradation profile of the TPP/genipin crosslinked chitosan beads in terms of the increments in free amino group content in the incubation medium vs time..	20
4.1 Polystyrene mold for MC film casting.....	22
4.2 Plastic box in moisture absorption test.....	25
4.3 Scheme of biodegradation test in this study.....	26
4.4 Plastic box in composting degradation test.....	27
5.1 Viscosity of 5wt% MMT suspension at various pre-swelling times using a speed of 6500 rpm for 1 min.....	43
5.2 Viscosity of MMT suspension at various contents of MMT using a speed of 6500 rpm for 1 min.....	44

5.3	MMT suspensions at various contents of MMT using a speed of 6500 rpm of 1 min.....	45
5.4	Viscosity of 5wt% MMT suspension at various mixing speeds using for 1 min.....	46
5.5	Viscosity of 5wt% MMT suspension at various mixing times using a speed of 13500 rpm.....	47
5.6	MC/MMT nanocomposite films at various contents of MMT.....	49
5.7	XRD patterns of MMT powder and MC/ 5 phr MMT nanocomposite films at various MMT preparations.....	50
5.8	XRD patterns of pure MC, MMT and MC/MMT nanocomposite films at various contents of MMT.....	51
5.9	TEM micrographs of MMT powder.....	52
5.10	TEM micrographs of MC/ 1 phr MMT nanocomposite.....	53
5.11	TEM micrographs of MC/ 5 phr MMT nanocomposite.....	54
5.12	TEM micrographs of MC/ 10 phr MMT nanocomposite.....	55
5.13	TGA thermograms of pure MC and MC/MMT nanocomposite films at various contents of MMT.....	56
5.14	DSC thermograms showing glass transition temperature of pure MC and MC/MMT nanocomposite films at various contents of MMT.....	57
5.15	Storage modulus of MC/MMT nanocomposite films at various contents of MMT.....	58
5.16	$\tan\delta$ of MC/MMT nanocomposite films at various contents of MMT.....	59
5.17	Tensile modulus of MC/MMT nanocomposite films at various contents of MMT.....	60
5.18	Tensile strength & elongation at break of MC/MMT nanocomposite films at various contents of MMT.....	61
5.19	Moisture absorption of MC/MMT nanocomposite films at various contents of MMT.....	62
5.20	Pure MC, MC/MMT nanocomposite and MC crosslinked films.....	63
5.21	FTIR spectra of pure MC and MC crosslinked films at various contents of glutaraldehyde.....	64

5.22	Moisture absorption of MC crosslinked films at various contents of glutaraldehyde.....	65
5.23	Tensile modulus of MC crosslinked films at various contents of glutaraldehyde.....	66
5.24	Tensile strength & elongation at break of MC crosslinked films at various contents of glutaraldehyde.....	67
5.25	Storage modulus of pure MC and MC crosslinked films at various contents of glutaraldehyde.....	68
5.26	tan δ of pure MC and MC crosslinked films at various contents of glutaraldehyde.....	69
5.27	Biodegradability of pure MC and nanocomposite films at various contents of MMT under soil field with time.....	70
5.28	Biodegradability of MC crosslinked films various contents of glutaraldehyde under soil field with time.....	71
5.29	Time dependence of degree of biodegradation i.e. CO ₂ evolution of pure MC, MC/MMT nanocomposite, and crosslinked films at various compositions under compost.....	72
5.30	Water solubility of pure MC, MC/MMT nanocomposite, and crosslinked films.....	73

CHAPTER I

INTRODUCTION

1.1 Introduction

In the past 20 years, the production and the use of plastics in the world have been enormously increased, worsening the problems of the waste disposal. The growing interest in environmental impact of discarded plastics has directly researched on the development of plastics that degrade more rapidly in the environment, leading to a complete mineralization or bioassimilation of the plastics (Aminabhavi et al., 1990; Crosby, 1981; Doi, 1990). Biopolymers should be used in those applications where biodegradability and/or the derivation of natural resources gives added value, particularly, where valuable petroleum-based plastics are used for applications with a short life time (Avella et al., 2005). For these reasons, throughout the world today, the development of biodegradable materials with controlled properties has been a subject of great research challenge to the community of material scientists and engineers.

Methyl Cellulose (MC), a biodegradable polymer, is a modified type of cellulose which is the most abundant biopolymer in nature. MC is well known and of interest to be used as environmental friendly products, especially as coating or mulching film, because of its large availability, low cost, and easy processability. However, due to a limitation in biodegradable behavior of MC, it can be used only in some applications.

There are two methods that can be used to potentially improve the biodegradability of MC. The first method is nanoreinforcement of pristine polymers to increase the lengths of the tortuous paths in nanocomposites in the presence of high clay content. When the lengths of the tortuous paths increase, the clay with high aspect ratio obstructs the diffusion of microorganism in the bulk of the film. That

forces the decrease of biodegradability rate (Lee et al., 2002). The second one is to promote covalent linkages between polymer chains by crosslinking agent such as glutaraldehyde (GA). When cross linkages occur, the gaps between polymer chains reduce. The water molecules, which are the media of microorganism, cannot penetrate through the nanocomposite. Both methods should to modulate the biodegradability of polymer.

Polymer/clay nanocomposites have been the focus of academic and industrial attention in recent years because the final composites often exhibit a desired enhancement of physical and/or chemical properties relative to the pure polymer matrix e.g. increasing of strength, enhancement of thermal stability, and especially decreasing of biodegradability rate even at very low clay contents (Li et al., 2004; Lee et al., 2002; Wang et al., 2005). Montmorillonite (MMT) is one of the most important natural clays. The filler originally inherits a stacked structure of parallel silicate layers (Sinha Ray and Okamoto, 2003). Depending on the extent of compatibility between the clay and the matrix, a microphase-separated conventional composite, intercalated, or exfoliated morphology can be obtained when direct mixing with polymer matrix (Krikorian et al, 2003).

Crosslinking is one of the most popular methods used to modify water-soluble polymer in order to achieve desired properties. Some polymer characteristics could be altered by crosslinking such as swelling, permeability (Park and Ruckenstein, 2001; Coma et al., 2003), drug releasing, transport properties, water uptake, mechanical properties, chemical stability, sponge structure as well as biodegradation rate (Wach et al., 2003). Several crosslinking agents for MC have been employed including dialdehyde. However, one of the most popular crosslinkers is glutaraldehyde (GA), a small molecule dialdehyde (Park and Ruckenstein, 2001).

In this work, MC/MMT nanocomposite films are prepared by solution intercalation using a homogenizer at the MC gelatinized temperature of 50-55°C, to achieve intercalation of the stacked layers of MMT. The filler is suspended in water

and dispersed under ultra high shear rate to form MMT gel suspension. This preparation method is also to delaminate the layered silicate of MMT in order to homogeneously disperse the nanoparticles in MC matrix. Crosslinked MC is prepared by using GA as a chemical crosslinking and hydrochloric acid as a catalyst in an aqueous solution. The effects of MMT and GA crosslinking agent content used on the biodegradability, physical properties, thermal properties and mechanical properties of nanocomposite and crosslinked films will be investigated.

1.2 Objectives

This present study is aimed primarily at the following objectives.

1. To develop MC-based biodegradable polymer with broader range of biodegradability.
2. To investigate the effect of MC nanocomposites and crosslinked MC on the morphology, thermal properties, dynamic mechanical properties, tensile properties, moisture absorption, water solubility and biodegradability.

1.3 Scopes of Research

1. Appropriate MMT suspension for MC/MMT nanocomposite film fabrication will be prepared. Four parameters will be studied i.e. pre-swelling times (0 to 14 days), MMT contents (1, 3, 5, 7, and 9wt%), mixing speeds (6500, 9500, 13500, 17500, 21500, and 24000 rpm), and mixing times (1 to 10 min).
2. MC/MMT nanocomposite films will be prepared by solution intercalation technique using a homogenizer at various weight ratios of MMT to obtain final MC/MMT weight ratios of 100:0, 100:1, 100:2, 100:3, 100:5, and 100:10.
3. Crosslinked MC films will be studied using GA as a chemical crosslinking agent and hydrochloric acid as a catalyst in an aqueous solution at various contents of GA of 0.5, 1.5, 3.0, 4.5, 6.0, and 12.0% by weight.
4. The effects of MMT loadings and GA contents on the resulting films will be examined as follows:

- 4.1 The degree of MMT dispersion of nanocomposites will be evaluated by XRD and TEM microscopy.
- 4.2 Crosslinking density of MC with GA will be observed by FTIR and moisture absorption (ASTM D 570-98).
- 4.3 Thermal properties of nanocomposites will be studied by DSC and TGA.
- 4.4 Tensile properties of nanocomposites and crosslinked MC will be examined by DMA and universal testing machine.
- 4.5 Biodegradability of nanocomposites and crosslinked MC will be investigated accordingly to ASTM D5988-96.



สถาบันวิทยบริการ
จุฬาลงกรณ์มหาวิทยาลัย

CHAPTER II

THEORY

2.1 Biodegradable Polymers

The term “biodegradable” materials is used to describe those materials which can be degraded by enzymatic action of living organisms, such as bacteria, yeasts, fungi. The ultimate end-products of the degradation process are CO₂, H₂O, and biomass under aerobic conditions and hydrocarbons, methane and biomass under anaerobic conditions (Doi and Fukuda, 1994).

The degradation of biodegradable polymer proceeds either by hydrolysis through the bulk and/or by enzymatic degradation. The latter comprises of endoenzyme and exoenzyme as shown in Figure 2.1. Hydrolysis (so called bioerosion) necessitates a certain degree of hydrophilicity of the polymer, so that water molecule can access to sample bulk. Materials such as PET characterized by a strong hydrophilic character and/or a high degree of crystallinity will generally show good tolerance to hydrophilic breakdown. Enzyme attacks a polymeric material from the surface, degrading first the amorphous and easily accessible regions (Chielline and Solora, 2003).

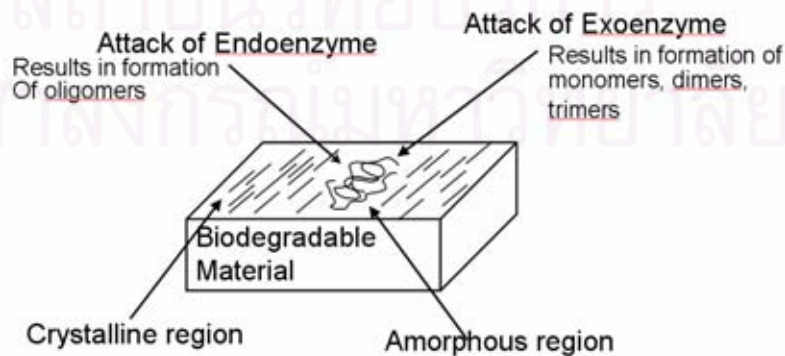


Figure 2.1: Biodegradation by surface of biodegradable material: action of exo- and endo-enzymes (Chielline and Solora, 2003).

2.2 Cellulose and Methyl Cellulose

2.2.1 Cellulose

Cellulose constitutes the main structural component of plants and the most abundant source of carbohydrate in nature. Cellulose consists of $\beta(1,4)$ -glycopyranose units. Cellulose exhibits a strong tendency to form intra- and inter- molecular hydrogen bonding. Because of its highly crystalline nature, it is insoluble and unswellable in water. In order to solubilize cellulose e.g. for processability purpose, various substituents have been incorporated into its anhydroglucose backbone to decrease its crystallinity (Hirrien et al., 1996; Sarkar and Walker, 1995; Hirrien et al., 1998).

2.2.2 Methyl Cellulose

In Methyl Cellulose (MC), some hydroxyl groups are replaced with methoxyl groups and thus the hydrogen-bonding, which is responsible for the crystallinity of cellulose, is weakened. For this reason MC becomes water soluble. MC is prepared on a commercial scale by the etherification of alkali-cellulose with methyl chloride (BeMiller, 1986). Chemical structure of MC is showed in Figure 2.2.

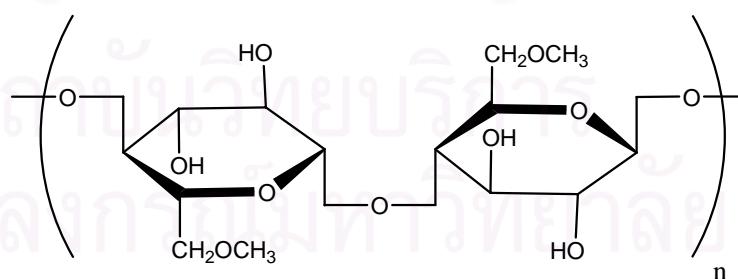


Figure 2.2: Methyl Cellulose.

MC is a powder which can be mixed with distilled or de-ionized water to form a paste. It is not lumpy (completely soluble in water) and has a neutral pH (pH 6.5-8.5 at 1% solution), non-toxic, odorless and smellless. It is soluble even in cold

water because of the existing of hydrophilic group. MC provides high-strength films which are transparent, water soluble, oil resistant, and have low oxygen and moisture vapor transmission rates (BeMiller, 1986; Park et al., 1993). Its biodegradability rate is rather high, i.e. 55 to 73 wt% of polymer degraded in 20 days using bath-type activated sludge tests (Blanchard et al., 1976).

2.3 Polymer/clay Nanocomposites

Polymer nanocomposites represent a novel class of multiphase materials in which ultrafine particles, typically in the range of 1–100 nm, are dispersed. These polymer/clay nanocomposites are of particular interest because of their demonstrated significant enhancement which is relative to an unmodified polymer resin. The enhancement is of a large number of physical properties, including barrier, flammability resistance, thermal and environmental stability, solvent uptake, and rate of biodegradability of biodegradable polymers (Shen et al., 2004).

The main reason for these improved properties in polymer nanocomposites is the strong interfacial interactions between matrix and clay as opposed to conventional composites. The most common reinforcements that have been used are the layered natural silicates–clays, such as mica, montmorillonite (MMT), hectorite, and saponite. Among them the most commonly used is MMT because it offers favorable enthalpy of mixing for good dispersion (Manias et al., 2001).

2.3.1 Structure and Properties of Montmorillonite

MMT is the most commonly used layered silicates consisting of two types of structures: tetrahedral-substituted and octahedral-substituted. In the case of tetrahedrally substituted layered silicates, the negative charge is located on the surface of silicate layers, and hence, the polymer matrices can interact more readily with these clays than with octahedrally-substituted material. Each clay layer is slightly less than 1 nm thick, with surface dimensions extending to about 1 μm or 1000 nm. The aspect

ratio is about 1000 to 1 and the surface area is in the range of $750 \text{ m}^2/\text{g}$. Details regarding the structure of these layered silicates are provided in Figure 2.3 (Sinha Ray and Okamoto, 2003). Scanning electron microscope (SEM) micrograph of MMT depicting very fine particle size is shown in Figure 2.4.

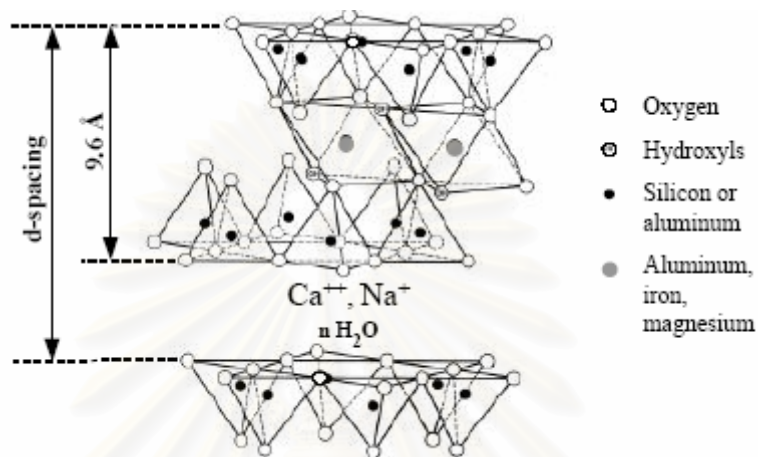


Figure 2.3: Structure of 2:1 phyllosilicates (Sinha Ray and Okamoto, 2003).

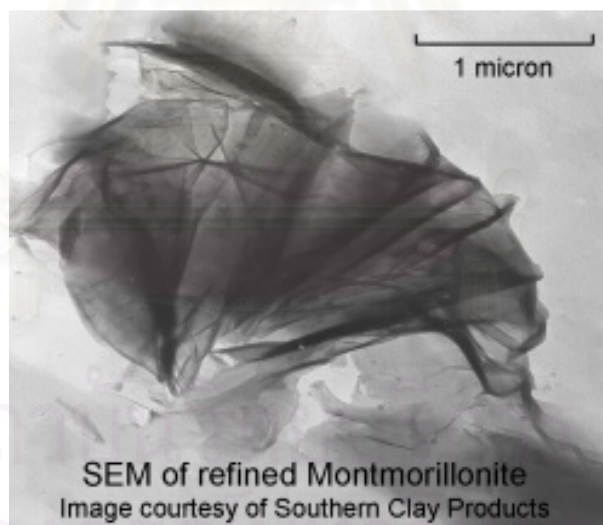


Figure 2.4: SEM micrograph of Montmorillonite (<http://www.netcomposites.com>).

2.3.2 Types of Polymer Nanocomposites

On the basis of the strength of the polymer/clay interaction, two structurally different types of nanocomposites are thermodynamically achievable (see Figure 2.5).

The former type of nanocomposites is intercalated nanocomposites, where insertion of polymer chains into the silicate structure occurs in a crystallographically regular fashion, regardless of polymer to clay ratio with a repeat distance of a few nanometers. The latter type of nanocomposites is exfoliated nanocomposites, in which the individual silicate layers are separated in polymer matrix by average distances that totally depend on the clay loading (Liu et al., 2004). The exfoliated nanocomposites generally provide superior properties than the intercalated nanocomposites (Avella et al., 2005).

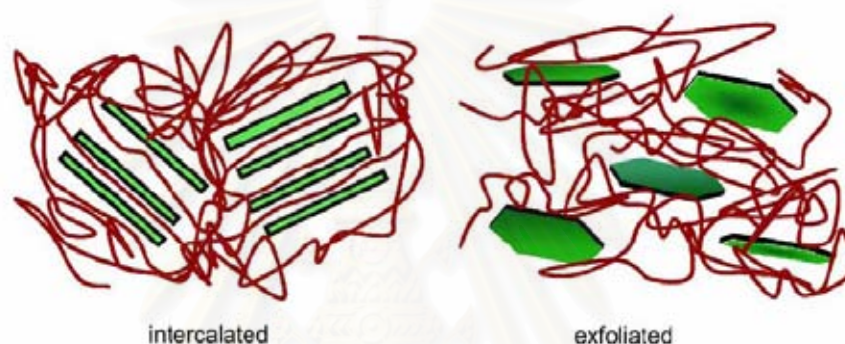


Figure 2.5: Schematic illustration of two different types of thermodynamically achievable polymer/layered silicate nanocomposites (Liu et al., 2004).

2.3.3 Techniques Used for the Characterization of Nanocomposites

To general, the state of intercalation and exfoliation of nanoparticles has typically been established using X-ray diffraction (XRD) analysis and transmission electron micrographic (TEM) observation (see Figure 2.6). Due to its easiness and availability, XRD is most commonly used to probe the nanocomposite structure. By monitoring the position, shape, and intensity of the basal reflections from the distributed silicate layers, the nanocomposite structure (intercalated or exfoliated) may be identified. For example, in an exfoliated nanocomposite, the extensive layer separation associated with the delamination of the original silicate layers in the polymer matrix results in the eventual disappearance of any coherent XRD from the distributed silicate layers. On the other hand, for intercalated nanocomposites, the finite layer expansion associated with the polymer intercalation results in the

appearance of a new basal reflection corresponding to the larger gallery height. The spacing was calculated by Bragg's equation as shown in Equation (2.1).

$$2d\sin\theta = n\lambda \quad (2.1)$$

Where λ = the wavelength of the XRD used in the diffraction experiment (1.542 Å)

d = the spacing between diffractive lattice planes

θ = the measured diffraction angle

n = peaks correspond to the {001} basal reflection ($n=1$).

Although XRD offers a convenient method to determine the interlayer spacing of the silicate layers in the original layered silicates and in the intercalated nanocomposites (within 1-4 nm), little can be said about the spatial distribution of the silicate layers or any structural non-homogeneities in nanocomposites. Additionally, some layered silicates initially do not exhibit well-defined basal reflections. Thus, peak broadening and intensity decreases are very difficult to study systematically. Therefore, conclusions concerning the mechanism of nanocomposite formation and the structure based solely on XRD patterns are only tentative. On the other hand, TEM allows a qualitative understanding of the internal structure, spatial distribution and dispersion of the nanoparticles within the polymer matrix, and views of the defect

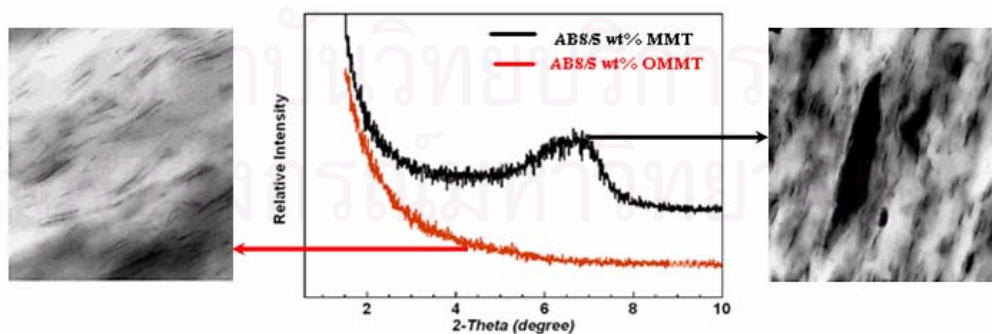


Figure 2.6: The state of intercalation and exfoliation of nanoparticles has typically been established using XRD analysis and TEM (<http://www.psrc.usm.edu>)

structure through direct visualization. However, special care must be exercised to guarantee a representative cross section of the sample.

Both TEM and XRD are essential tools for evaluating nanocomposite structure. However, TEM is time-intensive, and only gives qualitative information on the sample as a whole, while wide-angle peaks in XRD allow quantification of changes in layer spacing. Typically, when layer spacing exceed 6-7 nm in intercalated nanocomposites or when the layers become relatively disordered in exfoliated nanocomposites, associated XRD features weaken to the point of not being useful. However, recent simultaneous small angle X-ray scattering (SAXS) and XRD studies yielded quantitative characterization of nanostructure and crystallite structure in some nanocomposites (Bafna and Gilman, 2003).

2.3.4 Preparative Techniques of Nanocomposites

Typical preparation methods of these nanocomposites include solution intercalation, melt intercalation, and in-situ polymerization (Liu et al., 2004). Solution intercalation, in particular, has been very successful in incorporating delaminated clay into polymers (Pinnavaia and Beal, 2001). In this case, dilute concentrations of organophilic swelling clays dispersed in a polymer matrix have unusual and valuable mechanical, thermal, and permeability properties relative to the pure polymer (Vaia and Giannelis, 2001). The effect of clay on these properties is significant if the clay has an intercalated tactoid structure. Alternatively, exfoliated materials, in which the clay is dispersed at the level of individual platelets, are thought to provide even greater potential for material property enhancement.

2.4 Crosslinking of Methyl Cellulose

Crosslinking of MC, which could be used as biodegradable materials, can be considered as a useful approach to prepare non-water soluble polymer with interesting moisture barrier properties. Keslter and Fennema (1986) studied the method to enhance barrier characteristics by crosslinking modified polysaccharides chains. They

reported that, crosslinking would decrease polymer chain mobility, and increases the resistance to vapor and gas transport. This study corresponds to the reports of Coma et al. (2003). They reported that crosslinking of the hydroxypropylmethylcellulose (HPMC), hydrophilic polymers, induced a strong influence on water solubility and an improvement in the water vapor barrier of about 34% under conditions of 50% RH and 23°C. It is evident that highly water soluble MC crosslinked to various extents should offer the possibility to modulate its biodegradability.

2.4.1 Crosslinking Reaction of Methyl Cellulose with Glutaraldehyde

Crosslinking agents for MC have been employed in various reports such as dialdehyde (e.g. glutaraldehyde (GA), glyoxal, succinaldehyde, trichlorotriazine, epihalohydrin, benzoquinone and bisepoxiranes) in the presence of a strong acid to generate a hydrogel (Horkay and Zrinyi, 1982; Tomita and Ikada, 1997; Gimenez et al., 1999; Yeom and Lee, 1996). However, the most popular crosslinker is GA, a small molecule dialdehyde. That is due to the fact that GA provides higher crosslink density than other crosslinking agents with the same consumption (Park et al., 2001).

Using acid as a catalyst, crosslinking reaction between MC and GA occurs from hydroxyl groups of MC and aldehyde groups of GA via hemi-acetal formation, as shown in Figure 2.7 (Hennink and Nostrum, 2002). This reaction starts with the breakages of O-H bonds in alcohol and C=O in aldehydes. Then, carbonyl groups of aldehydes react with H⁺ ions of alcohols from O-H. In addition, RO⁻ ions of alcohol form with carbon atoms of aldehydes to be C-RO.

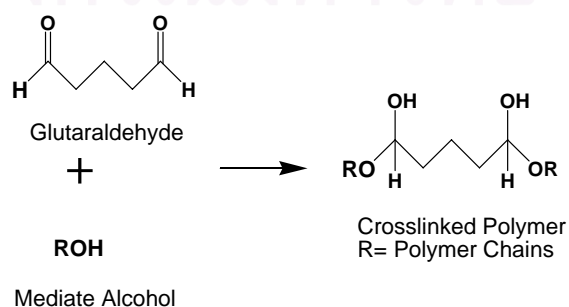


Figure 2.7: Aldehyde-mediated crosslinking of polymers containing hydroxyl groups.

2.4.2 Crosslinking procedure of methyl cellulose with glutaraldehyde

Crosslinking reaction between MC with GA depends on temperature, concentration of MC, concentration of GA and the amount of employed acid. Moreover, crosslinking condition plays important roles in the obtained MC properties. These methods can be divided into two categories, i.e. homogeneous crosslinking (Oungbho and Muller, 1997; Fang et al., 1998) and heterogeneous crosslinking (Andrady and Xu, 1997; Denkbasi and Odabasi, 2000). Homogeneous crosslinking is the method that a crosslinking agent is mixed with MC solution. Heterogeneous crosslinking is the method that MC in solid form is soaked in a crosslinking agent. Homogeneous crosslinking method is easier because crosslinker can be well dispersed in MC solution. Hence, homogeneous crosslinking method is used in this study.

2.4.3 Techniques Used for the Characterization of Crosslinked MC

Crosslink reaction of MC with GA is easily observed by Infrared (IR) spectroscopic technique. There are many absorbance peaks related to crosslinking reaction. Kurita et al. (1986) reported that the excess glutaraldehyde shows the absorption peak at 1710 cm^{-1} (aldehyde group in FTIR spectra). Peak assignment of the spectra is listed in Table 2.1

สถาบันวิทยบริการ
จุฬาลงกรณ์มหาวิทยาลัย

Table 2.1: Peak assignments of IR spectra of glutaraldehyde, methyl cellulose and crosslinked methyl cellulose (Coma et al., 2003; Kurita et al., 1986; Sannino et al., 2005; Zaccaron et al., 2005).

Peak (cm^{-1})	Possible assignment
GA	
2740, 2855	C–H stretching vibration
1710	C=O stretching vibration
1645	C=O stretching vibration (shift by conjugating)
1114	C–O stretching vibration of trimer or polymer
MC	
3430	O–H stretching vibration
3000-2800	C–H stretching vibration
1645	C=O stretching vibration
1371	C–H stretching vibration of methyl group
1153	C–O stretching vibration (asymmetric oxygen bridge)
1066	C–O stretching
948	ring stretching
Crosslinked MC	
1710	C=O stretching vibration

CHAPTER III

LITERATURE REVIEWS

3.1 Biodegradable Polymers and Their Nanocomposite Properties

Li et al. (2004) showed that three methacrylated anhydride monomers of citric acid (MCA), sebacic acid (MSA) and 1,4-bis(carboxyphenoxy) butane (MCPB) were utilized to prepare biodegradable nanocomposites with homogeneously distributed hydroxyapatite (HAp) nanoneedles in crosslinking polyanhydride network. The incorporation of HAp into the polyanhydrides can significantly increase the maximum of compressive strength of the composites. The modulus of the nanocomposite was about three times the corresponding polyanhydride alone. In addition, HAp played an important role in reducing the cumulative mass loss and in enhancing the mechanical integrity of the nanocomposite during the biodegradation process. The studies of biodegradation behavior were carried out in the simulated body fluid, SBF, at pH 7.25 and 37°C. SBF solution was changed every 24 hr. The cumulative mass loss and the retention of elastic modulus were measured as a function of degradation time. At 600 hr of the test period, the cumulative mass loss of PMCA was 57%, while that of the HAp/PMCA nanocomposite with the HAp contents of 10%, 20%, and 30% was suppressed to 44%, 38%, and 32%, respectively. The same trend can also be found in the nanocomposites of HAp/PMSA and HAp/PMCPB during their biodegradation process. Therefore, HAp played a major role in decreasing the cumulative mass loss and in enhancing the mechanical integrity of the nanocomposite during the biodegradation process.

Lee et al. (2002) prepared aliphatic unsaturated polyester, APES, copolymer having a molecular weight of about 60000. The copolymer was prepared by polycondensation of aliphatic glycols (ethylene glycol and 1, 4-butane diol) with succinic and adipic acids. Its clay nanocomposite was obtained by melt intercalation

method. Two kinds of organoclays, Cloisite 30B and Cloisite 10A were chosen for the nanocomposites preparation. Both product clays which contain different ammonium cations: methyl tallow bis-2-hydroxyethyl ammonium for Cloisite 30B and dimethyl benzyl hydrogenated-tallow ammonium for Cloisite 10A, respectively. The XRD patterns of the mixtures of APES with various amounts of Cloisite 30B or Cloisite 10A are shown in Figure 3.1. For APES/Cloisite 30B hybrids with the content of Cloisite 30B less than 15wt%, the interlayer spacing has increased from 2.097 nm of the original Cloisite 30B to around 10 nm while those containing higher amounts of Cloisite 30B showed almost no peaks, indicating an exfoliation of the Cloisite 30B in the APES matrix. For APES/Cloisite 10A hybrids with the Cloisite 10A contents less than 15wt%, two peak exist corresponding to the interlayer spacing of 10 and 3.25 nm, much larger than of the original Cloisite 10A i.e. 1.902 nm. Almost the same trend appeared with increased the amount of Cloisite 10A as that of Cloisite 30B, that is the peak nearly disappeared in the XRD patterns when the Cloisite 10A contents exceeded 15wt%. This is attributed to the strong interaction or miscibility between APES and Cloisite 30B which originates from the strong hydrogen bonding between the carboxyl group of APES and the hydroxyl group in the gallery in the Cloisite 30B.

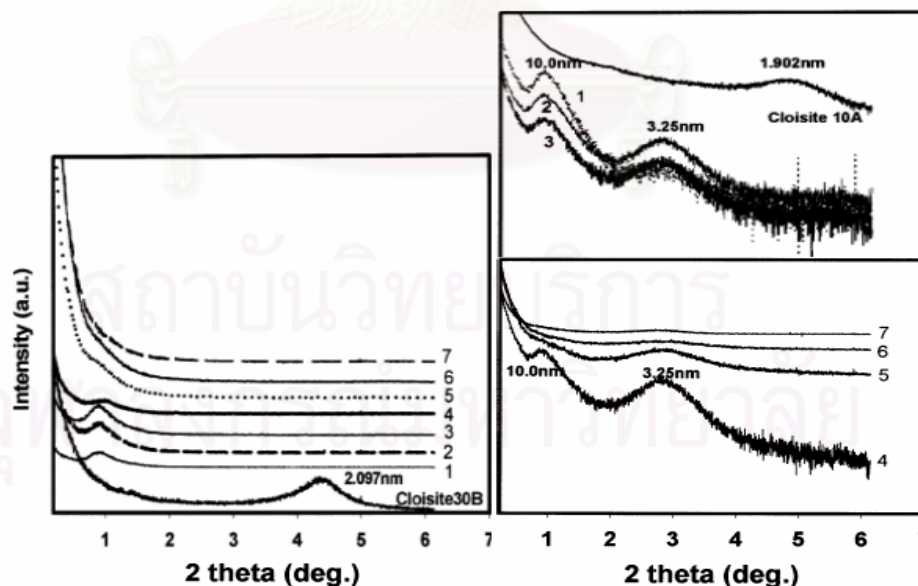


Figure 3.1: XRD patterns of APES/Cloisite 30 and APES/Cloisite 10A with various contents of Cloisite 30B, 10A; (1) 1wt%; (2) 3wt%; (3) 5wt%; (4) 10wt%; (5) 15wt%; (6) 20wt%; (7). 30wt% (Lee et al., 2002).

To evaluate the biodegradability as shown in Figure 3.2, The films were buried in the activated soil, which consisted of 50% of soil, 30% of sand and 20% of composted manure with pH 7.0 ± 0.5 , and kept at the temperature of 60°C and the relative humidity of $60 \pm 5\%$. At predetermined intervals, the specimens were recovered from the soil, cleansed with ethanol solution, and dried in a vacuum oven. The dried films were weighted to calculate the weight loss. From the above results, APES/Cloisite 30B hybrids showed higher of intercalation than the Cloisite 10A hybrids. This leads to higher tensile properties and lower biodegradability under composting for APES/Cloisite 30B hybrids than for APES/Cloisite 10A hybrids.

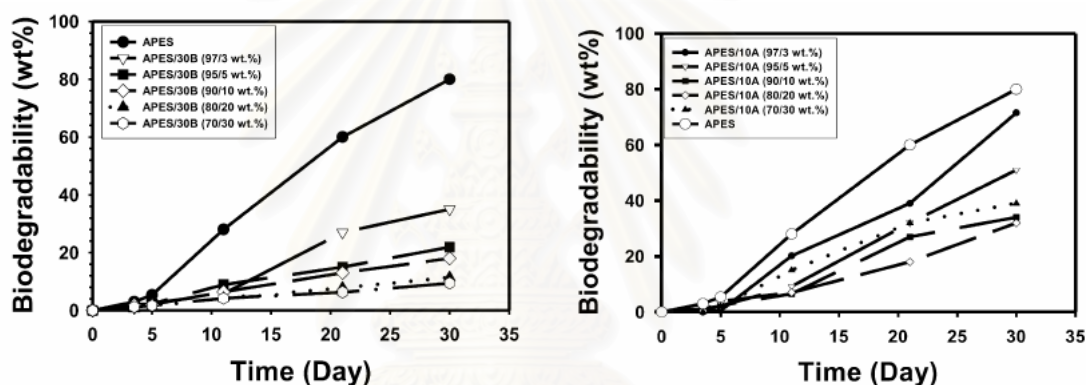


Figure 3.2: Biodegradability of APES/Cloisite 30B and APES/Cloisite 10A nanocomposites with different contents of Cloisite 30B, 10A (Lee et al., 2002).

Maiti et al. (2002) reported the biodegradability of the Poly(3-hydroxybutyrate), PHB, and its organophilic montmorillonite nanocomposites under compost. Figure 3.3 represents the percentage weight loss of PHB and its nanocomposites as a function of time. Apparently, the degradation started just after one week and at the initial stage the weight loss was almost the same for both PHB and its nanocomposites. Deviation occurred after three weeks of exposure, but degradation tendency of nanocomposites was suppressed. They assumed that the retardation of biodegradation of PHB was due to the improvement of the barrier

properties of the matrices after nanocomposites preparation with organophilic montmorillonite.

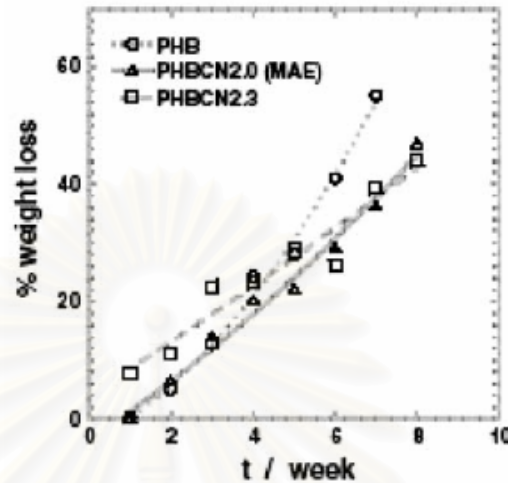


Figure 3.3: Percentage in the compost media at 60°C and 90% relative humidity as a function of exposure time (Maiti et al., 2003).

Wang et al. (2005) concluded that melting temperature, T_m and enthalpy of fusion, ΔH_m of Poly (3-hydroxybutyrate-co-3-hydroxyvalerate)/organophilic montmorillonite, PHBV/OMMT, nanocomposites decreased with increasing amount of OMMT in the nanocomposites. It was demonstrated that the small-sized PHBV spherulites were formed and the crystallinity of PHBV reduced whereas the range of the processing temperature i.e. temperature between T_m and T_p , of the nanocomposites enlarged by intercalation of OMMT with PHBV. Simultaneously, the biodegradability of PHBV/OMMT nanocomposites in soil suspension decreased with increasing amount of OMMT. At the tested degradation period of 350 hr, the cumulative mass loss of PHBV was 46.62%, while that of the PHBV/OMMT nanocomposite with OMMT content of 3, 5, and 10 phr was decreased to 30.53%, 4.12%, and 4.18%, respectively. The biodegradability of PHBV/OMMT nanocomposites related to the interaction and adhesion of PHBV and OMMT, water permeability, degree of crystallinity, and anti-microbial property of the OMMT. The biodegradable PHBV/OMMT nanocomposites with low OMMT content would offer the opportunities to reduce the cost of PHBV and show a better application potential of biodegradable PHBV in future.

3.2 Biodegradable Polymers and Their Crosslinking properties

Park and Ruckenstein (2001) studied suitable condition by solution casting method for MC gel crosslinked with glutaraldehyde (GA) in the presence of hydrochloric acid prepared. In case of GA-crosslinked MC, 5wt% MC solutions was prepared by dissolving MC powder in water with constant stirring at room temperature and then GA and hydrochloric acid were added for crosslinking. The films were fabricated by casting on a glass plate. Films of 50-80 μm were obtained by drying at ambient temperature for 72 hr. The swelling test has shown that the MC gels were insoluble in water with GA content of over 5.0×10^{-3} mol/l, and hydrochloric acid concentrations of more than 1.0×10^{-2} mol/l. The swelling ratio of MC gel, which is a measure of their degree of crosslinking density, was observed to increase with increasing GA and hydrochloric acid concentrations. Finally, the tensile strength was increased through crosslinking while the elongation was slightly decreased.

Kurita et al. (1986) prepared and studied the crosslinked water-soluble chitin to varying extents with glutaraldehyde in homogeneous aqueous solutions to improve the properties as an adsorbent for metal cations. They reported that the excess glutaraldehyde shows the absorption peak at 1710 cm^{-1} (aldehyde group in FTIR spectra). In addition, complete insolubilization was achieved with the fivefold excess aldehyde, but in terms of adsorptivity of Cu^{2+} the chitin crosslinked at an aldehyde/amino group ratio of 1.0 was found to exhibit remarkable capacity and was much superior to others.

Mi et al. (2003) showed the effects of crosslinking mechanism with degradable properties. Figure 3.4 presents the degradation profile of the TPP/genipin crosslinked chitosan beads in terms of the increments in free amino group content within 8 weeks of lysozyme incubation. It was showed that the increment in free-amino-group content of medium incubated with fresh chitosan gel bead (without crosslinking) was significantly greater than that observed in the media incubated with the TPP/genipin co-crosslinked chitosan beads. The biodegradation rates of

TPP/genipin co-crosslinked chitosan networks showed slower than fresh chitosan gel beads.

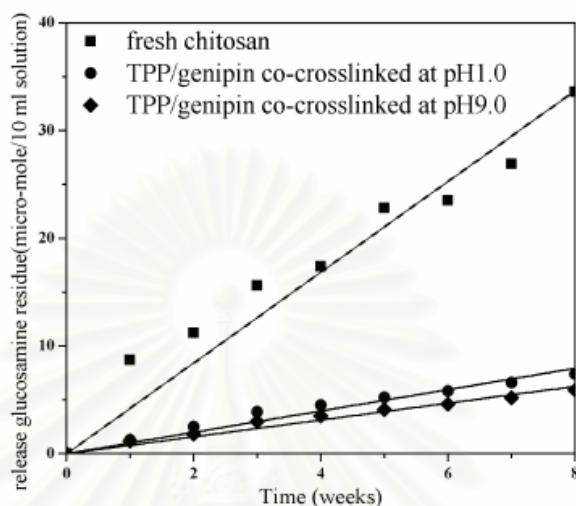


Figure 3.4: Degradation profile of the TPP/genipin crosslinked chitosan beads in terms of the increments in free amino group content in the incubation medium vs. time.

Lee et al. (2000) reported the effect of biodegradable poly(aldehyde guluronate), obtained by oxidation with periodate of partially depolymerized alginate. The polymer can be converted into a hydrogel by crosslinking with adipic acid dihydrazide. The swelling and degradation of the gels could be systematically controlled by the amount of adipic acid dihydrazide. When daunomycin presented during the hydrogel formation process, drug was grafted onto the polymer matrix through a covalent linkage. Due to hydrolysis of this linkage, daunomycin was released in a time frame from 2 days to 6 weeks.

CHAPTER IV

EXPERIMENTAL

4.1. Materials

Methyl Cellulose (MC), Tylose H 6000 YP2, was purchased from SE Tylose GmbH & Co. KG, Germany whereas Polargel HV powder, trade name of montmorillonite (MMT) commercial grade was supplied by VOLCLAY International Co., Ltd. Glutaraldehyde (GA) solution (25wt%, MW = 100.11, Bp = 106°C) under trade name of UNILAB was obtained from Ajex Finechem, New Zealand.

4.2 Preparation of Nanocomposite Films

4.2.1 Preparation of Montmorillonite Suspension

MMT suspension was prepared at ambient temperature using a homogenizer. There were four essential parameters to be studied as listed in Table 4.1.

Table 4.1 Lists of parameters studied in this work.

Item	Parameter	Variables	Condition
1	Pre-swelling times	0 to 14 days	5wt% MMT suspension using a speed of 6500 rpm for 1 min
2	MMT contents	1, 3, 5, 7 and 9wt%	The appropriate system from Item 1
3	Mixing speeds	6500, 9500, 13500, 17500, 21500, and 24000 rpm	The optimal system from Item 1 and 2
4	Mixing times	1, 2, 4, 6, 8, and 10 min.	The best condition of Item 1, 2 and 3

4.2.2 Preparation of Methyl Cellulose Nanocomposite Films

MC/MMT nanocomposite films were prepared by mixing appropriate MMT suspensions obtained from section 4.2.1 with aqueous MC solutions (2wt%) by solution intercalation technique over the gelation temperature of MC (50-55°C). In this study, mixing temperature was about 80°C. A homogenizer (IKA T25 basic) was used for high shear mixing at 13500 rpm for 5 min. The weight ratio of MC/MMT was varied as 100:0, 100:1, 100:2, 100:3, 100:5 and 100:10. About 30 ml of the obtained MC/MMT solution was poured into a polystyrene mold, as shown in Figure 4.1, to render a dried film then after solvent. The yielded thickness of the nanocomposite films was in the range of 70-80 μm .



Figure 4.1: Polystyrene mold for MC film casting.

4.3 Preparation of Crosslinked Methyl Cellulose Films

Aqueous MC solutions (2wt%) were prepared by dissolving MC powders in water and mixed for 1 min at 80°C using a homogenizer with a speed of 13500 rpm. GA and hydrochloric acid were added after the MC solution was cooled to room temperature. The investigated GA contents were varied at 0.5, 1.5, 3.0, 4.5, 6.0, and 12.0wt%. In each solution, 2 drops of hydrochloric acid were added to yield a solution of pH 3. The homogeneous blend solution was obtained using a magnetic stirrer at 700 rpm for 1 hr. Finally, the resulting dried films were washed by distilled water for

3 hr to neutralize the film. The thickness of each crosslinked film was approximately the same as that of the nanocomposite film.

4.4 Specimen Characterizations

4.4.1 Viscometer

Viscosity of MMT suspension was measured by Physica Rheolab MC1: Standard measuring system MS-Z3 DIN/MC1, at shear rate of 10-1000 s⁻¹ for 10 min. The volume of measured suspension was about 17-20 ml. The raw data was plotted between shear rate and viscosity of the suspensions. Appropriate suspension with highest viscosity would be used for MC/MMT nanocomposite films preparation.

4.4.2 X-ray Diffraction (XRD)

Interlayer spacing of MMT in nanocomposites was investigated by XRD technique. Samples were detected by X-Ray diffractometer (Bruker model D8 ADVANCE) with CuK α radiation (1.541 Å). The voltage and the current used were 40 kV and 30 mA, respectively. The measurement was scanned at 2θ in range of 1.5° to 30.0°. The scan speed was 5.0 sec/step with the step size of 0.01°. The basal spacing of the silicate layers (d) was calculated according to Bragg's equation.

4.4.3 Transmission Electron Microscope (TEM)

A qualitative understanding of the internal structure, spatial distribution of the various phases and direct visualization of defect structure was allowed by TECNAI 20 TWIN at an accelerating voltage of 80 kV. The ultrathin film, approximately 90 nm was sectioned at ambient temperature using a Reichert cryoultramicrotome without staining.

4.4.4 Differential Scanning Calorimetry (DSC)

The thermal behaviors of the MC samples were investigated by Perkin Elemer Diamond DSC in a nitrogen atmosphere. The measurement was performed using a sample mass of 6-10 mg. The sample was placed in a sealed aluminum pan. The first heating scan, which was conducted to eliminate water residual, was carried out at a rate of 20°C/min from room temperature to 150°C. The second scan was carried out at a heating rate of 10°C/min from 0 to 300°C. Glass transition temperature (T_g) values were identified by using the temperature of the step transition midpoint in the thermogram.

4.4.5 Thermogravimetric Analysis (TGA)

The thermal stability of nanocomposites and crosslinked MC were investigated by Perkin Elemer Diamond TG/DTA. The sample mass used was about 15 mg. The first heating scan, which was conducted to eliminate water residual, was carried out at a rate of 20°C/min from room temperature to 150°C. The second scan was heated from 40 to 500°C at a heating rate of 20°C/min in a nitrogen atmosphere. The nitrogen purging flow rate was 100 ml/min. Weight loss of a sample was measured as a function of time or temperature.

4.4.6 Dynamic Mechanical Analysis (DMA)

Dynamic properties of nanocomposites and crosslinked MC films were investigated by NETZSCH DMA 242C in the tensile mode at a frequency of 1 Hz. The samples were heated from 30 to 250°C at a rate of 2°C/min in a nitrogen atmosphere. The films with dimensions of about $5 \times 10 \times 0.1 \text{ mm}^3$ were subjected to sinusoidal deformation with a 5 mm amplitude. The storage modulus (G'), loss modulus (G''), and damping curve ($\tan\delta$) were determined. The T_g was taken as the maximum point on the loss modulus curve in the temperature sweep tests.

4.4.7 Universal Testing Machine

The tensile strength, elongation at break and tensile modulus values of nanocomposites and crosslinked MC films were using a universal testing machine (Instron 5567) with a speed of 5.0 mm/min for a gauge length of 50.0 mm at ambient temperature. Samples were cut by scalpel to $130 \times 10 \text{ mm}^2$ in dimension. The reported values were taken from an average of five measurements.

4.4.8 Fourier Transform Infrared Spectroscopy (FTIR)

To investigate functional groups and the structure of crosslinked MC films, FTIR technique was used (Perkin Elmer spectrum GX) at the resolution of 4.0 cm^{-1} , at scan number of 64, and frequency of $4000\text{-}400 \text{ cm}^{-1}$. The thickness of the films was prepared in the range of 25-30 μm .

4.4.9 Moisture Absorption

The water absorption testing of ASTM D570-98 was modified to find out the moisture absorption of nanocomposites and crosslinked MC films with 70-80 μm thickness were determined. The test specimens have the dimension of $50 \times 50 \times 0.07 \text{ mm}^3$. The test specimens were dried at 40°C for 24 hr, then cooled in a desiccator, and immediately weighed as the initial weight. The specimens were placed on the aluminum net inside a plastic box ($300 \times 200 \times 110 \text{ mm}^3$) at 100% RH for 24 hr, as shown in Figure 4.2.



Figure 4.2: Plastic box in moisture absorption test.

After 24 hr, the specimens were then weighed immediately to obtain the final weight. The moisture absorption of the sample was calculated using Equation (4.1):

$$\text{Water Absorption (\%)} = \frac{(W_f - W_i)}{W_i} \times 100 \quad (4.1)$$

Where W_i and W_f are the weight of composite MC films before and after absorbing moisture.

4.4.10 Degree of Biodegradation

The controlled composite testing of ASTM D5988-96 was modified to find out the degree of biodegradability of nanocomposite and crosslinked films as a function of time. Quantitative tests were performed in an air-tight vessel during a period of 6 weeks.

The composting test was performed as summarized in Figure 4.3. Add 100 g of mixture soil (topsoil: composted manure=70:30) in a 900 ml vessel. Then, add 5 g of the tested specimen in the form of fragments to 100 g the mixture soil and mix the soil thoroughly. After that, add distilled water to bring the moisture content to 80 to 100%. Keep the vessel and lid (with the necessary amount of stopcock grease) in a dark cabinet at ambient temperature. The amount of CO_2 produced was determined every week using gas chromatography (GC-8A).

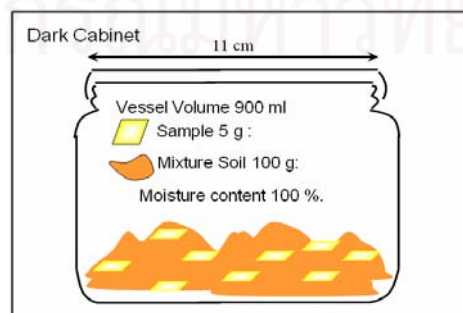


Figure 4.3: Scheme of biodegradation test in this study.

GC-8A was equipped with a thermal conductivity detector (TCD) and 2 m stainless column packed with Porapak Q (80/100 mesh). The temperatures of the injection port, the column and the detector were maintained at 50°C. Helium was used as a carrier gas at a flow rate of 25 ml/min. The volume of injected biogas was 0.5 ml.

The area of CO₂ peak, representing CO₂ concentration, was reported. The test method is based on the determination of the net CO₂ evolution, the main product of the biodegradation reaction evolved from the mixture compost minus the CO₂ evolved from the unamended compost (blank).

4.4.11 Composting degradation

The film samples were placed on the mixed soil and stored under controlled conditions (100% RH at room temperature, as seen in Figure 4.4) in plastic box (300×200×110 mm³). The test specimens were prepared in the dimension of 45×55×0.07 mm³. The film appearance was observed, and then the photographs were taken.

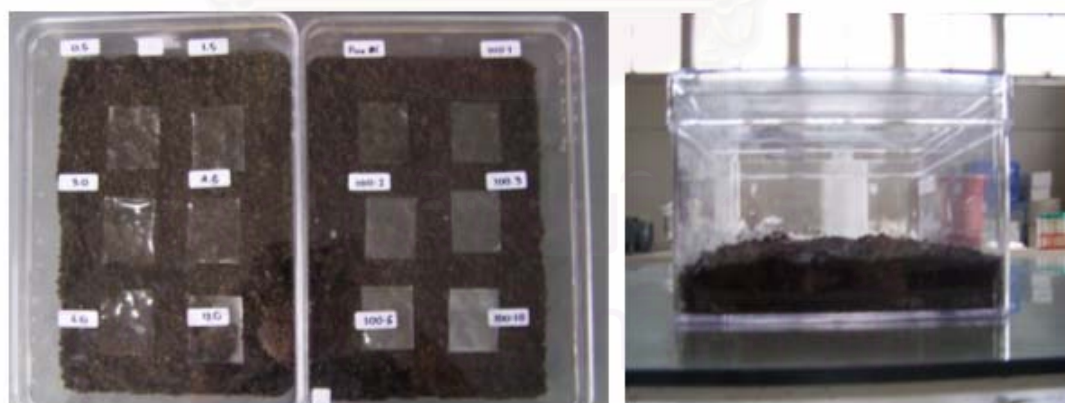


Figure 4.4: Plastic box in composting degradation test.

CHAPTER V

RESULTS AND DISCUSSION

5.1 Suitable Conditions for MMT Suspension Preparation

Dilute concentrations of organophilic swelling clays dispersed in a polymer matrix have unusual and valuable mechanical, thermal, and permeability properties relative to the pure polymer (Vaia., 2001). It is well known that the distribution of clay has a significant effect on the nanocomposite properties. The types of distribution can be classified into intercalated tactoid structure and exfoliated structure. The exfoliated materials provide greater distribution, which leads to higher potential for material property enhancement. Therefore, the preparation of well-dispersed clay suspension for high quality of nanocomposite film will be investigated via viscosity measurement of the MMT suspension.

MMT aqueous suspension was prepared at ambient temperature using a homogenizer. There are four parameters to be studied including pre-swelling times, MMT contents, mixing speeds, and mixing times. The measured viscosity expressed in centipoises (cps) was recorded and the results are shown in Figure 5.1, 5.2, 5.4, and 5.5.

5.1.1. Effect of Pre-swelling Times on Viscosity of MMT Suspension

Polargel HV powders, trade name of MMT, were added into water before mixing to achieve intercalation of stacked layers. Before applying a high shear force by a homogenizer for 1 min, the suspension with 5wt% of MMT powder was prepared at pre-swelling time of 0, 2, 4, 6, 8, 10, 12 and 14 days. Then their suspension viscosities were examined. The rheological behaviors of MMT suspensions in the shear rate range of 200 to 1000s⁻¹ are presented in Figure 5.1. All suspension exhibited shear thinning characteristics. It was clearly seen that the greater

pre-swelling time, the higher viscosity with more deviation from the Newtonian behavior were observed, i.e. greater shear-thinning.

At the shear rate of 600s^{-1} , the relation of pre-swelling time and viscosity of the suspension is shown in the inset of Figure 5.1. The viscosity of MMT suspension slightly increased with an increasing in pre-swelling times, while the pre-swelling times of at least 8 days yielded a maximum suspension viscosity approximately at 19-20 cP.

As pre-swelling time increases, water molecules can achieve intercalation into the stacked layers (Frost et al., 2000). Moreover, long immersion period provides a high swelling possibility of the layered silicate. Therefore, the pre-swelling time of 8 days was chosen for the preparation of MMT suspension in this work.

5.1.2 Effect of MMT Contents on Viscosity of MMT Suspension

The effects of MMT content on rheological behavior are presented in Figure 5.2. The suspension preparation was based on a homogenizer speed of 6500 rpm for 1 min. The MMT contents were varied from 1wt% to 9wt% at fixed pre-swelling time of 8 days. The change of suspension viscosity was not clearly observed when a small amount of 1wt% of MMT was used. The exponential increase of the MMT suspension viscosity was evidently observed, when the MMT content was increased from 3wt% to 9wt%. Furthermore, it can be noticed that the higher MMT contents, the more pronounced shear-thinning behavior was observed.

At the shear rate of 600s^{-1} , the relation of MMT contents and viscosity of the suspension is shown in the inset of Figure 5.2. It can be noted that the viscosity of suspension exponentially increased with the increase of MMT contents. The suspensions at 1wt% and 3wt% were precipitated after leaving the MMT suspension for 24 hr, as depicted in Figure 5.3. Therefore, the MMT suspension at 5wt% was selected for further investigation since it was the lowest concentration that provided

homogeneous suspension with the lowest MMT content for effective dispersion of layered silicate.

5.1.3 Effect of Mixing Speeds on Viscosity of MMT Suspension

The 5wt% of MMT suspension pre-swelling time for days was prepared using a homogenizer with various mixing speeds. Figure 5.4 shows the relationship between the varied shear rates and viscosities of MMT suspension prepared at various mixing speeds of 6500, 9500, 13500, 17500, 21500 and 24500 rpm. At the mixing speed of 6500 rpm, the relatively low viscosity in the range of 20-45 cP of the 5wt% MMT suspension was obtained. At the higher mixing speed of 9500, 13500, 17500, 21500 and 24500 rpm, the observed viscosities were in the range of 25-70 cP. This phenomenon signifies that the increasing of shear rate enhances dispersion of the stack of MMT layered silicate.

Based on the shear rate of 600s^{-1} , the relationship between the mixing speed and the viscosity of the MMT suspension is shown in the inset of Figure 5.4. It can be noticed that the viscosity of the suspension drastically increased from 19 cP to 29 cP with increasing the mixing speed from 6500 rpm to 13500 rpm, respectively. Beyond 13500 rpm, the viscosity did not significantly change with a further increase of the shear rate. Hence, this mixing speed was chosen for maximizing the dispersion of MMT. It can be observed that when the mixing speed was 24500 rpm, the viscosity was slightly raised to 31 cP. This phenomenon signifies that high shear force applied by a homogenizer effectively disperses the stack of MMT.

5.1.4 Effect of Mixing Times on Viscosity of MMT Suspension

The effect of mixing time on viscosity of 5wt% MMT suspension prepared a mixing speed of 13500 rpm after pre-swelling 8 days is illustrated in Figure 5.5. Viscosity of MMT suspension was found to slightly increase with an increase of the mixing time. At the applied shear rate of $200\text{-}1000\text{ s}^{-1}$, the viscosity of the MMT suspension exhibited shear thinning behavior in the range of 21-80 cP.

At the shear rate of 600s^{-1} , the relationship between mixing time and viscosity of the suspension is obtained and plotted in the inset of Figure 5.5. It was revealed that the viscosity obtained by using a mixing time over 4 min approached a maximum value of about 33 cP. Therefore, the optimal mixing times of 4 min was chosen for the MMT suspension preparation in our investigation.

Conclusively, the mixing conditions to prepare MMT suspension are summarized in terms of viscosity maximization at the shear rate range of 200 to 1000s^{-1} as shown in Table 5.1. All MMT suspensions with the maximum viscosity at each condition were selected for MMT suspension preparation used in MC/MMT nanocomposite films. Table 5.1 suggested that at 1000s^{-1} , the viscosity of MMT suspension prepared by condition 3 greatly increases from that prepared by condition 1 and 2 while that of MMT suspension prepared by condition 4 and 5 do not significantly increase for that prepared by condition 3. Maximum viscosity of the system is first noticed at the mixing speed of 13500 rpm in condition 3. However, to ensure a completely exfoliated suspension, condition 4 was applied for the preparation of MMT suspension. The performed condition is Polargel HV suspension at 5wt% and pre-swelling times of 8 days using a homogenizer at a constant mixing speed of 13500 for 4 min.

5.2 Characterization of MC/MMT Nanocomposites

In this study, the thickness of the obtained MC/MMT nanocomposite films at various contents of MMT was controlled to be in the range of 70-80 μm . Figure 5.6 shows the comparison of the MC/MMT nanocomposite films filled with 0-10 phr of MMT particles. Normally for high translucency, the dispersed phase should have an average size smaller than the wavelength of visible light, i.e. 400-800 nm (Chang et al., 2003). In our nanocomposite films, the translucency slightly decreased with increasing MMT content possibly because of agglomeration of MMT particles. It can be observed that the film with 10 phr of MMT particles was the least translucent. This suggests that some agglomeration of the MMT nanoparticles existed in the composite films thus resulting in the decreased translucency of the films. To confirm the

formation of the nanocomposite in our MC/MMT mixture, its morphology has also been investigated.

5.2.1 Morphology of Nanocomposite Films

The state of intercalation and exfoliation of nanoparticles has typically been established using X-ray diffraction (XRD) analysis. When the interlayer basal spacing increases relative to the original MMT, it is called intercalation. In case that the basal interlayer of the MMT is completely disrupted, it is called exfoliation. (Xia et al., 2003). In addition, transmission electron micrographic (TEM) observation is often used to support XRD results on the nanocomposite morphology.

Figure 5.7 shows XRD patterns of MMT powder and MC/ 5 phr MMT nanocomposite films based on non pre-swelled MMT and pre-swelled MMT, in the region of $2\theta = 1.5^\circ$ to 10° . The characteristic peak of MMT powder, a sharp peak, was observed at $2\theta = 6.7^\circ$. This value corresponds to the interlayer spacing, $d(001)$, = 1.3 nm, which is similar to a previous report (Park et al., 2004). In the case of MC/ 5 phr MMT nanocomposite films using non pre-swelled MMT, a peak was observed at $2\theta = 2.2^\circ$ which corresponded to the interlayer spacing, $d(001) = 4.3$ nm. The angle of the characteristic peak was shifted to the smaller value than that of the MMT powder. This indicates that the molecules of MC were able to intercalate into the layered silicate of MMT, expanding the basal spacing of the MMT. Therefore, an intercalated structure (within 1.3 nm – 4.3 nm) was observed. In the case of MC/ 5 phr MMT nanocomposite films prepared from pre-swelled MMT, there were no peaks observed in the diffraction pattern. The phenomenon implied MMT layers in the composites were disordered, thus nanocomposite tended to exhibit exfoliated structure. The proper pre-swelling condition therefore has a positive effect to promote the dispersion of the MMT layers resulting in a highly exfoliated nanocomposite.

XRD patterns of the pure MC, MMT powder and MC/MMT nanocomposite films at various MMT contents in the 2θ region of 0.5° to 30° are shown in Figure 5.8. The diffraction intensities were divided by a factor of 100 relative to the

nanocomposite intensities in order to place them on the same plot for comparison. The nanocomposite diffraction intensities were vertically overlaid for clarity of presentation. The diffraction pattern of MMT powder had three characteristic peaks with one broad peak at $2\theta = 6.7^\circ$ ($d = 1.3$ nm), which indicated the spacing between the silicate layers and two narrow peaks at $2\theta = 19.8^\circ$, and 21.9° . There was no evidence of an MMT basal spacing peak at 1.3 nm in all nanocomposites. The lack of intergallery in MMT diffraction was due to the complete exfoliation and random distribution of the MMT platelets within the MC matrix, which suggests relatively high miscibility of MMT filler and MC matrix. It can be concluded from the XRD study that the nanocomposite containing 1 to 10 phr of MMT exhibited an exfoliated morphology. However the presence of order at higher d-spacing (>5.8 nm or $2\theta = 1.5^\circ$) could not be confirmed from the XRD data in this study. Further investigation with TEM was, therefore, performed.

For the pure MC film, some broad diffraction peaks were observed between $2\theta = 9^\circ$ to 21° , indicating some order intermolecular structures of this polymer. For nanocomposite, the area under these peaks, which indicates the crystallinity of the MC matrix, gradually decreased with increasing the MMT content up to 10 phr. This is probably related to the changes of crystalline morphology for semi-crystalline MC possibly owing to heterogeneous nucleation of MMT particles, which might lower or destroy the crystal perfection or crystallinity of the matrix. The addition of MMT even at the content as low as 1 phr into some polymeric matrices such as Nylon 66 was reported to considerably decrease the crystallinity of the matrix by about 10% (Shen et al., 2004).

TEM analysis can be used to support XRD results by visualizing MMT dispersion on nanoscale. Nanometer-range intercalated MMT tactoids are shown in Fig. 5.9(b). Dark lines correspond to the cross section of a MMT sheet ca. 1 nm thick and the gap between two adjacent lines is the interlayer spacing or gallery of the MMT. The measured interlayer spacings between adjacent clay layers of intercalated tactoids obtained from TEM are consistent with the XRD data.

By using different magnifications in the imaging, Figures 5.10 to 5.12 show TEM micrographs of MC/MMT nanocomposite films at various MMT contents of 1, 5, and 10 phr respectively. Nanocomposites of MC and MMT clearly reveal disordered platelets of MMT layers in the MC matrix. A low magnification TEM micrograph (Figure 5.10(a)) shows a general view of the dispersed MMT layers in MC matrix. In this figure, a relatively homogeneous dispersion of MMT layers was achieved suggesting a high level of miscibility between the MMT and the MC. All the nanocomposites at the MMT contents of 1 to 10 phr under this investigation show an exfoliated morphology. The nanocomposite with 5 and 10 phr of MMT content rendered the uniform and dense dispersion. Figure 5.10 (b) and (c) present a close-up view of the miscible MMT layers with some agglomeration of the MMT particles. Dark lines correspond to the cross section of MMT sheets possibly due to some ionic interaction among the MMT layers. The gap between two adjacent lines was the interlayer spacing or gallery. Conclusively from Figure 5.10 to 5.12, TEM images of the MC/MMT nanocomposite system with 1, 5, and 10 phr of MMT confirm a well dispersion of MMT layered silicate in the MC matrix with some degree of agglomeration of the MMT layers.

In summary, the results of XRD patterns seen in Figure 5.8 suggested that the order of MMT layers was eliminated in the MC matrix. This result was confirmed by TEM images. However, the formations of MMT layers in communities were found in the images. Therefore, the direct visual information of the morphology provides information on the phase distribution and exfoliation behavior with some degree of agglomeration of the MMT, which is similar to a previous work reported by Wibowo et al. (2005).

5.2.2 Thermal Properties of Nanocomposite Films

The thermal degradation of the pure MC and MC/MMT nanocomposites as a function of MMT content is presented in Figure 5.13. It can be noticed that a slight weight loss (~1-3wt%) of MC and MC nanocomposites started below 100°C. The possible causes for the initial weight loss are probably due to moisture and high

water-retention capacity of MC, which is similar to a reported work on hydroxypropylmethylcellulose, HPMC systems (Sannino et al., 2005; Park and Ruckenstein, 2001). The major weight decrease of pure MC and its nanocomposites took place in the temperature range of 330-400°C because of the structure degradation of MC. It can be noticed that the thermal decomposition of nanocomposite shifted slightly toward higher temperature from that of the pure MC, which confirmed the enhanced thermal stability due to a barrier effect of the layered MMT on the confined polymers. Beyond 400°C, all curves were consistent as mainly inorganic residue remained. Like other nanocomposites in the determination of the residual weight, a small amount of MMT also increased the residual weight of MC/MMT because of its inorganic nature. The residual weight of these specimens at 500°C increased in the order of pure MC < MC/MMT01 < MC/MMT02 < MC/MMT03 < MC/MMT05 < MC/MMT10 (here number indicates phr of MMT). The improved thermal degradation properties are also observed in the system of chitosan/MMT (Darder et al., 2003). The authors reported that the addition of MMT enhanced the performance of the char formed, by acting as a superior insulator and mass transports barrier to the volatile products generated during decomposition.

The role of MMT in the nanocomposite structure may be the main reason for the difference in TGA results of these systems compared to the previously reported systems. The MMT acts as a heat barrier, which enhances the overall thermal stability of the system, and occasionally assists the char formation after thermal decomposition. However, this heat barrier effect would sometimes result in a reverse thermal stability. In this case, the stacked silicate layers could hold accumulated heat that could be used as a heat source to accelerate the decomposition process, in conjunction with the heat flow supplied by the outside heat source. This thermal degradation acceleration had been discussed by Sinha Ray and Bousmina, 2005.

The DSC thermograms showing glass transition temperature (T_g) of pure MC and MC/MMT nanocomposites films at various MMT contents are presented in Figure 5.14. T_g values were taken as the midpoint temperature of the change in specific heat in the transition region. MC curve exhibited T_g at 176°C, which is

similar to T_g of hydroxypropylmethylcellulose, HPMC (Zaccaron et al., 2005). The T_g of the MC nanocomposites slightly shifted to 182°C with increasing the content of MMT to 10 phr. In theory, an increase in T_g was attributed to the restricted thermal motion of polymer in the vicinity of the silicate layers. The slight change of T_g was possibly due to the highly rigid anhydroglucose unit of MC. In this type of molecule, the rigidity of the sugar backbone was not changed in a major way by nanoreinforcement, even though there exists a strong bonding between the hydroxyl groups of the anhydroglucose units of MC with the hydroxyl groups on the surfaces and the edges of the exfoliated clay particles (Park and Ruckenstein, 2001).

5.2.3 Dynamic Mechanical Analysis of Nanocomposite Films

Figure 5.15 shows the storage modulus (G') of MC/MMT nanocomposite films in the range of 30-250°C at various MMT contents. This figure show G' of the nanocomposite at 10 phr of MMT was higher than that of pure MC and 1 phr of MMT content for all testing temperatures. In comparison with pure MC at 30°C, the storage modulus of 10 phr nanocomposite increased from 2.4 GPa of pure MC to 3.3 GPa. For all samples, the transition regions from glassy state to rubbery state were in the range of 170°C to 200°C. Additionally, the improvement of storage modulus was obviously found in the rubbery plateau. This phenomenon can be caused from mechanical reinforcement by the silicate layers (Sinha Ray et al., 2003).

Figure 5.16 indicates mechanical loss tangent ($\tan\delta$) of the MC and MC/MMT nanocomposite as a function of temperature. The relaxation peaks of the pure MC curve could be observed at 190°C. That corresponds to the glass transition temperature of the MC, which is similar to the reported T_g of same polymer (Park et al., 2001). The $\tan \delta$ curve for the MC nanocomposites shows the slight shift of the relaxation peaks to higher temperature with increasing MMT. The T_g value was 194°C for the nanocomposite at 10 phr of MMT. This behavior indicates that the silicate layers in the polymer hybrids have some influence on the MC chain mobility.

This behavior has been described to the restricted segmental motions at the organic–inorganic interface neighborhood of intercalated nanocomposites.

5.2.4 Tensile Properties of Nanocomposite Films

Figure 5.17 shows the changes of the tensile modulus values at various MMT contents. The tensile modulus of the nanocomposite can be improved by about 65% from 2.0 GPa for pure MC to 3.3 GPa for the nanocomposites contained only 10 phr of MMT. The enhancement of the modulus can be directly attributed to the reinforcement provided by the exfoliation of MMT in the MC. This affected polymer can be thought of as the region of the polymer matrix that is physisorbed on the silicate surface, and is thus stiffened through its affinity for and adhesion to the filler surfaces (Shia et al., 1998). It is well-known that, high aspect ratio fillers as layered silicate layers and its high surface area exposed to the polymer play a key role in an increase in the modulus with very low filler content. In some cases, the modulus of nanocomposite could be raised about 300% higher than that of the bulk matrix at only 4wt% of the MMT (Strawhecker and Manias, 2000).

The tensile strength and the elongation at break of MC/MMT nanocomposite films at various MMT contents are shown in Figure 5.18. A considerable improvement in tensile strength with a slight decrease in elongation at break was observed with increasing MMT content. The tensile strength was found to increase from 68 MPa for pure MC to 92 MPa for the 10 phr nanocomposites, whereas the elongation at break was slightly reduced from 22.5% of the MC to 18.9% for the 10 phr nanocomposite. This behavior is mainly due to reinforcing effect of MMT from its high aspect ratio and its enormous surface area discussed above, which leads to high strength improvement.

5.2.5 Moisture Absorption of Nanocomposite Films

Figure 5.19 shows a moisture absorption study of pure MC and the MC nanocomposites. The nanocomposites exhibited not only superior mechanical

properties but also enhanced water resistance. The moisture absorption of nanocomposite films decreased systematically with MMT loading. In this Figure, the MC/MMT nanocomposite films process lower moisture absorption than that of pure MC, i.e. from 133% of pure MC compared to 108% for the 10 phr nanocomposite. This phenomenon can be explained by the fact that the large aspect ratio MMT layers inherit outstanding mass barrier properties because of the formation of a tortuous path in the presence of layered silicates, which can hinder water diffusion through the nanocomposite specimens.

5.3 Characterization of Crosslinked MC

The crosslinking of MC can be achieved using crosslinking agents. Glutaraldehyde (GA) is one of crosslinking agents that is often used to crosslink MC. Figure 5.20 shows the films of the crosslinked MC film, pure MC film, and MC nanocomposite film. From this figure, it can be observed that the crosslinking film at 12wt% of GA was as clear as the pure MC film. In addition, the nanocomposite film at 10 phr of MMT was the least translucent.

5.3.1 FTIR Spectroscopy Investigation of the Crosslinked Reaction

The FTIR spectra for pure MC and crosslinked films at various amount of GA crosslinker are showed in Figure 5.21. Pure MC had absorption bands related to O–H stretching at 3447 cm^{-1} , C–H stretching at 2837 cm^{-1} , C–O carbonyl stretching from the glucose of the cellulose at 1643 cm^{-1} , C–O stretching from asymmetric oxygen bridge at 1163 cm^{-1} , and ring stretching at 896 cm^{-1} . These values were consistent with those reported by Wang et al., 2004. For crosslinked MC, the peaks at 1710 cm^{-1} (C=O stretching from aldehyde group of GA) is used to indicate the crosslinking reaction. With an increase in the GA over 6.0 wt% in the crosslinked MC, the peak at 1710 cm^{-1} (C=O from the aldehyde group) substantially increases. The optimal GA content was thus below 6.0 wt%. The appearance of the absorption

spectrum also suggested the formation of intermolecular hydrogen bonding, similar to the results reported for chitosan crosslinked with GA (Kurita et al., 1986).

5.3.2 Moisture Absorption of Crosslinked MC

The effect of the crosslinking agent (GA) contents (wt% based on the MC) on moisture absorption capacity of crosslinked MC is presented in Figure 5.22. All crosslinked MC films in the GA contents range from 0.5 to 12.0 wt% were insoluble in water. When the GA contents increased, moisture absorption also systematically decreased from 133% of uncrosslinked MC to 96% of the crosslinked MC. It can be explained that as the crosslinking of MC increased, the number of hydroxyl groups of MC decreased. Then, the reaction between hydrogen bonds and water molecules reduced. Moreover, the crosslinking made the polymer chains difficult to move. As a result, the moisture absorption decreased with increasing GA contents. This phenomenon was similar to that reported for chitosan crosslinked with tripolyphosphate and genipin at pH 7.4 (Mi et al., 2003). They reported that, the moisture absorption decreased with increasing degrees of crosslinking.

5.3.3 Tensile Properties of Crosslinked MC

Tensile modulus, tensile strength, and percent elongation at break were also determined experimentally for crosslinked MC chemistries with varying quantities of GA crosslinker. The testing conditions are the same as those used for nanocomposite films evaluation.

Figure 5.23 illustrates a relationship between tensile modulus of crosslinked MC films at various contents of GA. Comparing with uncrosslinked MC film, the tensile modulus of crosslinked MC film at 4.5wt% of GA improved by about 45% (from 2.0 to 2.9 GPa). From 6.0wt% to 12.0wt%, this value slightly decreased. This phenomenon can be explained that GA led to network structures, which decreased the mobility of the polymer chains. Therefore, the crosslinked materials were rigid. When

the GA content was in excess, i.e. higher than 4.5wt% in this case, it might function as a plasticizer that softened the composite.

The tensile strength and the elongation at break at various contents of GA are shown in Figure 5.23. An improvement in tensile strength with a considerable decrease in elongation at break was observed with increasing GA content while the tensile strength increases with increasing the GA content up to 4.5wt%. From the plots, the tensile strength values show the values of 68 MPa in pure MC to 70 MPa in crosslinked MC. We can conclude that the tensile strength improved by about 3% when compared with that of pure MC and then the tensile strength slightly decreased for the composite with 6.0wt% to 12.0wt% of GA. Elongation at break of crosslinked MC was decreased about 87% for the GA contents of 12 wt%. This is because the excess amount of the crosslinking agent started to act as a plasticizer.

5.3.4 Dynamic Mechanical Analysis of crosslinked MC

For all MC crosslinked films, significant enhancement of storage modulus (G') can be seen in the investigated temperature ranges as presented in Figure 5.25. At 250°C (temperature in the rubbery plateau region), the addition of GA increases plateau modulus of the crosslinked films which relates to an increase in degree of crosslinking in the specimen. The MC crosslinked film at 4.5 wt% of GA showed the highest crosslinking density. The higher degree of crosslinking led to denser network structures, which decreased the mobility of the polymer chains. Therefore, the higher crosslinked materials have more rigidity in nature. When the contents of GA were 6wt% (i.e. excess level), the crosslink density became lower than its highest plateau, i.e. at 4.5wt% GA. This is because GA acted as a plasticizer that softened the composite.

Figure 5.26 presents the DMA thermograms of MC and MC crosslinked films as mechanical loss tangent ($\tan\delta$) against temperature. The relaxation peak corresponded to the T_g of the pure MC can be observed at 190°C. The $\tan\delta$ curves for the MC crosslinked films show the shift of the relaxation peaks to higher temperature with increasing the GA from 0.5 to 4.5wt%. That means the film with 4.5wt% of GA

rendered the highest T_g (219°C). When the amount of GA was greater than 4.5wt%, the T_g decreased due to the plasticizing effect mentioned earlier. Generally, the height of $\tan \delta$ exhibits the ratio between viscous and elastic behaviors. In this figure, $\tan \delta$ peak of pure MC is highest. It can be observed that the height of the curves decreased with an addition of the GA crosslinker. At 4.5wt% of GA which is about the optimal GA quantity, the films showed the highest elastic behavior from the highest network density thus showing the small $\tan \delta$ peak.

5.4 Biodegradability of MC/MMT Nanocomposite and Crosslinked MC Films

Figure 5.27 and 5.28 shows the physical appearance of nanocomposite films and crosslinked films placed on mixing soils at various observing times, respectively. The effect of MMT content on the degradation behavior of films was presented in Figure 5.27. The degradation behavior of all nanocomposite films started with swelling appearance. Then they decayed and finally disappeared. This period of consumption time can be prolonged when MMT was increased. It can be noticed that at the observation period of 5 days, the film with 10 phr (highest MMT content) was the only one that was not disappeared. In Figure 5.28, the appearance of the crosslinked films with all compositions at the observation period of 5 days was still the same as those new films.

The quantitative study on the relationship between net CO_2 evolution from pure MC film, nanocomposite films, and crosslinked films during 6 weeks is shown in Figure 5.29. When comparing the results of nanocomposite films and crosslinked films, the amount of CO_2 from crosslinked films < nanocomposite films < pure MC film. That means the crosslink formation could have a greater effect on prolonging biodegradation of MC films than the addition of MMT.

To clarify that water diffusion was the greatest factor on degradation for MC system, the water solubility test was performed. Figure 5.30 illustrates the different

behaviors of water solubility of pure MC film, nanocomposite film (10 phr of MMT), and crosslinked MC film (4.5wt% of GA). It is found that pure MC film was soluble within 10 min, whereas nanocomposite film was swelled. After observation for 24 hr, crosslinked film was insoluble in water. This result confirms that the degrader had less effect on degradation than water diffusion.

The decrease of biodegradability of MC/MMT nanocomposites was possibly caused from the interaction and adhesion of MC and layered silicate surfaces of MMT. The interaction and adhesion restricted segmental motion at the interface. A Part of MC chains was hidden by the silicate layers on the surface of the film, which forced the degraders to diffuse into the bulk of the film through more tortuous paths. Therefore, the effective path length and time for the diffusion of degraders were increased, and the biodegradation of MC was hindered (Lee et al., 2002).

The decreased permeability may also be related to the decrease of the biodegradability. The hydrolysis of MC matrix was likely to depend on transporting water from the surface into the bulk of the film. The water permeability of MC crosslinked films was reduced with increasing amount of GA. Therefore, the biodegradability of MC crosslinked decreased with increasing amount of crosslinking agent (Waian et al., 2005).

Although both MMT and GA could delay the biodegradation of MC composite, the crosslinking could have a greater effect to delay erosion process than adding nanoparticles. As a consequence, the crosslinking provides the greater the reduction in the biodegradation process comparing with the modification of MC by nanoclay.

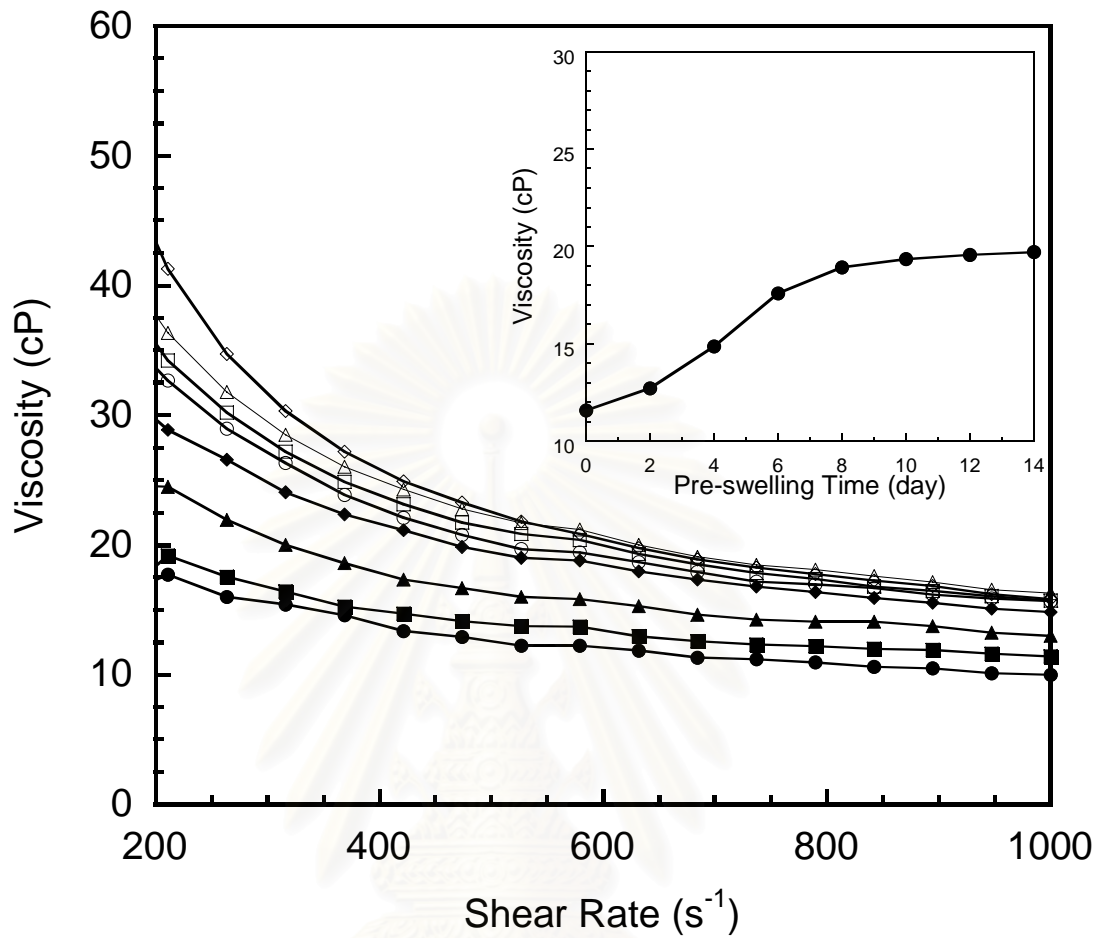


Figure 5.1: Viscosity of 5wt% MMT suspension at various pre-swelling times using a speed of 6500 rpm for 1 min: (●) 0 day , (■) 2 days, (▲) 4 days, (◆) 6 days, (○) 8 days, (□) 10 days, (△) 12 days, (◇) 14 days.

The inset: viscosity of 5wt% MMT suspension at the shear rate of 600s^{-1} at various pre-swelling time.

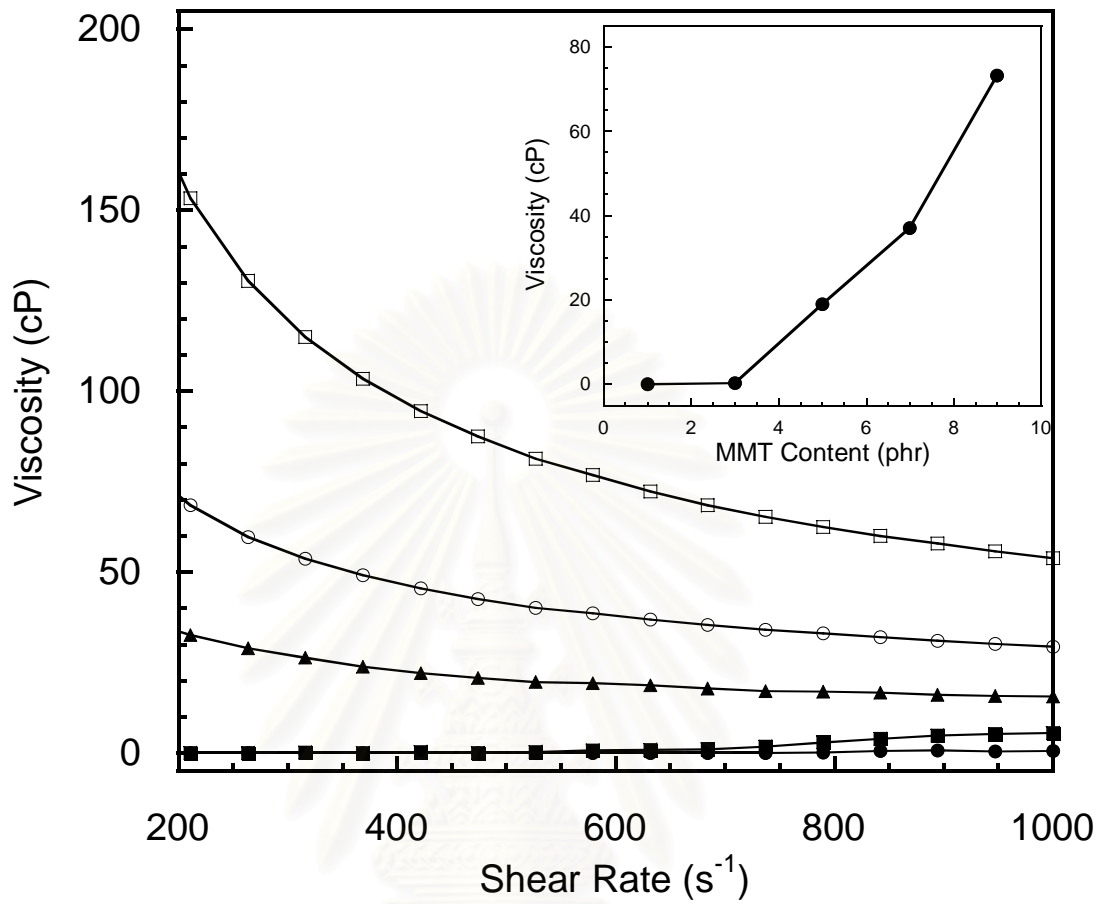


Figure 5.2: Viscosity of MMT suspension at various contents of MMT using a speed of 6500 rpm for 1 min: (●) 1wt%, (■) 3wt%, (▲) 5wt%, (○) 7wt%, (□) 9wt%.

The inset: viscosity of MMT suspension at the shear rate of 600s^{-1} at various contents of MMT.

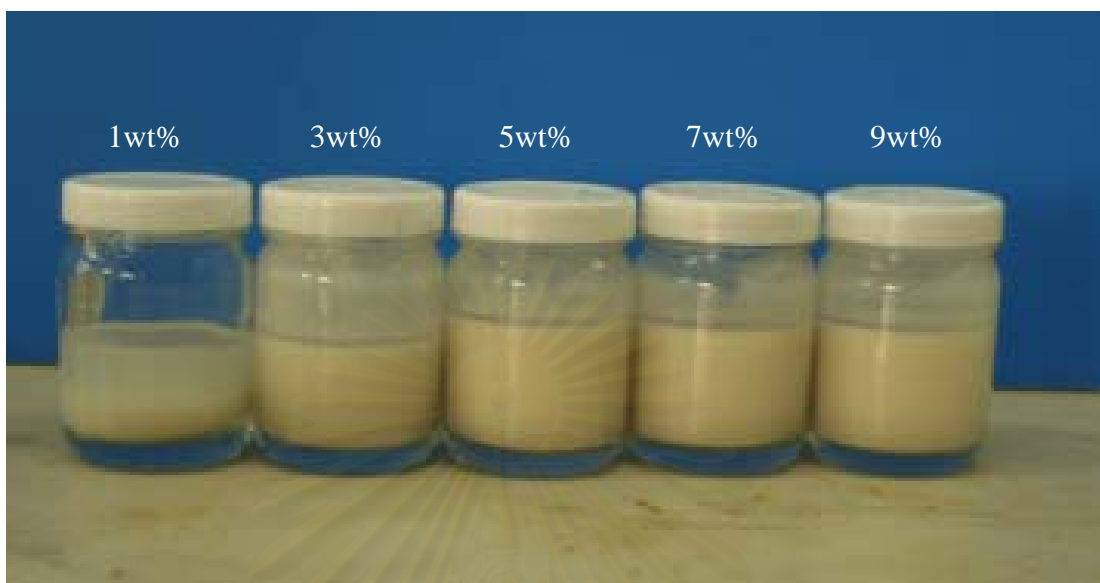


Figure 5.3: MMT suspensions at various contents of MMT using a speed of 6500 rpm of 1 min: 1wt%, 3wt%, 5wt%, 7wt%, 9wt%.

สถาบันวิทยบริการ
จุฬาลงกรณ์มหาวิทยาลัย

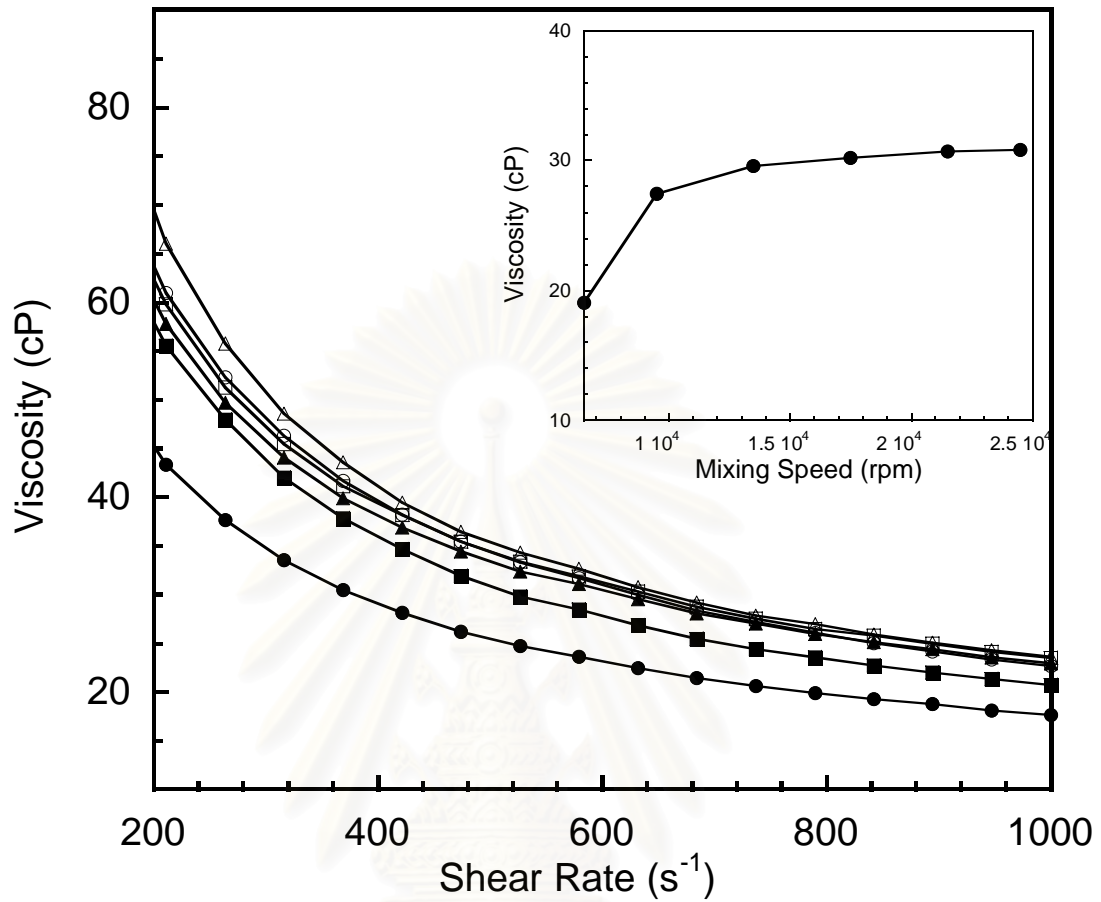


Figure 5.4: Viscosity of 5wt% MMT suspension at various mixing speeds for 1 min: (●) 6500 rpm, (■) 9500 rpm, (▲) 13500 rpm, (○) 17500 rpm, (□) 21500 rpm, (△) 24500 rpm.

The inset: viscosity of 5wt% MMT suspension at the shear rate of 600s⁻¹ at various mixing speeds.

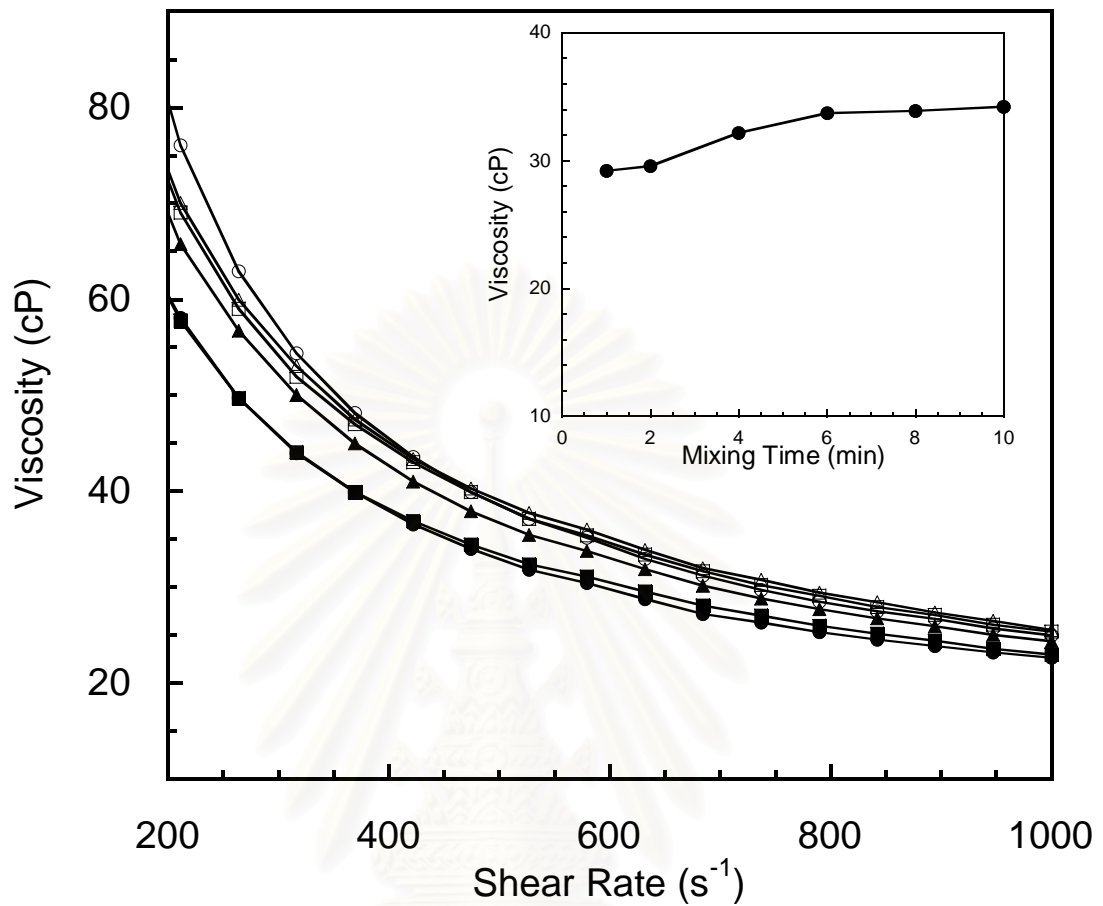


Figure 5.5: Viscosity of 5wt% MMT suspension at various mixing times using a speed of 13500 rpm: (●) 1 min, (■) 2 min, (▲) 4 min, (○) 6 min, (□) 8 min, (△) 10 min.

The inset: viscosity of 5wt% MMT suspension at the shear rate of 600s⁻¹ at various mixing times.

Table 5.1: Viscosity of MMT suspension at various mixing conditions*.

Shear rates (s ⁻¹)	Viscosity (cP)				
	Condition 1	Condition 2	Condition 3	Condition 4	Condition 5
200	17.7	32.7	57.8	65.7	70.0
400	13.3	22.1	36.9	41.0	43.4
600	11.8	18.6	29.5	31.8	33.9
800	10.9	16.9	25.9	27.6	29.4
1000	10.0	15.7	23.0	24.3	25.5

- * Condition 1: No pre-swelling..... , MMT 5wt%, 6500 rpm, 1 min
 Condition 2: Pre-swelling time (8 days), MMT 5wt%, 6500 rpm, 1 min
 Condition 3: Pre-swelling time (10 days), MMT 5wt%, 13500 rpm, 1 min
 Condition 4: Pre-swelling time (10 days), MMT 5wt%, 13500 rpm, 4 min
 Condition 5: Pre-swelling time (10 days), MMT 5wt%, 13500 rpm, 10 min

สถาบันวิทยบริการ
 จุฬาลงกรณ์มหาวิทยาลัย

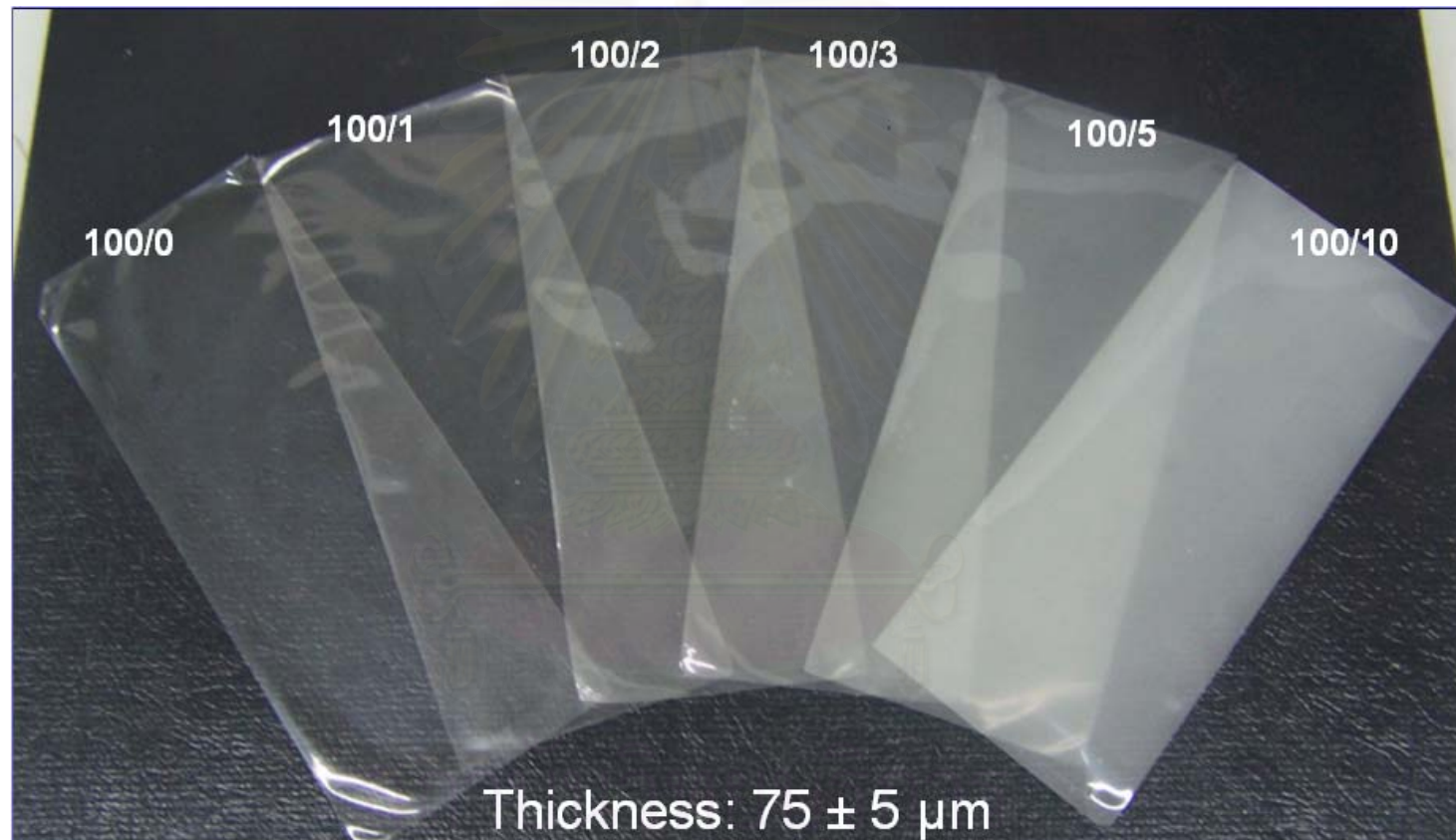


Figure 5.6: MC/MMT nanocomposite films at various contents of MMT.

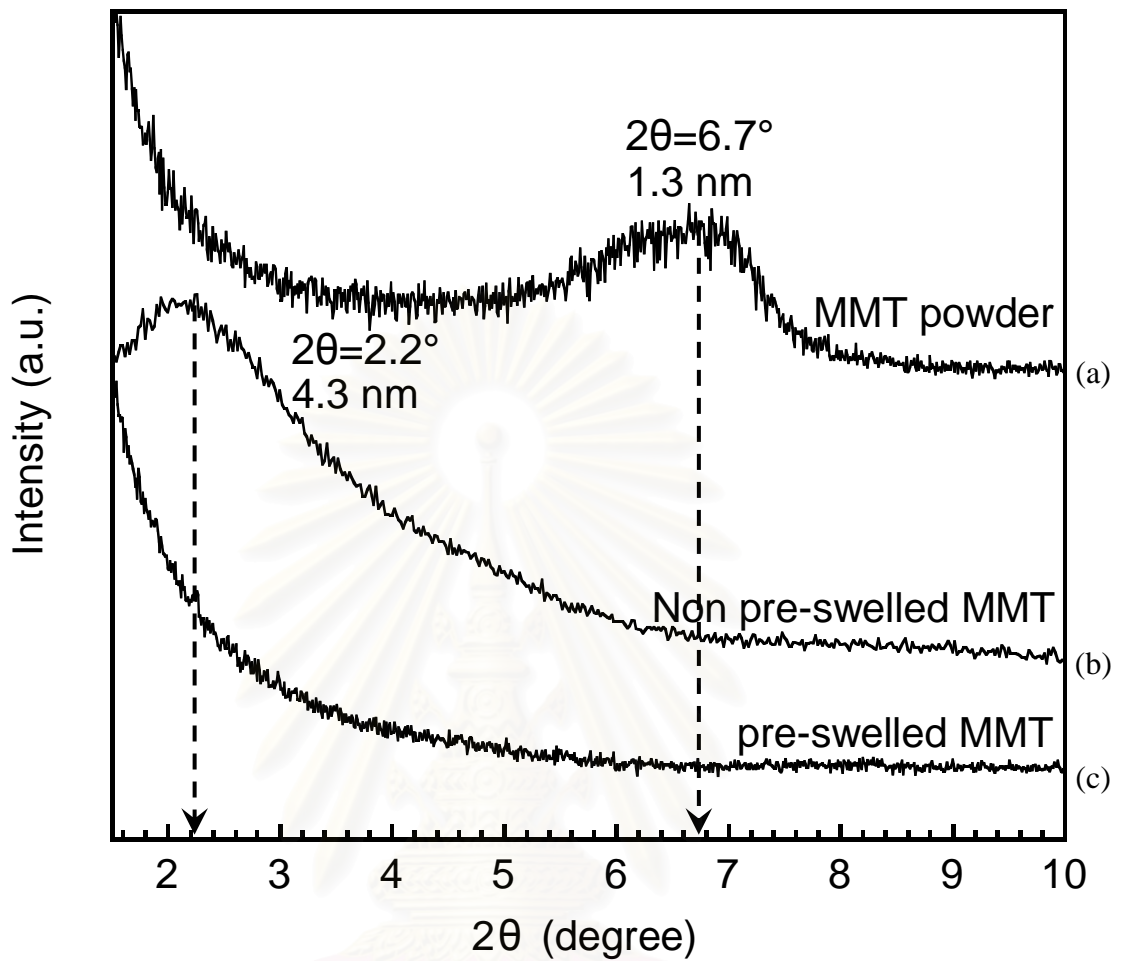


Figure 5.7: XRD patterns of MMT powder and MC/ 5 phr MMT nanocomposite films at various MMT preparations: (a) MMT powder, (b) non pre-swelled MMT, (c) pre-swelled MMT.

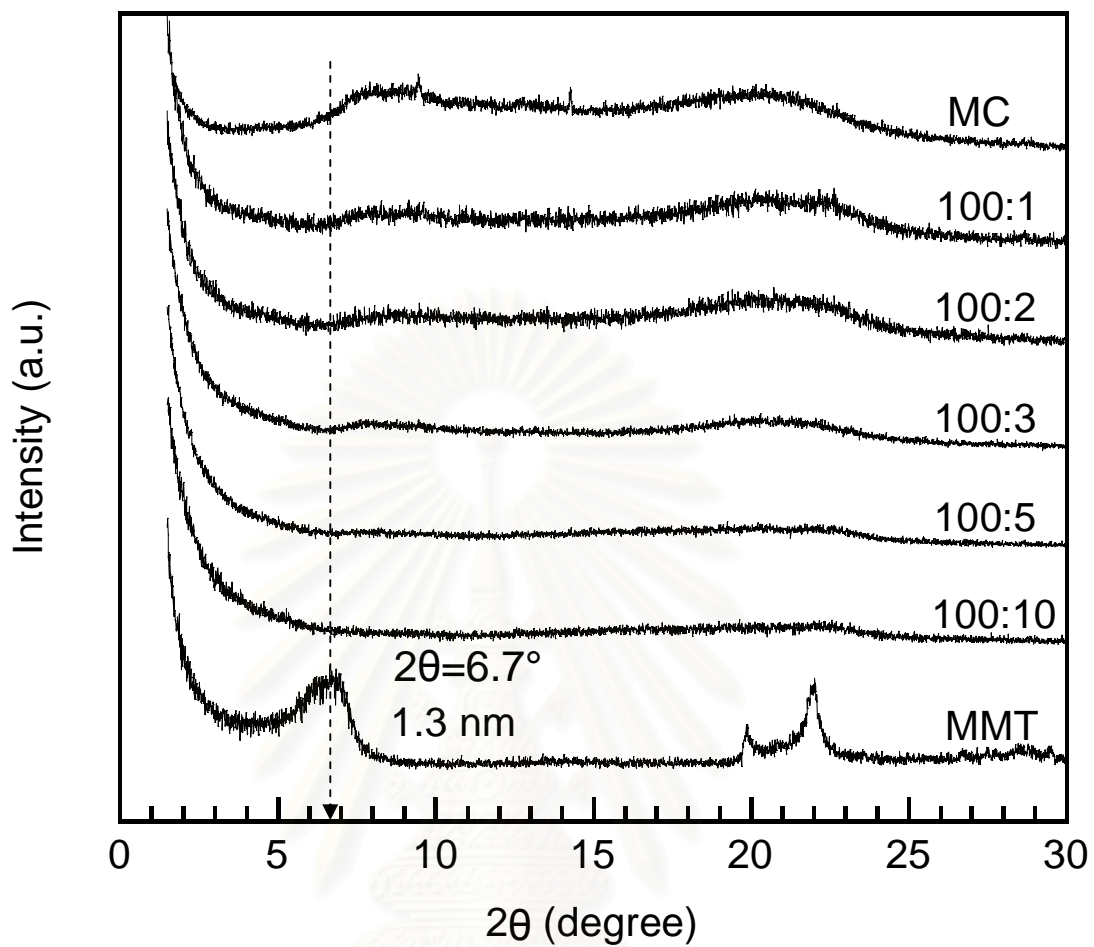


Figure 5.8: XRD patterns of pure MC, MMT and MC/MMT nanocomposite films at various contents of MMT.

สถาบันวิทยบริการ
จุฬาลงกรณ์มหาวิทยาลัย

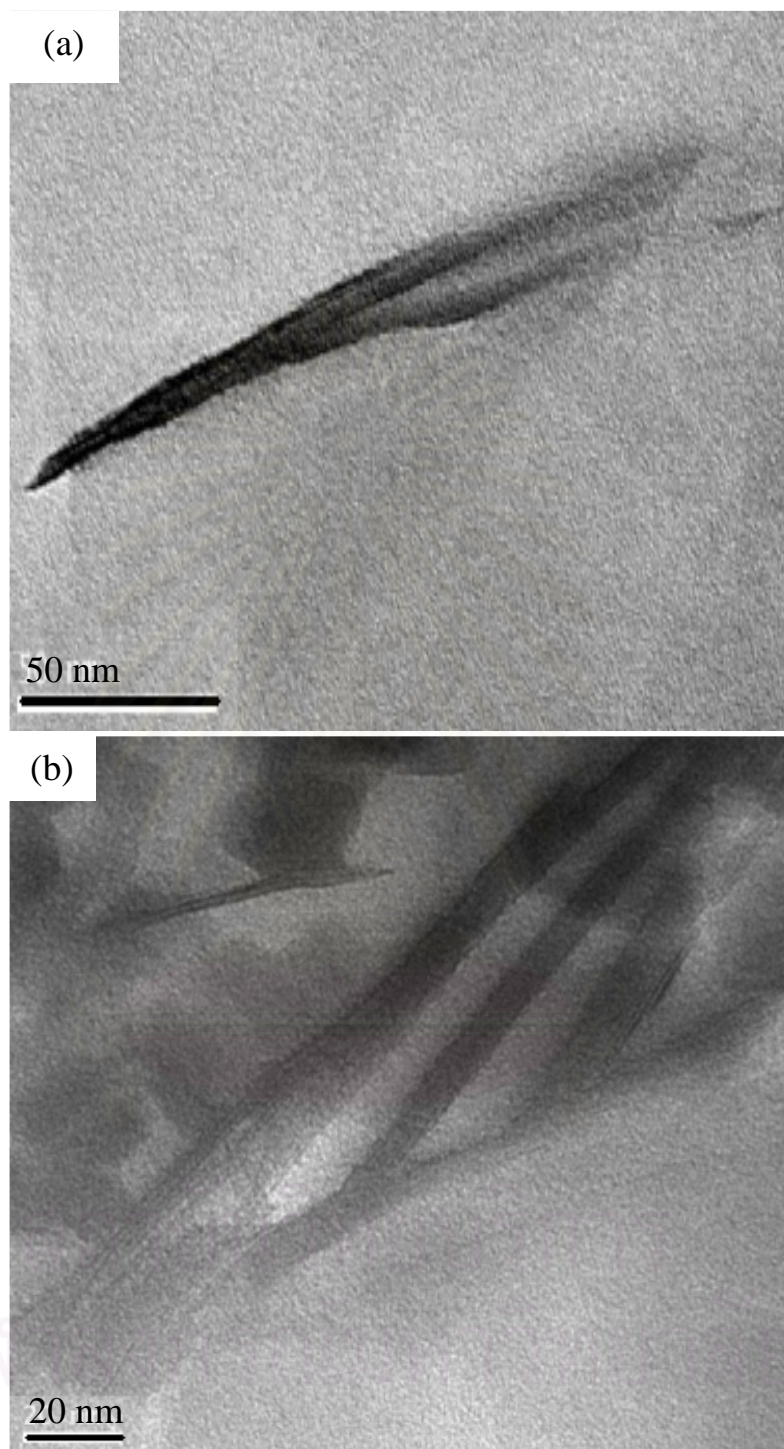


Figure 5.9: TEM micrographs of MMT powder at (a) $\times 62000$, and (b) $\times 80000$ magnifications.

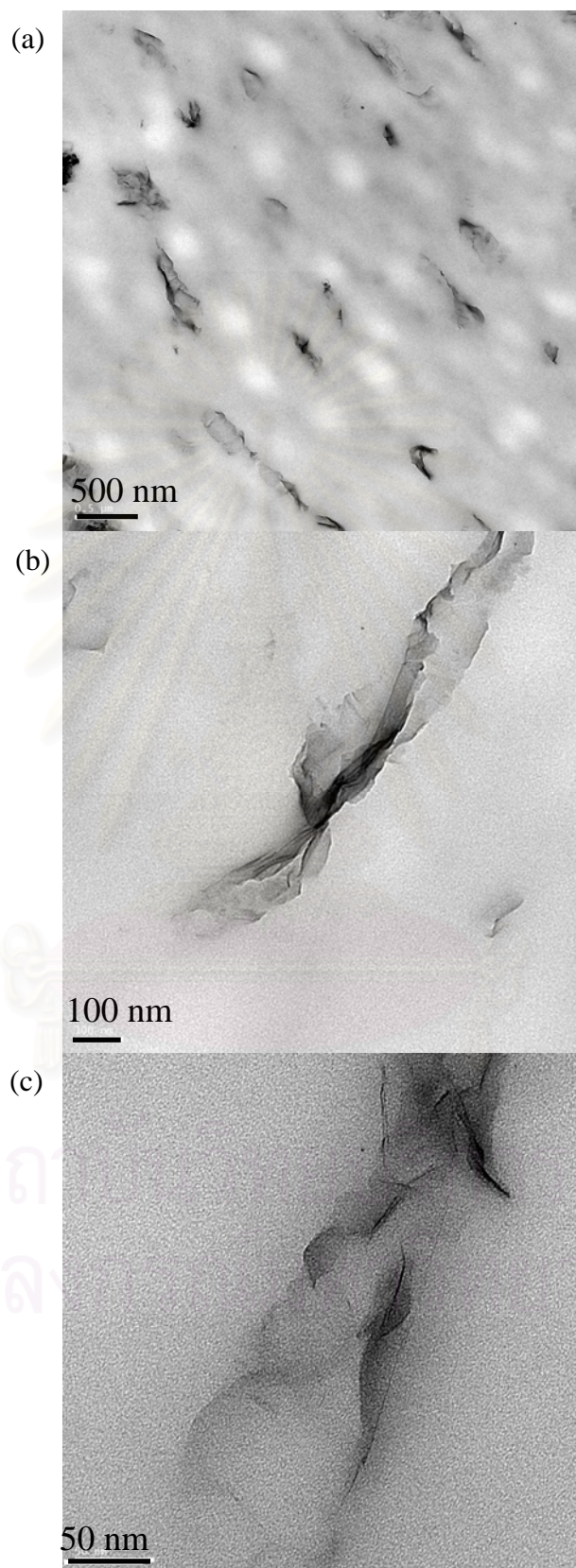


Figure 5.10: TEM micrographs of MC/ 1 phr MMT nanocomposite at (a) $\times 5000$, (b) $\times 19000$, and (c) $\times 62000$ magnifications.

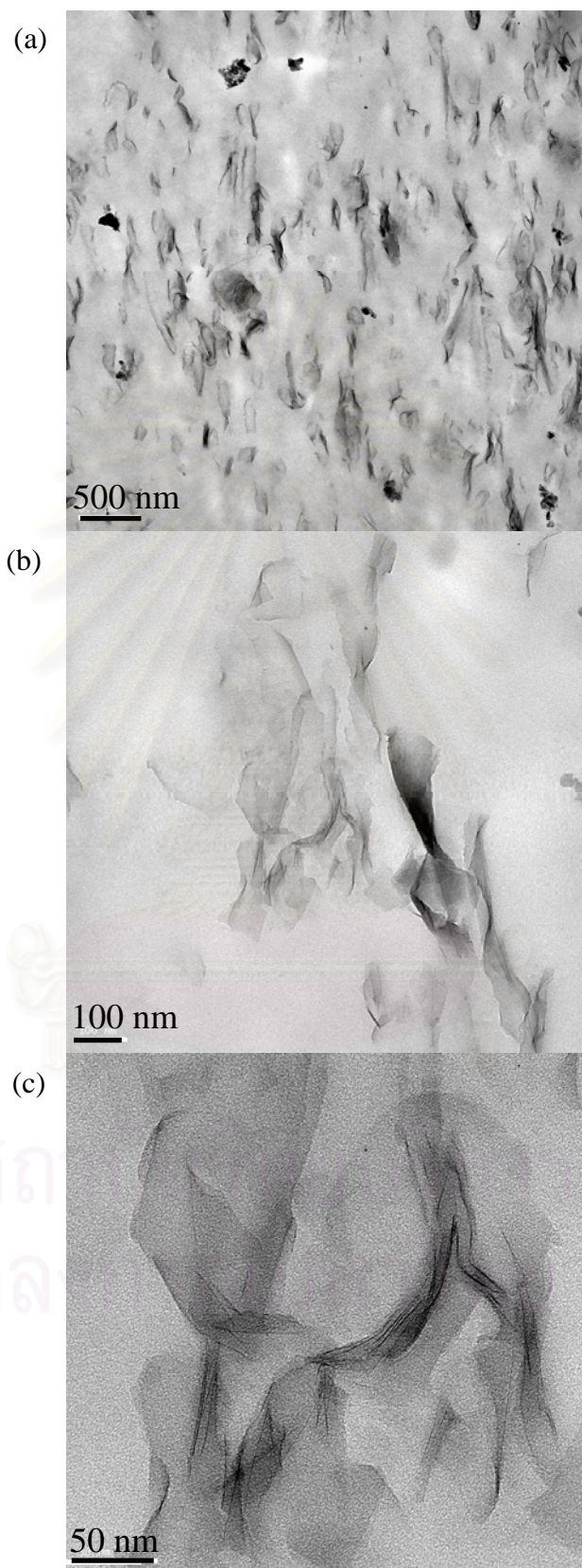


Figure 5.11: TEM micrographs of MC/ 5 phr MMT nanocomposite at (a) $\times 5000$, (b) $\times 19000$, and (c) $\times 62000$ magnifications.

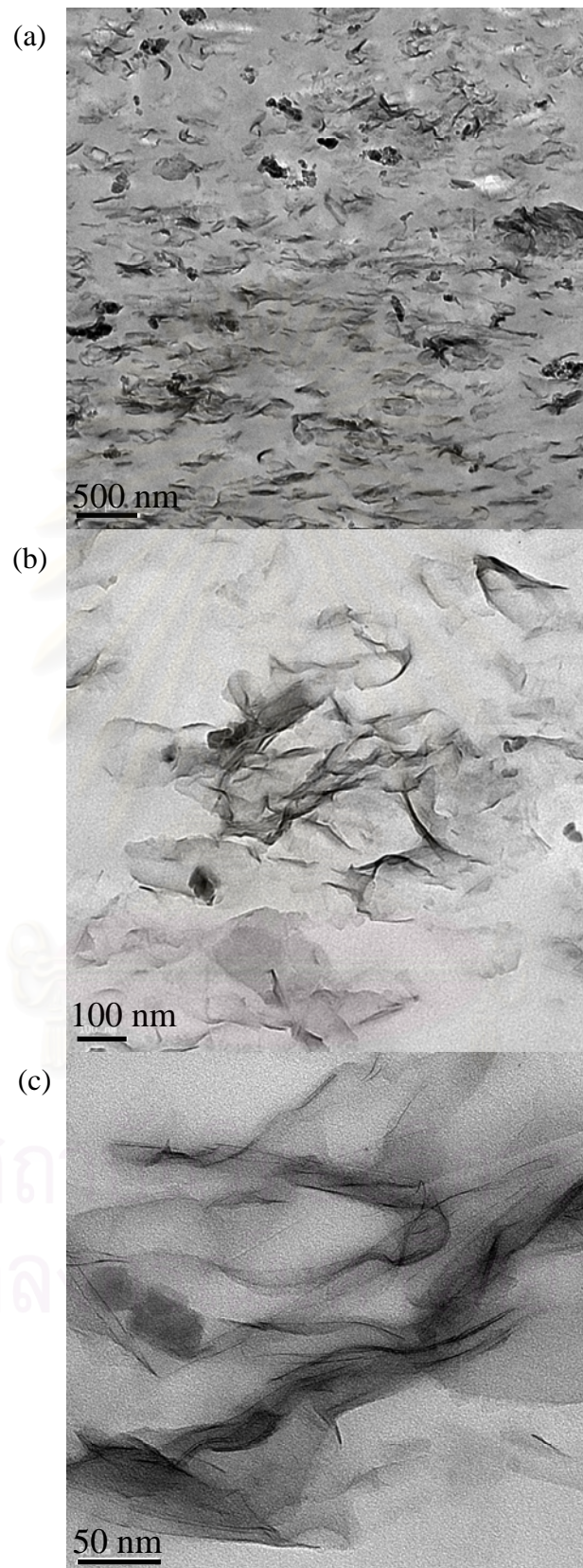


Figure 5.12: TEM micrographs of MC/ 10 phr MMT nanocomposite at (a) $\times 5000$, (b) $\times 19000$, and (c) $\times 62000$ magnifications.

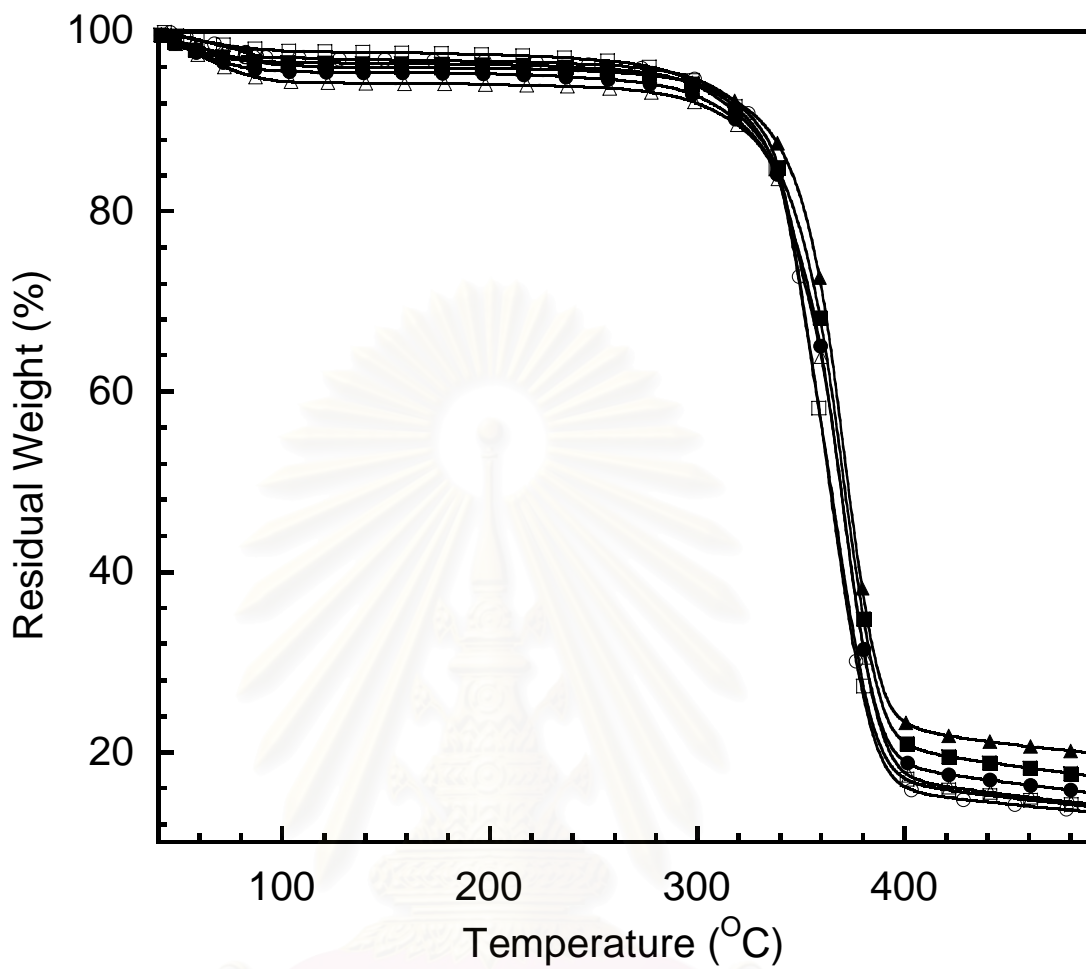


Figure 5.13: TGA thermograms of pure MC and MC/MMT nanocomposite films at various contents of MMT: (o) pure MC, (□) 100:1, (Δ) 100:2, (●) 100:3, (■) 100:5, (▲) 100:10.

จุฬาลงกรณ์มหาวิทยาลัย

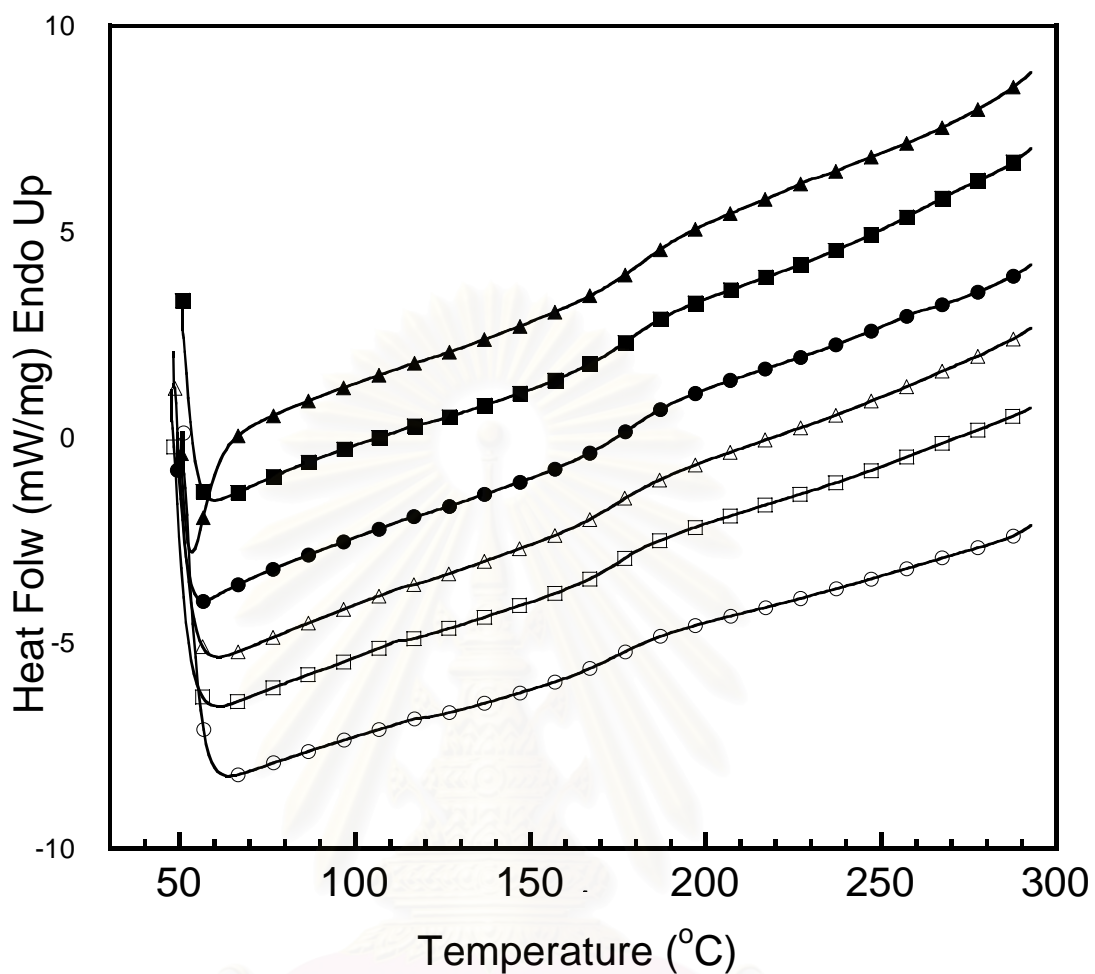


Figure 5.14: DSC thermograms showing glass transition temperature of pure MC and MC/MMT nanocomposite films at various contents of MMT: (o) pure MC, (□) 100:1, (Δ) 100:2, (●) 100:3, (■) 100:5, (▲) 100:10.

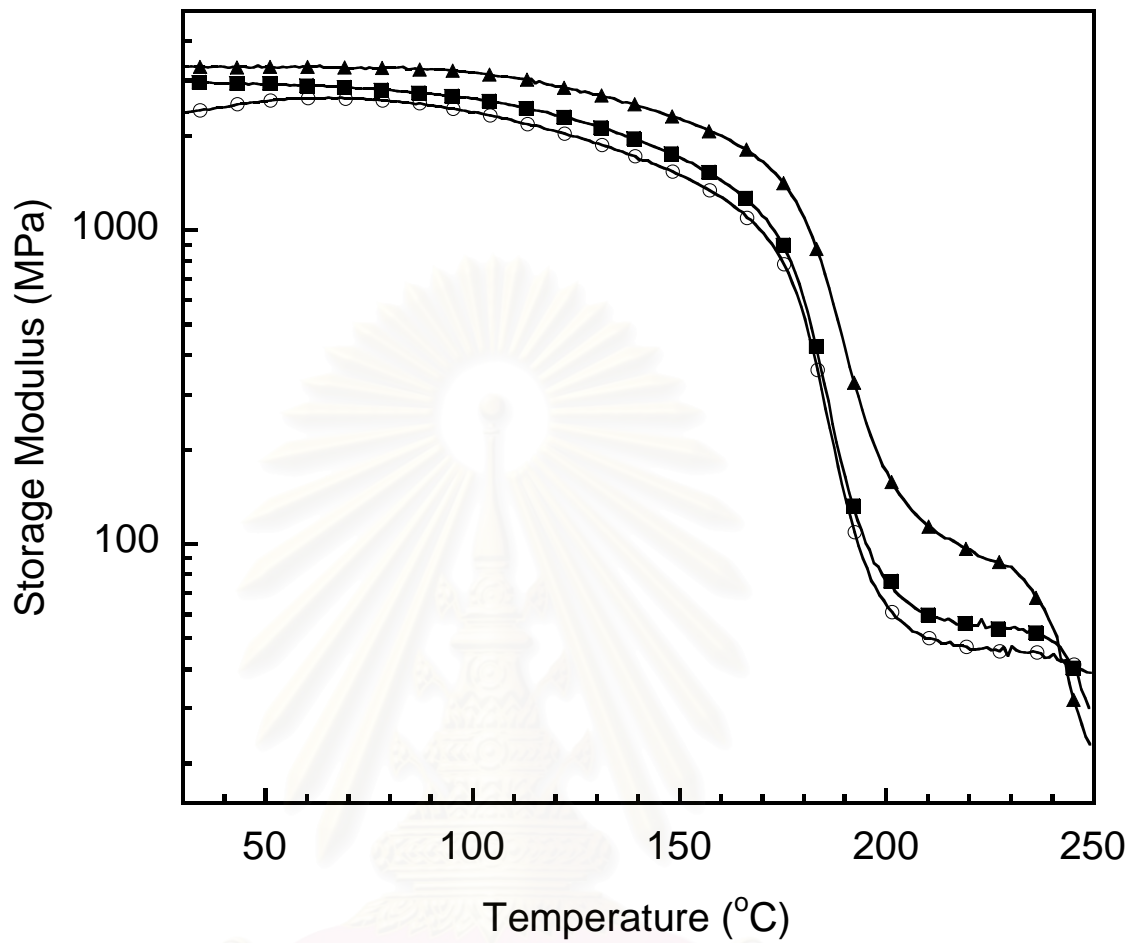


Figure 5.15: Storage modulus of MC/MMT nanocomposite films at various contents of MMT: (o) pure MC, (■) 100:1, (▲) 100:10.

สถาบันวิทยบริการ
จุฬาลงกรณ์มหาวิทยาลัย

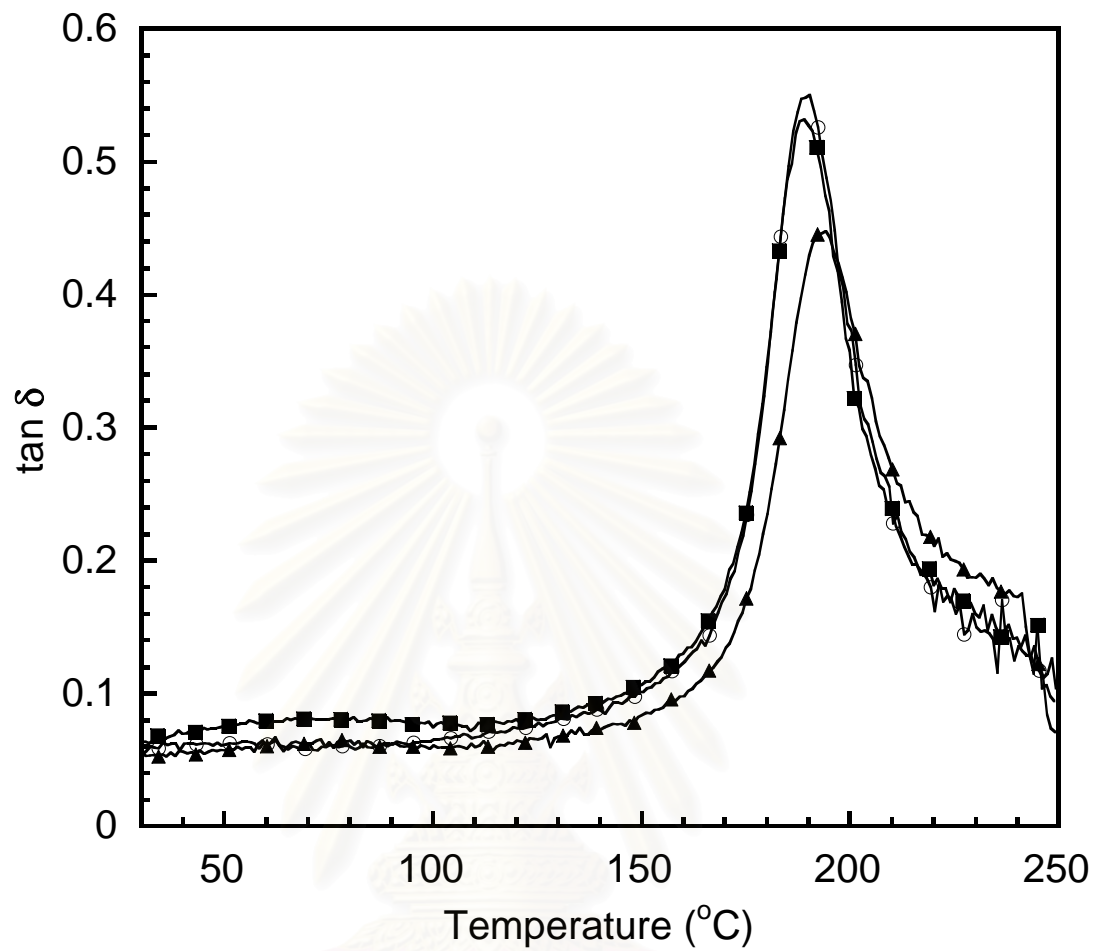


Figure 5.16: $\tan \delta$ of MC/MMT nanocomposite films at various contents of MMT: (o) pure MC, (■) 100:1, (▲) 100:10.

สถาบันวิทยบริการ
จุฬาลงกรณ์มหาวิทยาลัย

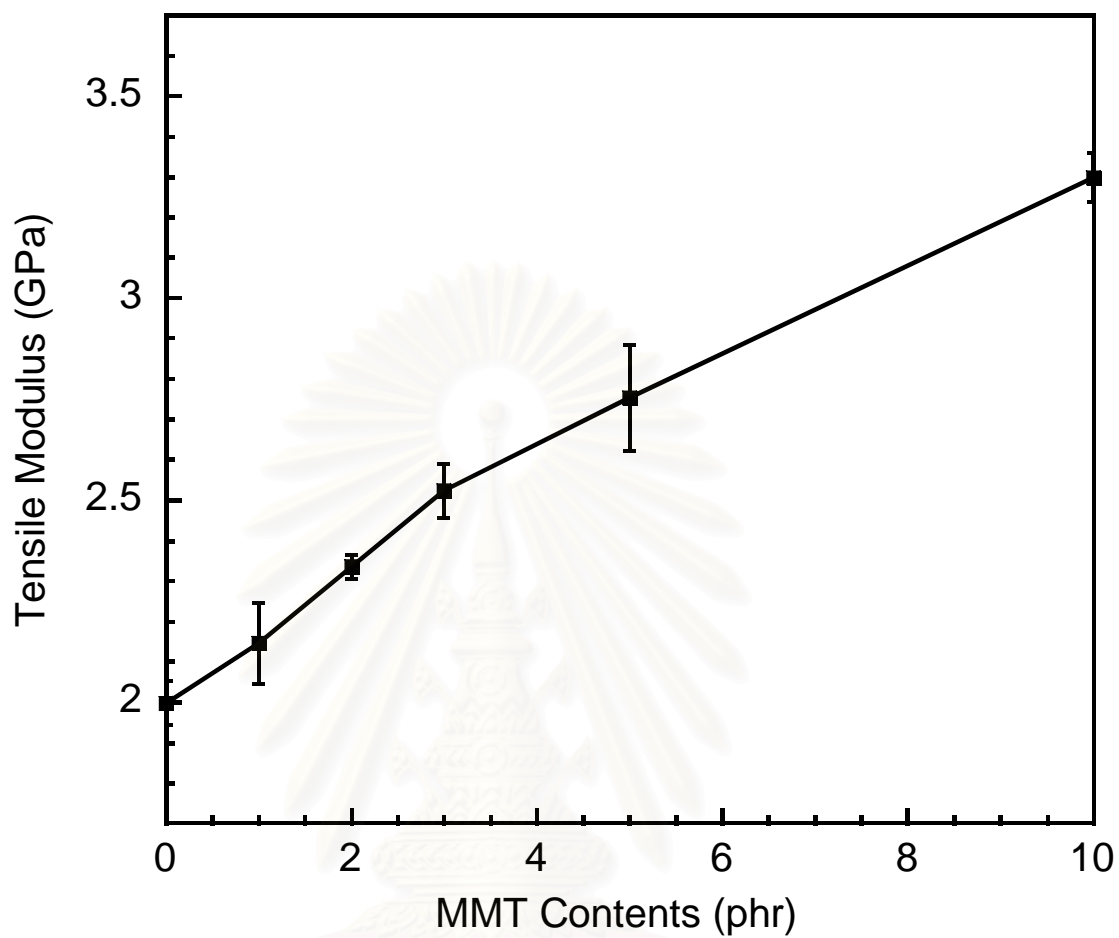


Figure 5.17: Tensile modulus of MC/MMT nanocomposite films at various contents of MMT.

สถาบันวิทยบริการ
จุฬาลงกรณ์มหาวิทยาลัย

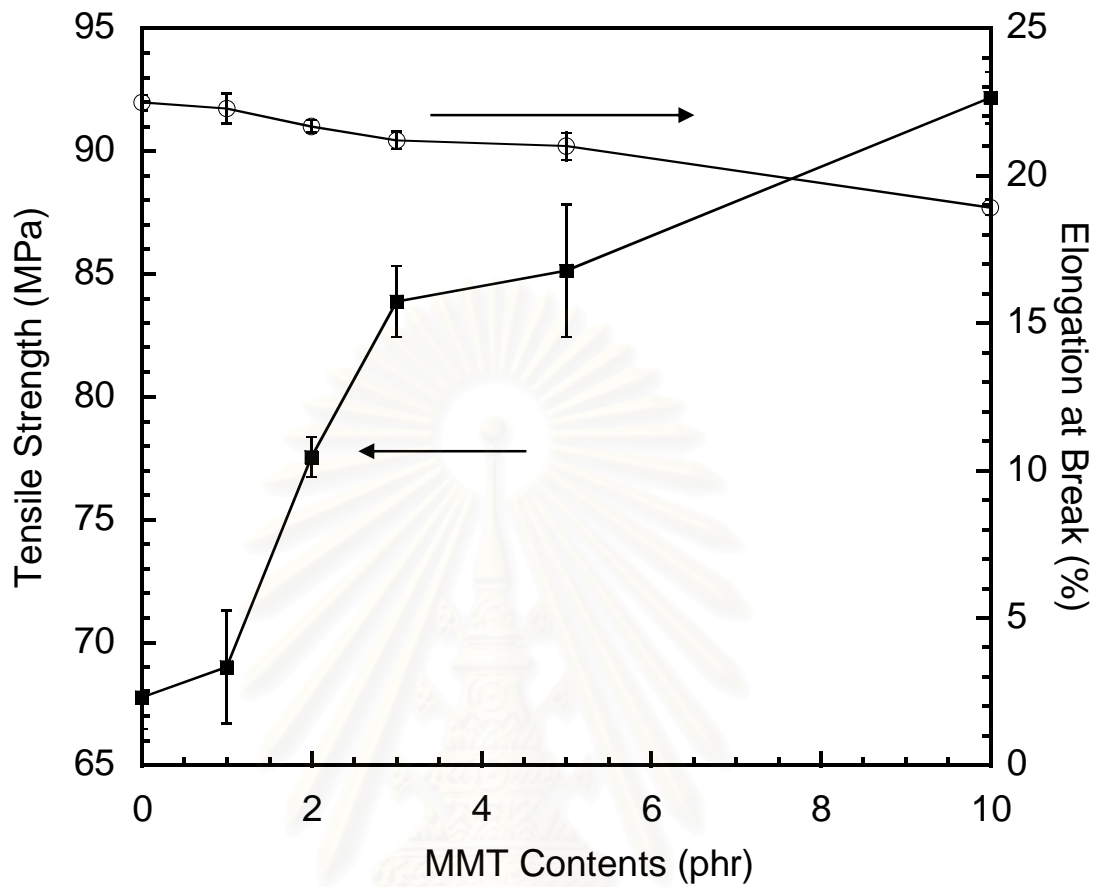


Figure 5.18: Tensile strength & elongation at break of MC/MMT nanocomposite films at various contents of MMT:
(■) tensile strength, (o) elongation at break.

สถาบันวิทยบริการ
จุฬาลงกรณ์มหาวิทยาลัย

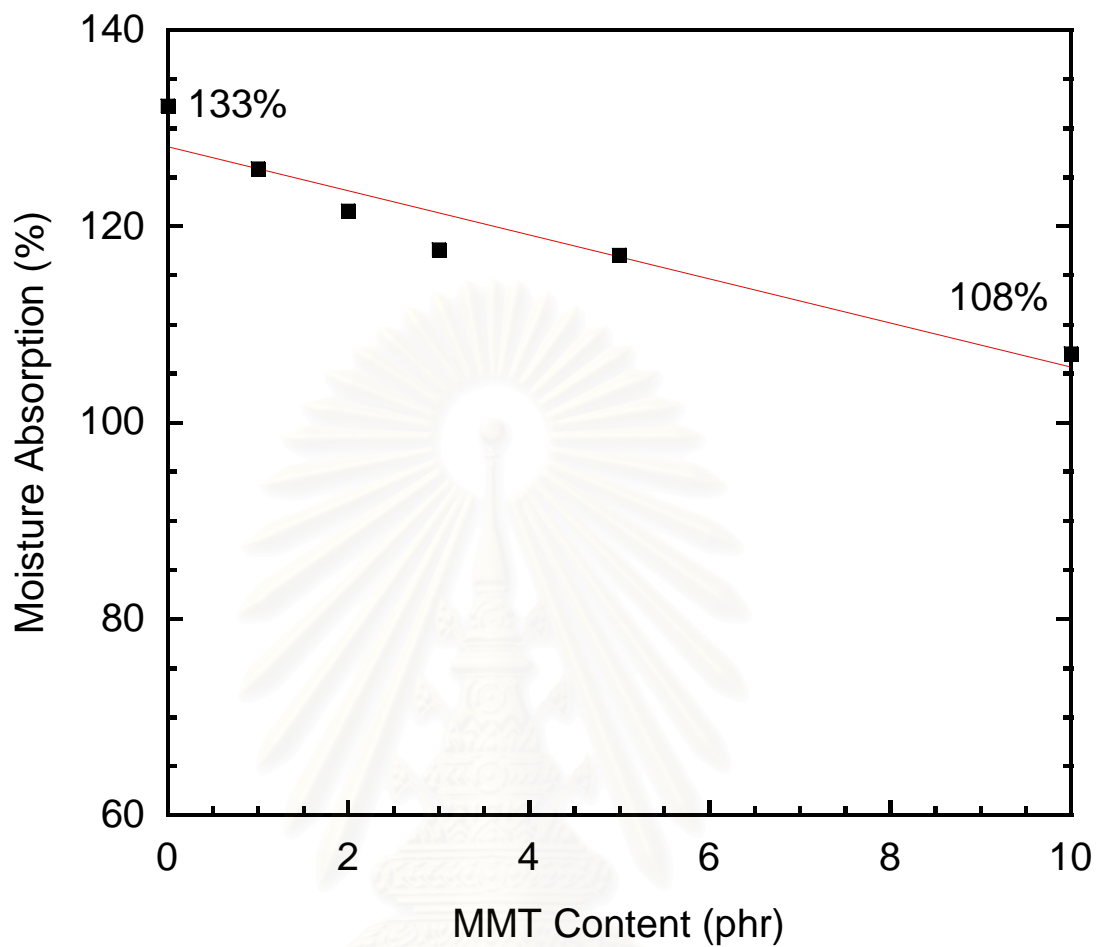


Figure 5.19: Moisture absorption of MC/MMT nanocomposite films at various contents of MMT.

สถาบันวิทยบริการ
จุฬาลงกรณ์มหาวิทยาลัย

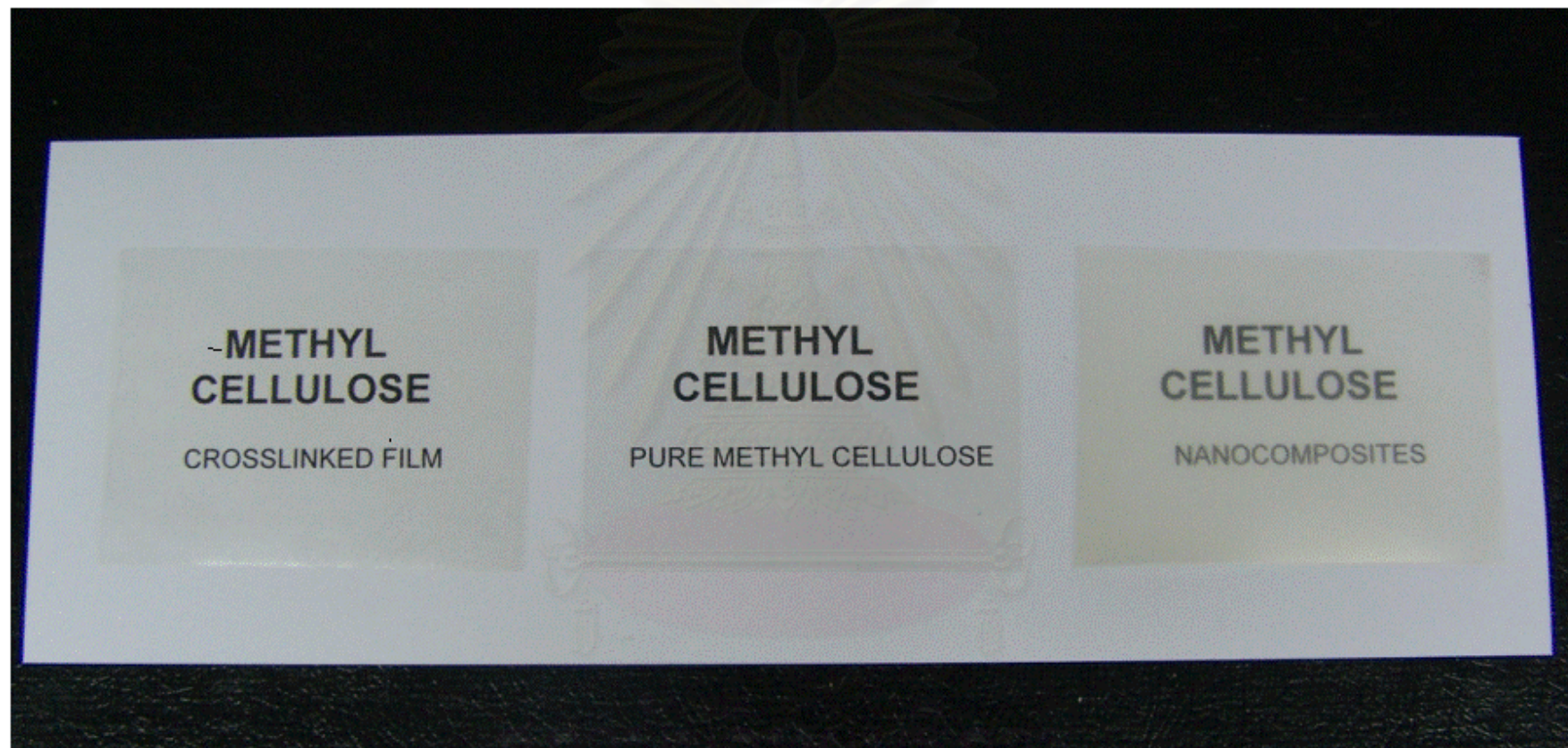


Figure 5.20: Pure MC, MC/MMT nanocomposite and MC crosslinked films.

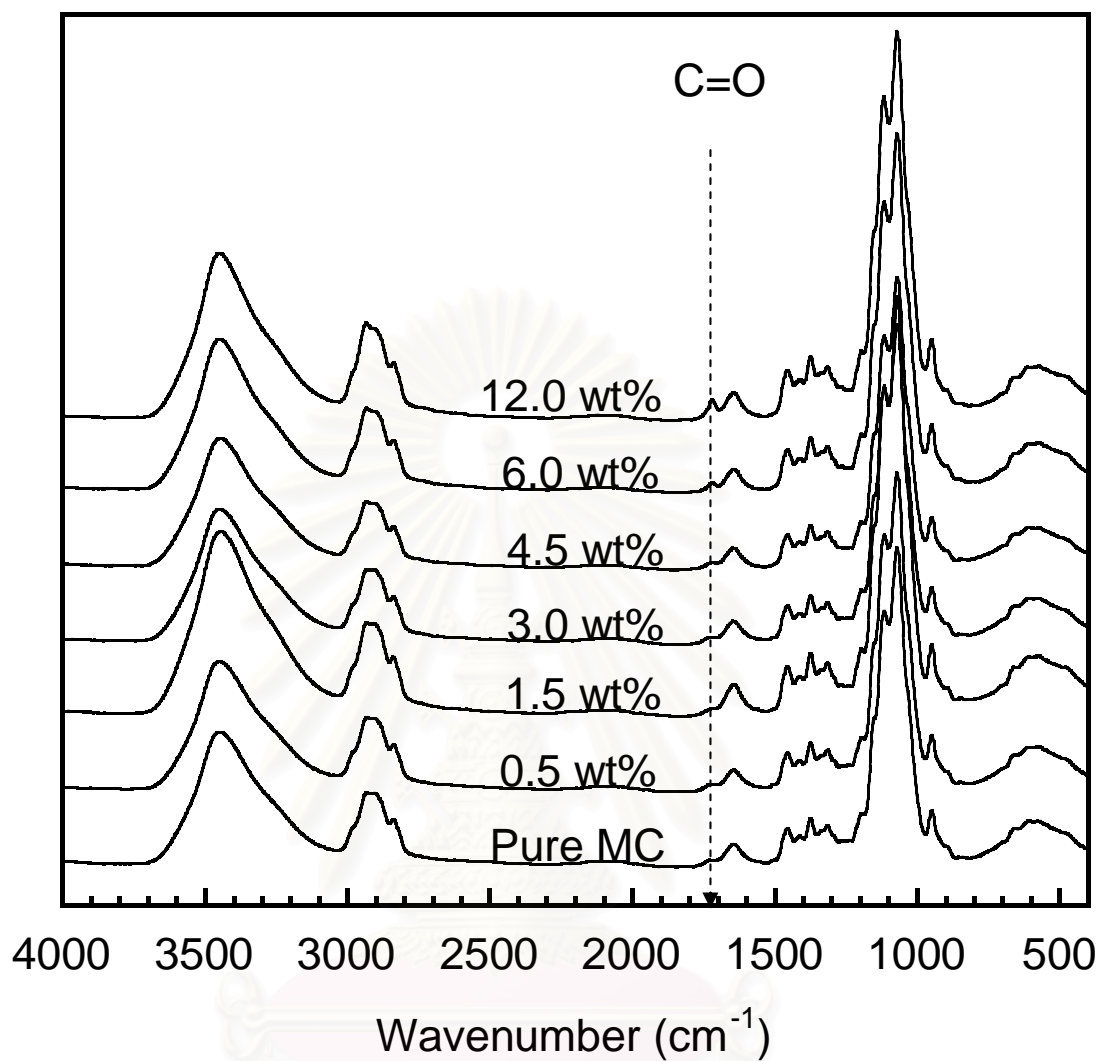


Figure 5.21: FTIR spectra of pure MC and MC crosslinked films at various contents of glutaraldehyde.

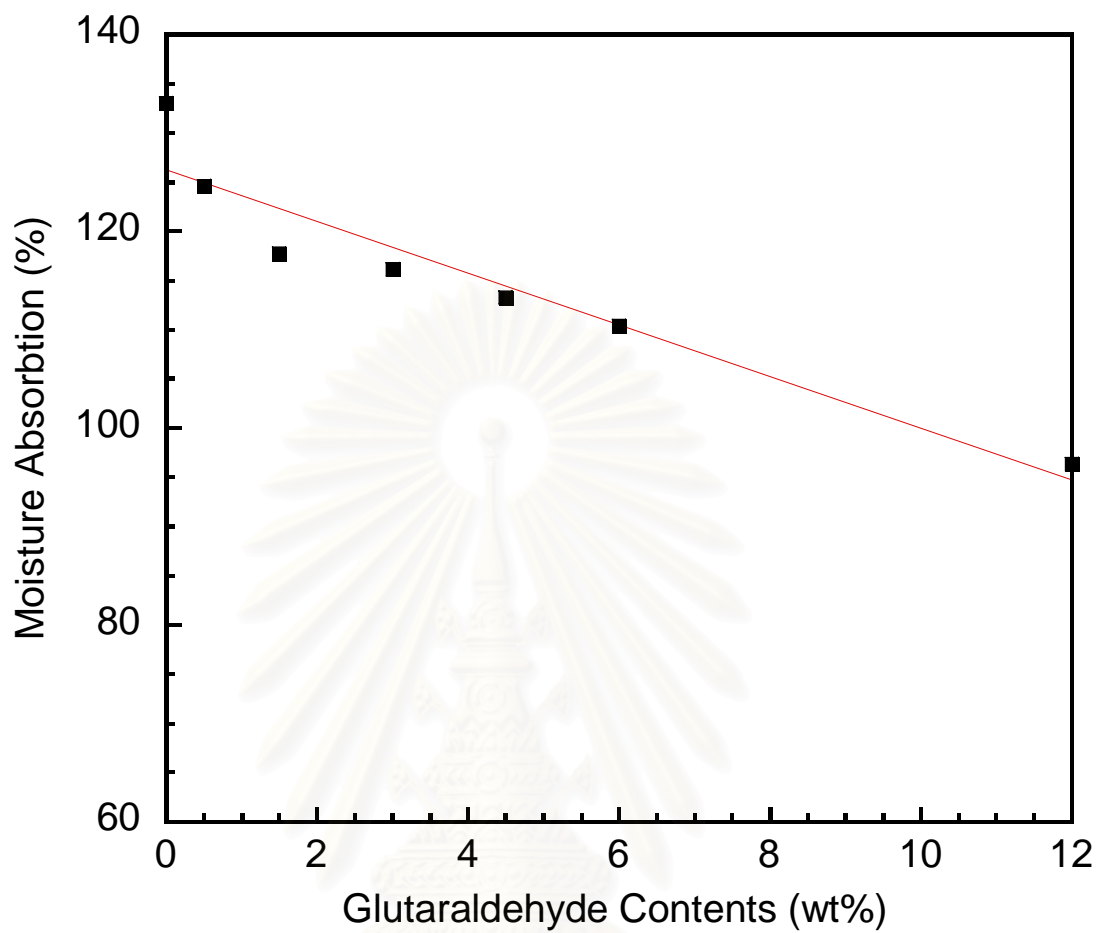


Figure 5.22: Moisture absorption of MC crosslinked films at various contents of glutaraldehyde.

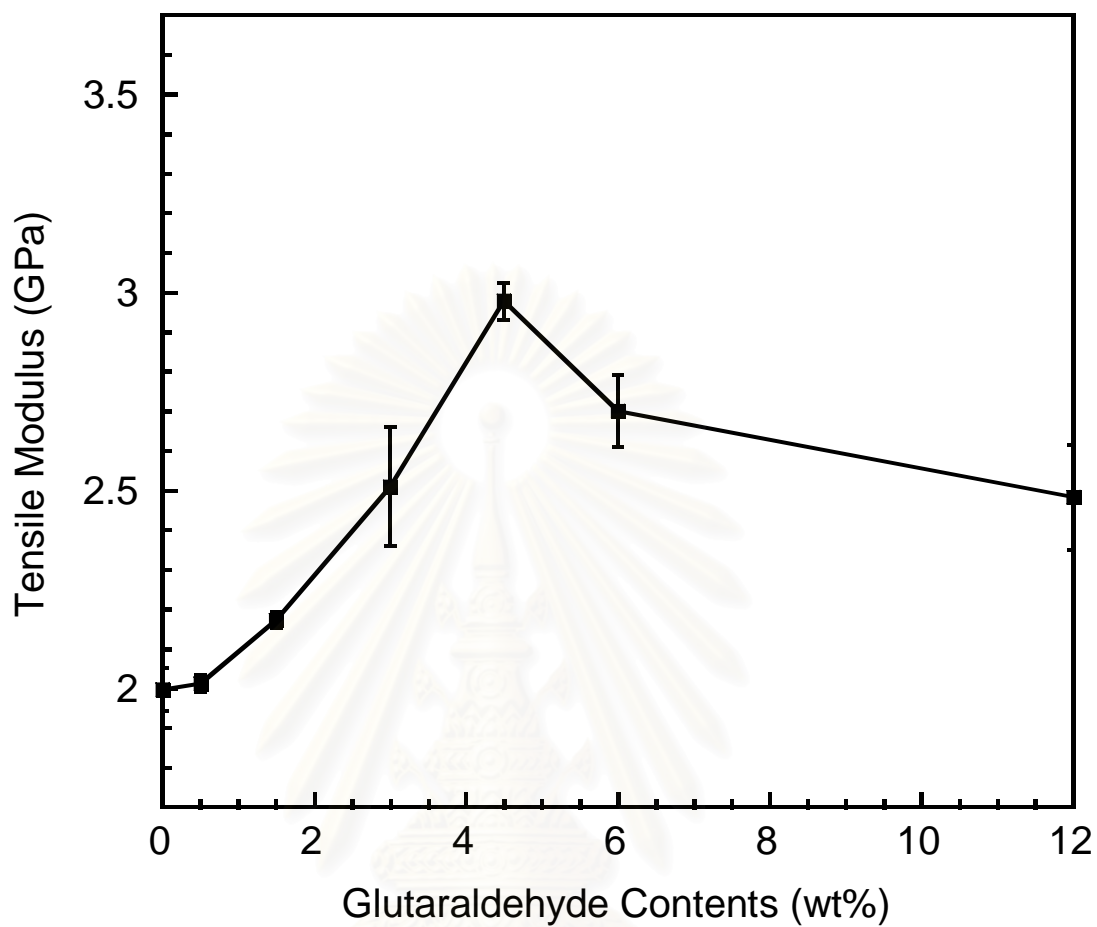


Figure 5.23: Tensile modulus of MC crosslinked films at various contents of glutaraldehyde.

สถาบันวิทยบริการ
จุฬาลงกรณ์มหาวิทยาลัย

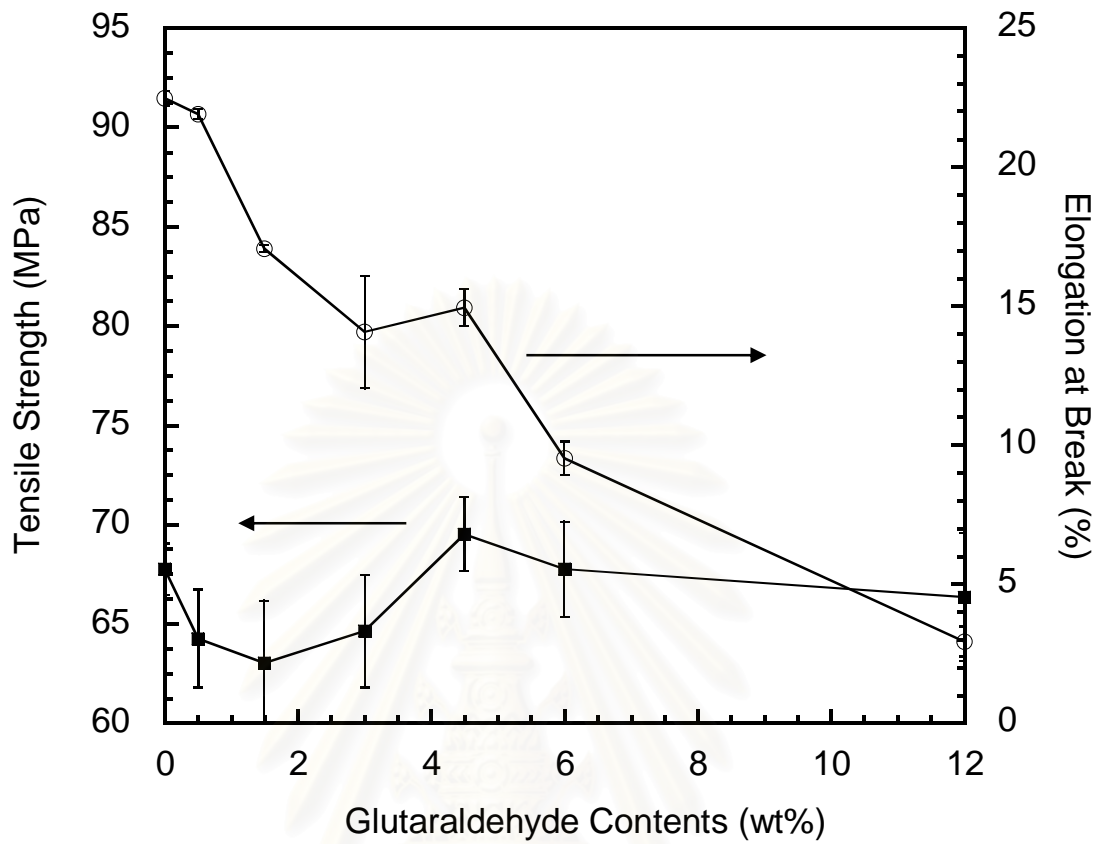


Figure 5.24: Tensile strength & elongation at break of MC crosslinked films at various contents of glutaraldehyde: (■) tensile strength, (○) elongation at break.

สถาบันวิทยบริการ
จุฬาลงกรณ์มหาวิทยาลัย

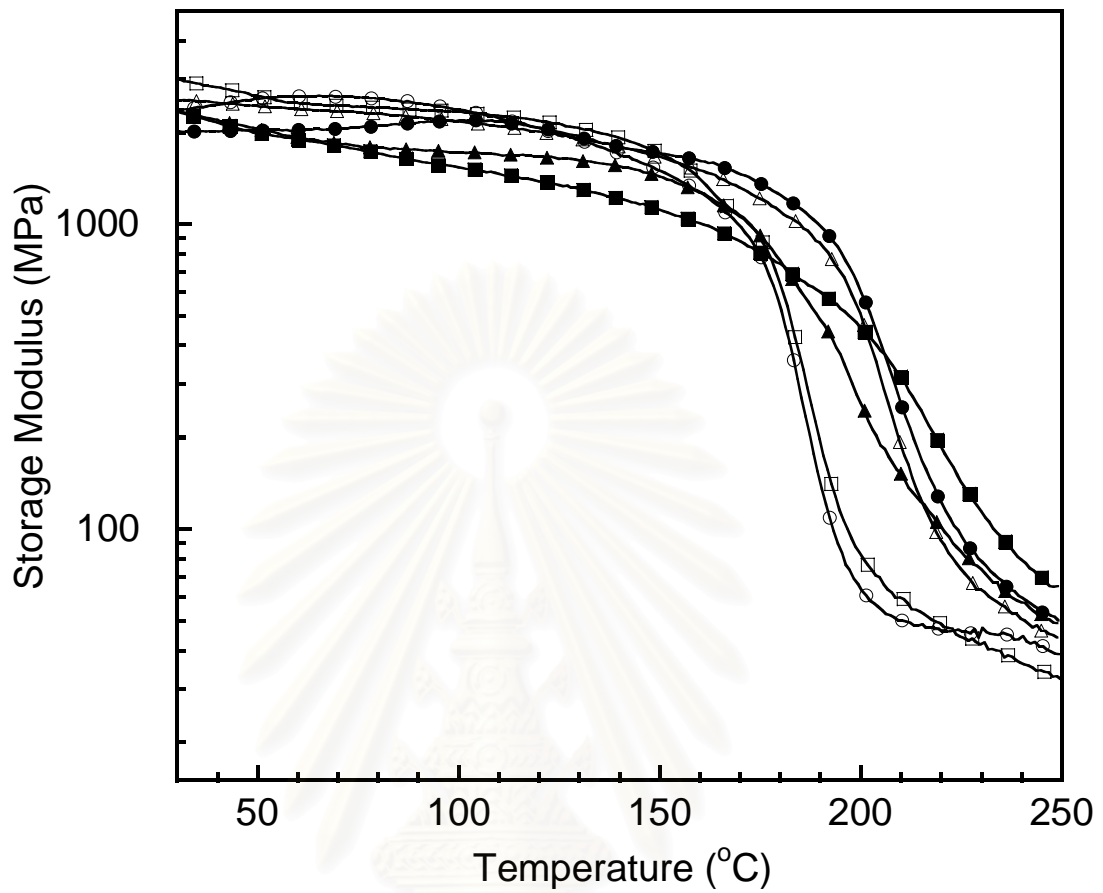


Figure 5.25: Storage modulus of pure MC and MC crosslinked films at various contents of glutaraldehyde: (o) pure MC, (□) 0.5wt%, (Δ) 1.5wt%, (●) 3.0wt%, (■) 4.5wt%, (▲) 6.0wt%.

สถาบันวิทยบริการ
จุฬาลงกรณ์มหาวิทยาลัย

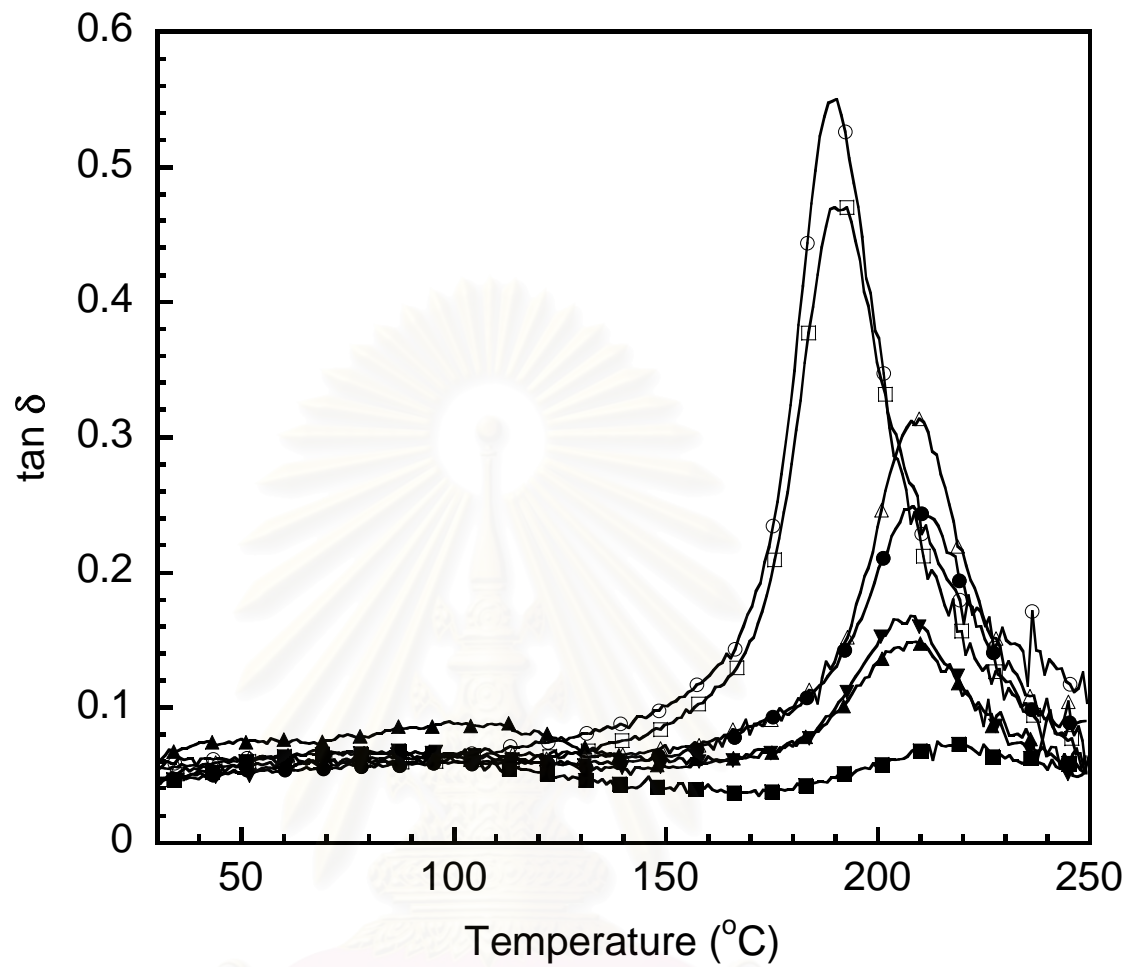


Figure 5.26: $\tan \delta$ of pure MC and MC crosslinked films at various contents of glutaraldehyde: (o) pure MC, (\square) 0.5wt%, (Δ) 1.5wt%, (\bullet) 3.0wt%, (\blacksquare) 4.5wt%, (\blacktriangle) 6.0wt%, (\blacktriangledown) 12.0wt%.

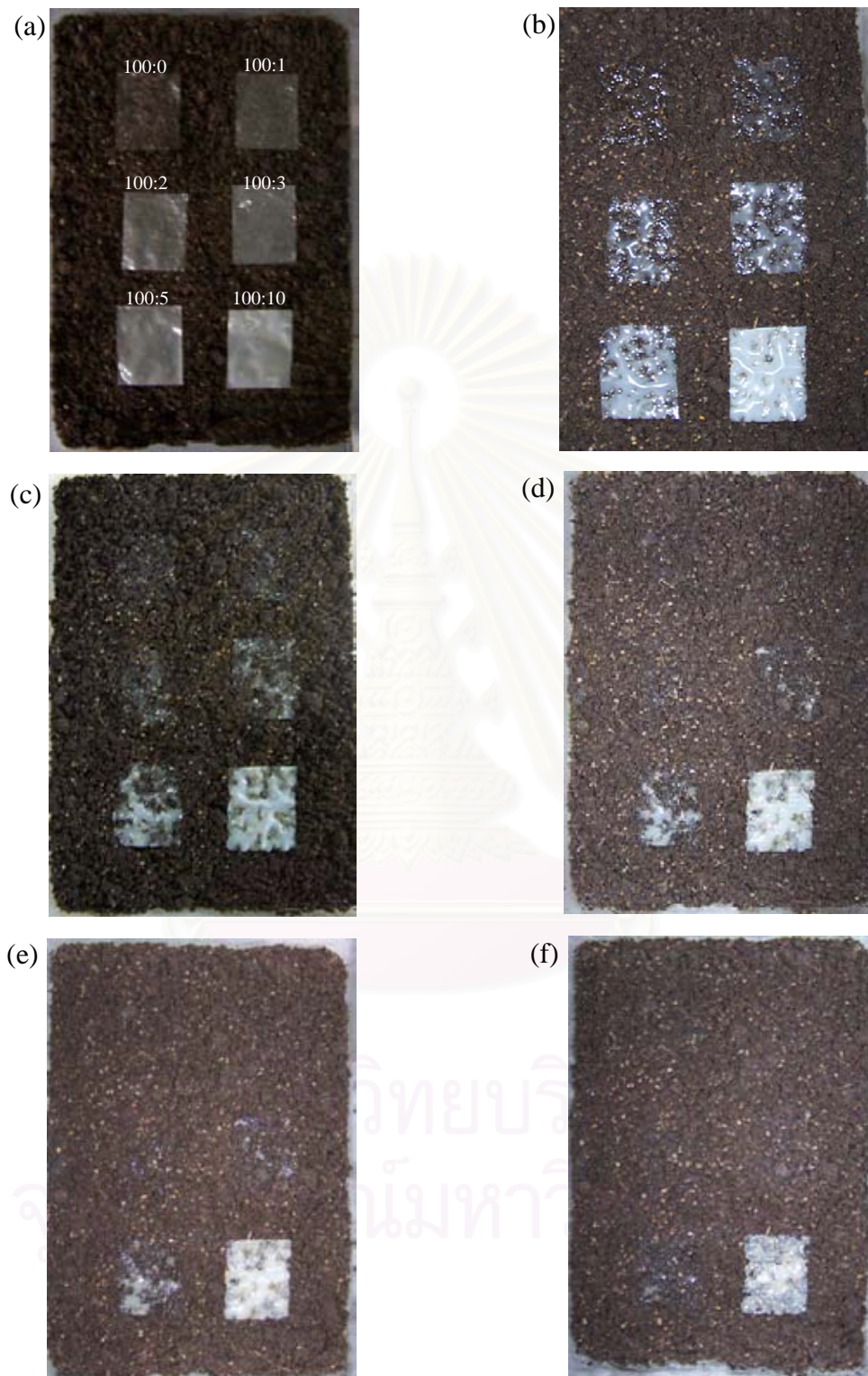


Figure 5.27: Biodegradability of pure MC and nanocomposite films at various contents of MMT under soil field with time at (a) 0 day, (b) 1 days, (c) 2 days, (d) 3 days, (e) 4 days, and (f) 5 days.

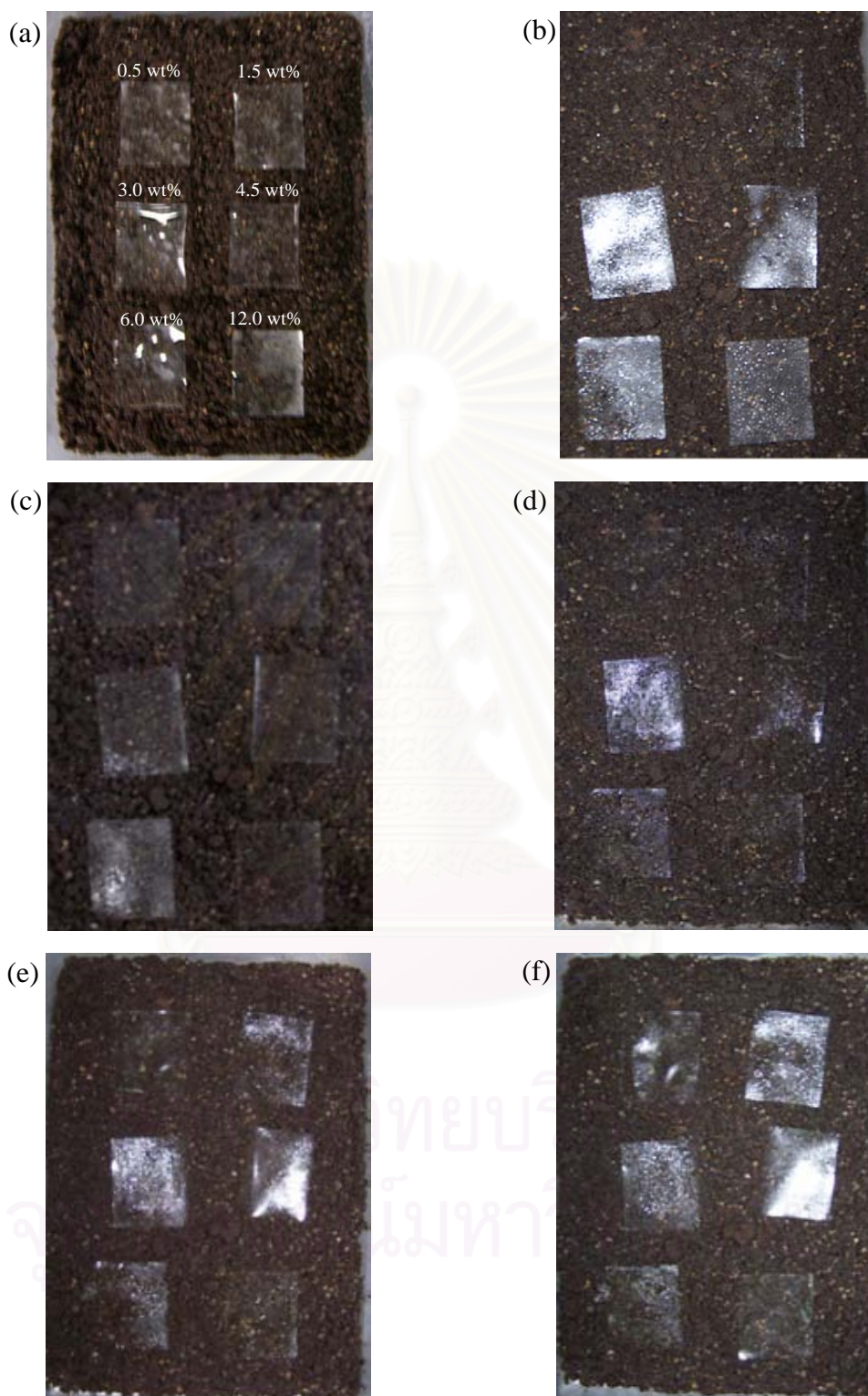


Figure 5.28: Biodegradability of MC crosslinked films various contents of glutaraldehyde under soil field with time at (a) 0 day, (b) 1 day, (c) 2 days, (d) 3 days, (e) 4 days, and (f) 5 days.

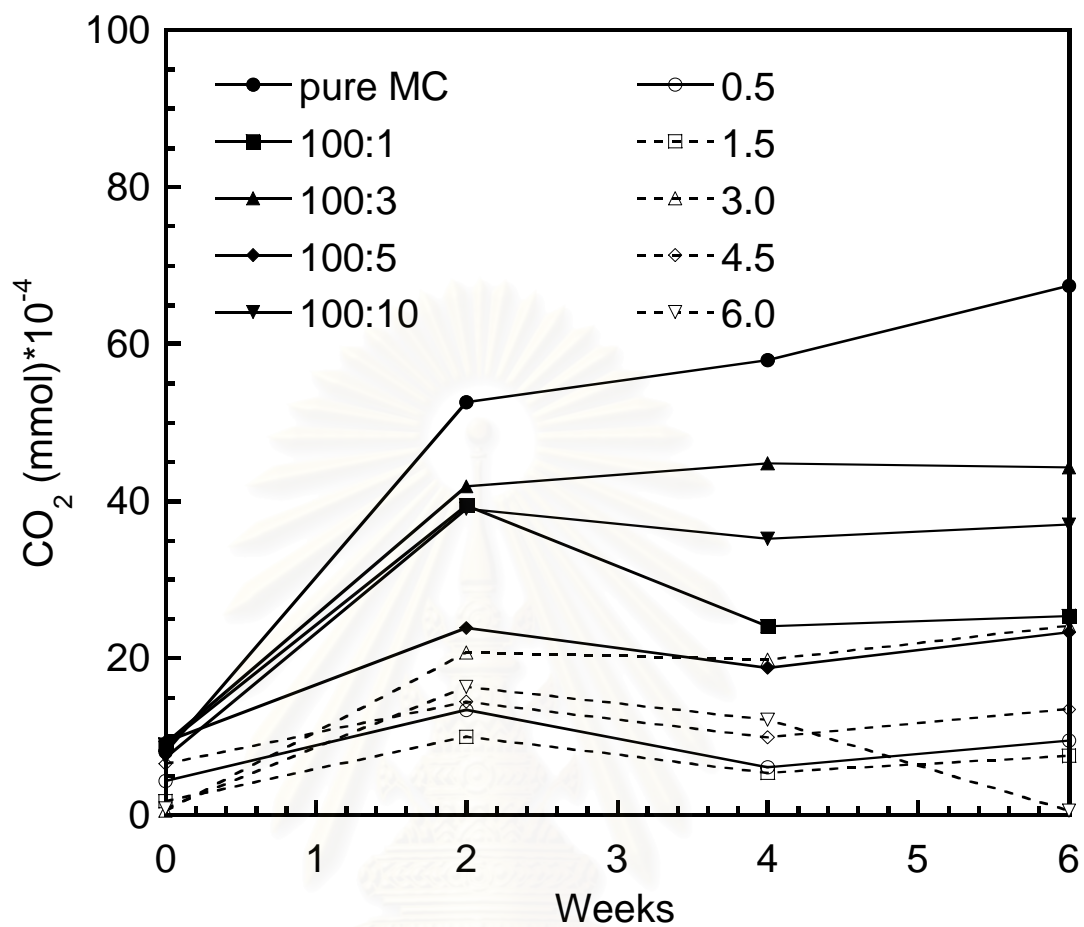


Figure 5.29: Time dependence of degree of biodegradation i.e. CO₂ evolution of pure MC and MC/MMT nanocomposite films: (●) Pure MC, (■) 100:1, (▲) 100:3, (◆) 100:5, (▼) 100:10, and MC crosslinked films at various compositions: (○) 0.5 wt%, (◻) 1.5 wt%, (△) 3.0 wt%, (◇) 4.5 wt%, (▽) 6.0 wt% under compost.

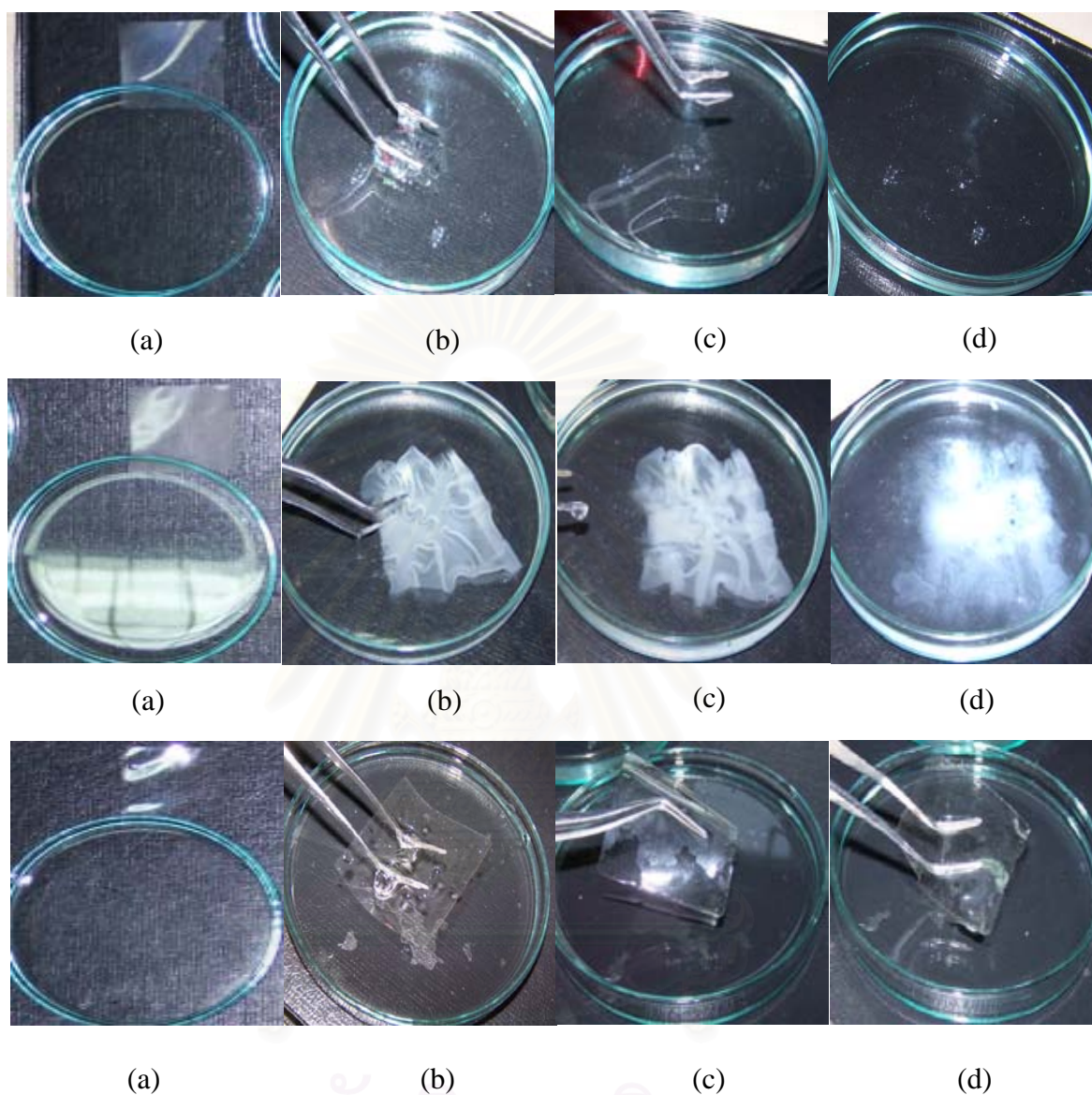


Figure 5.30: Water solubility of pure MC, nanocomposite film (10 phr of MMT), and crosslinked MC films (4.5wt% of GA) with time at (a) 0 min, (b) 10 min, (c) 12 hr, and (d) 24 hr.

CHAPTER VI

CONCLUSIONS

6.1 Conclusions

MC-based biodegradable polymer prepared by solution intercalation was achieved. The proper conditions for MMT suspension preparation were MMT grade Polargel HV at the suspension content of 5wt% and pre-swelling times of 8 days. High shear force was applied using a homogenizer at constant of 13,500 rpm for 4 min. The results showed that pre-swelling time, mixing speed, and mixing time had significant effects on the MMT suspension viscosity compared at the same MMT content. Viscosity at 5wt% of MMT was significantly affected with mixing speed because stack of MMT layered silicate was dispersed by increased shear force. The MC/MMT nanocomposites prepared by MMT suspension was exfoliated nanocomposite confirmed by XRD and TEM results. Both T_g and T_d of MC/MMT nanocomposite were slightly increased with MMT content (1-10 phr). The nanocomposite increased T_g with MMT content from 190°C (pure MC film) to 194°C (at 10 phr of MMT), whereas tensile strength and Young's modulus of the nanocomposites were improved notably with increasing the MMT loadings. When compared with pure MC film, the elongation at break slightly decreased about 16.0%. However, the modulus was increased about 65%. The tensile strength was increased 35%. In addition, moisture absorption of nanocomposite was reduced about 19%.

From the FTIR spectra, it can be noticed that there was a peak presenting excess aldehyde at the GA contents at 6.0wt%. This peak was not found at the concentration of at most 4.5wt%. That means the density of crosslinking between MC and GA was proportional to the GA content, and optimum GA content was 4.5wt%. The crosslinking increased T_g with GA content from 190°C (pure MC film) to 219°C (at 4.5wt% of GA). In addition, the crosslinking slightly improved the tensile properties. When comparing between pure MC film and the film at 4.5wt% of GA,

the modulus was increased about 45%. The tensile strength was increased 3%. The elongation at break remarkably decreased about 34%. In addition, moisture absorption of crosslinked film was reduced about 27%.

In the biodegradation test, MC based biodegradable polymers can enhance the period of biodegradability by both crosslinking and nanocomposite techniques. In comparison, the crosslinkage technique had more potential to hinder the biodegradation process. The main reason is that the crosslinkage could prevent water to diffuse through the bulk.

In summary, MC prepared by both MC/MMT nanocomposites and crosslinking methods was found to improve biodegradation properties. The MC/MMT nanocomposites could improve biodegradable and tensile properties. For MC crosslinked film, biodegradable and thermal properties were significantly enhance when compare with MC/MMT nanocomposites method.

6.2 Future Work

- 1 Study of the biodegradability of nanocomposite films crosslinked by GA.
2. Application of the composite films as a controlled release barrier for fertilizer.

REFERENCES

- Aminabhavi, T. M.; Balundgi, R. H.; and Cassidy, P. E. A review on biodegradable plastics. Polym-plast. Technol. 29 (1990): 235-262.
- Andrady, A.L. and Xu, P. Elastic behavior of chitosan films. J. Polym. Sci. Pol. Phys. 35 (1997): 517-521.
- Avella, M.; Vlieger, J.J.; Errico, M.E.; Fischer, S.; Vacca, P.; and Volpe, M.G. Biodegradable starch/clay nanocomposite films for food packaging applications. Food Chem. 93 (2005): 467-474.
- Bafna, A.; Beaucage, G.; Mirabella, F., and Mehta, S. 3D Hierarchical orientation in polymer–clay nanocomposite films. Polymer. 44(2003): 1103-1115.
- BeMiller, J.N. Encyclopaedia of polymer science and engineering. (p.601) New York: Wiley, 1986.
- Bharadwaj, R.K.; Mehrabi, A.R.; Hamilton, C.; Trujillo, C.; Murga, M.; Fan, R.; Chavira, A.; and Thompson, A.K. Structure-property relationships in cross-linked polyester/clay nanocomposites. Polymer. 43, (2002): 3699-3705.
- Blanchard, F.A.; Takahashi, I.T.; and Alexander, H.C. Biodegradability of [¹⁴C]Methylcellulose by Activated Sludge. Appl. Environ. Microbi. 32 (1976): 557-560.
- Chang, J.-H.; Ana, Y.U.; Choa, D.; and Giannelis, E.P. Poly(lactic acid) nanocomposites: comparison of their properties with montmorillonite and synthetic mica (II). Polymer. 44 (2003): 3715-3720.
- Chiellini, E. and Solara, R. Biodegradable polymers and plastics. New York: Kluwer Academic Plenum, 2003.
- Coma, V.; Sebt, I.; Pardon, P.; Pichavant, F.H.; and Deschamps, A. Film properties from crosslinking of cellulosic derivatives with a polyfunctional carboxylic acid. Carbohydr. Polym. 51 (2003): 265-271.
- Crosby, N. T. Food packaging material. Aspects of analysis and migration of contaminants. London: Applied Science Publisher Ltd., 1981.
- Denkbasi, E.B. and Odabasi, M. Chitosan microspheres and sponges: preparation and characterization. J. Appl. Polym. Sci. 76 (2000): 1637-1643.

- Darder, M.; Colilla, M.; and Ruiz-Hitzky, E. Biopolymer-clay nanocomposites based on chitosan intercalated in montmorillonite. Chem. Mater. 15 (2003): 3774-3780.
- Doi, Y. Microbial polyesters. New York: VCH Publishers, Inc, 1990.
- Doi, Y. and Fukuda, K. Biodegradable plastics and Polymers. (pp. 479-497). Amsterdam: Elsevier., 1994.
- Fang, Y.E.; Cheng, Q.; and Lu, X.B. Kinetics of in vitro drug release from chitosan/gelatin hybrid membranes. J. Appl. Polym. Sci. 68 (1998): 1751-1758.
- Frost, R.L., Kristof, K., Horvath, E., and Klopogge, T. Effect of water on the formamide-intercalation of kaolinite. Spectrochim. Acta. A. 56 (2000): 1711-1729.
- Gimenez, V, Reina, J.A.; Mantecon, A.; and Cadiz, V. Unsaturated modified poly(vinyl alcohol). Crosslinking through double bonds. Polymer. 40 (1999): 2759-2767.
- Gotoh, Y.; Fujimura, K.; Ohkoshi, Y.; Nagura, M.; Akamatsu, K.; and Deki, S. Preparation of transparent alumina film and fiber from a composite of aluminum polynuclear complex/methyl cellulose. Mater. Chem. Phys. 83 (2004): 54-59.
- Hennink, W.E. and Nostrum, C.F. Novel crosslinking methods to design hydrogels. Adv. Drug Deliver. Rev. 54 (2002): 13-36.
- Hirrien, H.; Chevillard, C.; Desbrieres, J.; and Rinaudo, M. Thermogelation of methylcellulose: new evidence for understanding the gelation mechanism. Polymer. 39 (1998): 6251-6259.
- Hirrien, M.; Desbrieres, J.; and Rinaudo, M. Physical properties of methylcellulose in relation with the conditions for cellulose modification. Carbohydr. Polym. 31 (1996): 243-252.
- Horkay, F. and Zrinyi, M. Halato-Telechelic polymer, 5 A Theoretical Approach to Gel Formation in Nonpolar Solvents. Macromolecules. 15 (1982): 1306-1310.
- Johnson, B.D.; Beebe, D.J.; and Crone, W.C. Effect of swelling on the mechanical properties of a pH-sensitive hydrogel for use in microfluidic devices. Mat. Sci. Eng. C-bio. S. 24 (2004): 575-581.

- Keslter, J. J. and Fennema, O. R. Edible films and coatings: a review. Food Technol. Biotech. 48 (1986): 47-59.
- Krikorian, V. and Pochan, D.J. Poly (L-Lactic Acid)/Layered Silicate Nanocomposite: Fabrication, Characterization, and Properties. Chem. Mater. 15 (2003): 4317-4324.
- Kurita, K.; Koyama, Y.; and Taniguchi, A. Studies on chitin.IX. Crosslinking of water-soluble chitin and evaluation of the products as adsorbents for cupric ion. J. Appl. Polym. Sci. 30 (1986): 1169-1176.
- Lee, K.Y.; Bouhadir, K.H.; Kruger, G.M.; and Mooney, D. Sustained and controlled release of daunomycin from cross-linked poly(aldehyde guluronate) hydrogels. J. Pharm. Sci. 89 (2000): 910-919.
- Lee, S.R.; Park, H.M.; Lim, H.L.; Kang, T.; Li, X.; and Cho, W.J. Microstructure, tensile properties, and biodegradability of aliphatic polyester/clay nanocomposites. Polymer. 43 (2002): 2495-2500.
- Li, H.-Y.; Chen, Y.-F.; and Xie, Y.-S. Nanocomposites of cross-linking polyanhydrides and hydroxyapatite needles: mechanical and degradable properties. Mater. Lett. 58 (2004): 2819-2823.
- Liu, T.; Phang, I.Y.; Shen, L.; Chow, S.Y.; and Zhang, W.-D. Morphology and Mechanical Properties of Multiwalled Carbon Nanotubes Reinforced Nylon-6 Composites. Macromolecules. 37 (2004): 7214-7222.
- Maiti, P.; Yamada, K.; Okamoto, M.; Ueda, K; and Okamoto, K. New polylactide/layered silicate Nanocomposites: role of organoclay. Chem. Mater. 14 (2002): 4654-4661.
- Manias, E.; Touny, A.; Wu, L.; Strawhecker, K; Lu, B.; and Chung, T.C. Polypropylene/Monmorillonite nanocomposites. Review of the Synthesis Routes and Materials properties. Chem. Mater. 13 (2001): 3516-3523.
- Mi, F.-L.; Sung, H.-W.; Shyu, S.-S.; Su, C.-C.; and Peng, C.-K. Synthesis and characterization of biodegradable TPP/genipin co-crosslinked chitosan gel beads. Polymer. (2003): 6521-6530.
- Morgan, A.B. and Gilman, J.W. Characterization of poly-layered silicate (clay) nanocomposites by transmission electron microscopy and X-ray diffraction: a comparative study. J. Appl. Polym. Sci. 87 (2003): 1329-1338.

- Oungbho, K. and Muller, B.W. Chitosan sponges as sustained release drug carriers. Int. J. Pharm. 156 (1997): 229-237.
- Park, H. J.; Weller, C. L.; Vergano, P. J.; and Testin, R. F. Permeability and mechanical properties of cellulose-based edible films. J. Food. Sci., 58(1993): 1361-1364.
- Park, H.-M.; Liang, X.; Mohanty, A.K.; Misra, M.; and Drzal, L.T. Effect of Compatibilizer on Nanostructure of the Biodegradable Cellulose Acetate/Organoclay Nanocomposites. Macromolecules. 37 (2004): 9076-9082.
- Park, J.-S.; Park, J.-W.; and Ruckenstein, E. Thermal and dynamic mechanical analysis of PVA/MC blend hydrogels. Polymer. 42 (2001): 4271-4280.
- Park, J.-S. and Ruckenstein, E. Viscoelastic properties of plasticized methylcellulose and chemically crosslinked methylcellulose. Carbohyd. Polym. 46 (2001): 373-381.
- Piner; R. D.; Xu, T. T.; Fisher, F. T.; Qiao, Y.; and Ruoff, S. Atomic force microscopy study of clay nanoplatelets and their impurities. Langmuir. 19 (2003): 7995-8001.
- Pinnavaia, T.J. and Beal, G.W., Eds. Polymer Clay Nanocomposites. New York, John: Wiley & Sons, 2001.
- Sannino, A.; Pappada, S.; Madaghiele, M.; Maffezzoli, A.; Ambrosio, L.; and Nicolais, L. Crosslinking of cellulose derivatives and hyaluronic acid with water-soluble carbodiimide. Polymer. 46 (2005): 11206-11212.
- Sarkar, N. and Walker, L.C. Hydration-dehydration properties of methylcellulose and hydroxypropylmethylcellulose. Carbonhyd. Polym. 27 (1995): 177-185.
- Shen, L.; Phang, I.Y.; Chen, L.; Liu, T.; and Zeng, K. Nanoindentation and morphological studies on nylon 66 nanocomposites. I. Effect of clay loading. Polymer. 45 (2004): 3341-3349.
- Shia, D.; Hui, C.Y.; Burnside, S.D.; and Giannelis, E.P. An interface model for the prediction of Young's modulus of layered silicate-elastomer nanocomposites. Polym. Compos. 19 (1998): 608-615.
- Sinha Ray, S. and Bousmina, M. Biodegradable polymers and their layered silicate nanocomposites: In greening the 21st century materials world. Prog. Mater. Sci. 50 (2005): 962-1079.

- Sinha Ray, S. and Okamoto, M. Polymer/layered silicate nanocomposites: a review from preparation to processing. Prog. Polym. Sci. 28 (2003): 641-1539.
- Sinha Ray, S.; Yamada, K.; Okamoto, M.; and Ueda, K. New polylactide-layered silicate nanocomposites. 2. Concurrent improvements of material properties, biodegradability and melt rheology. Polymer. 44 (2003): 857-866.
- Strawhecker, K.E. and Manias, E. Structure and properties of poly(vinyl alcohol)/Na⁺-montmorillonite nanocomposites. Chem Mater. 12 (2000): 2943-2949.
- Tomita, E. and Ikeda, Y. Crosslinking of hyaluronic acid with glutaraldehyde. J. Polym. Sci. Pol. Chem. 35 (1997): 3553-3559.
- Vaia, R. and Giannelis, E.P. Polymer nanocomposites: Status and opportunities. Mater. Res. Bull. 26 (2001): 394-401.
- Vuthipong, P. Use of ATR FT-IR Spectroscopy technique to determine the crosslinking density of chitosan film at various depths. Master's Thesis, Graduate School, Chulalongkorn University, 2001.
- Wach, R.A.; Mitomo, H.; Nagasawa, N.; and Yoshii, F. Radiation crosslinking of methylcellulose and hydroxyethylcellulose in concentrated aqueous solutions. Nucl. Instrum. Meth. B. 211 (2003): 533-544.
- Wang, Q. and Li, L. Effects of molecular weight on thermoreversible gelation and gel elasticity of methylcellulose in aqueous solution. Carbohydr. Polym. 62 (2005): 232-238.
- Wang, S.; Song, C.; Chena, G.; Guoa, T.; Liub, J.; Zhang, B.; and Takeuchi, S. Characteristics and biodegradation properties of poly(3-hydroxybutyrate-co-3-hydroxyvalerate)/organophilic montmorillonite (PHBV/OMMT) nanocomposite. Polym. Degrad. Stabil. 87 (2005): 69-76.
- Wang, X.L.; Yang, K.K.; Wang, Y.-Z.; Wang, D.Y.; and Yang, Z. Crystallization and morphology of a novel biodegradable polymer system: poly(1,4-dioxan-2-one)/starch blends. Acta Mater. 52 (2004): 4899-4905.
- Weian, Z.; Wei, L.; and Yue, F. Synthesis and properties of a novel hydrogel nanocomposites. Mater. Lett. 59 (2005): 2876-2880.
- Wibowo, A.C.; Manjusri, M.; Hwan, M.P.; Lawrence, T.D.; Richard, S.; and Amar, K.M. Biodegradable nanocomposites from cellulose from cellulose acetate:

- Mechanical, morphological, and thermal properties. Compos. Part A-Appl.S. 37 (2006): 1428-1433.
- Xia, X.; Yih, S.; D'Souza, N.A.; and Hu, Z. Swelling and mechanical behavior of poly(N-isopropylacrylamide)/Montmorillonite layered silicates composite gels. Polymer. 44 (2003): 3389-3393.
- Xu, J.; Li, R.K.Y.; Meng, Y.Z.; and Mai, Y.-W. Biodegradable poly(propylene carbonate)/montmorillonite nanocomposites prepared by direct melt intercalation. Mater. Res. Bull. 41 (2006): 244-252.
- Yeom, C.K. and Lee, K.H. Pervaporation Separation of water-acetic acid mixtures through poly(vinyl alcohol) membranes crosslinked with glutaraldehyde. J. Membr. Sci. 109 (1996): 257-265.
- Zaccaron, C.M.; Oliveira, R.; Guiotoku, M.; Pires, A.; and Soldi, A. Blends of hydroxypropyl methylcellulose and poly(1-vinylpyrrolidone-co-vinyl acetate): Miscibility and thermal stability. Polym. Degrad. Stabil. 90 (2005): 21-27.
- Zeng, X. and Ruckenstein, E. Cross-linked macroporous chitosan anion-exchange membranes for protein separation. J. Membr. Sci. 143 (1998): 207-218.
- Zhao, X.; Urano, K.; and Ogasawara, S. Adsorption of poly(ethylene vinyl alcohol) from aqueous solution on montmorillonite clays. Colloid. Polym. Sci. 267 (1989): 899-906.
- Zhou, Y. J.; Luner, P.; and Caluwe, P. Mechanism of crosslinking of papers with polyfunctional carboxylic acids. J. Appl. Polym. Sci. 58 (1995): 1523-1534.
- <http://www.netcomposites.com/images/montmorillonite.jpg>
<http://www.psrc.usm.edu>



APPENDICES

สถาบันวิทยบริการ
จุฬาลงกรณ์มหาวิทยาลัย

Appendix A

Viscosity of MMT suspension at various compositions

Shear Rate (s ⁻¹)	Viscosity of MMT suspension (cP)				
	Condition 1	Condition 2	Condition 3	Condition 4	Condition 5
0.9994	0.0	37.8	3191.0	6540.0	5191.0
53.58	13.8	54.7	153.7	187.5	198.8
106.2	8.7	45.1	92.1	109.1	116.3
158.7	15.6	37.6	69.7	80.8	86.0
211.3	17.7	32.7	57.8	65.7	70.0
263.9	15.9	28.9	49.7	56.7	59.9
316.5	15.4	26.3	44.0	50.0	53.1
369.1	14.6	23.8	39.9	45.0	47.5
421.6	13.3	22.1	36.9	41.0	43.4
474.2	12.9	20.8	34.4	37.9	40.3
526.8	12.2	19.7	32.3	35.4	37.7
579.4	12.2	19.4	31.1	33.8	36.0
631.9	11.8	18.6	29.5	31.8	33.9
684.5	11.3	17.9	28.1	30.1	32.0
737.1	11.2	17.1	27.0	28.8	30.7
789.7	10.9	16.9	26.0	27.7	29.4
842.3	10.6	16.7	25.1	26.7	28.4
894.8	10.5	16.2	24.4	25.9	27.4
947.4	10.1	15.9	23.5	25.0	26.4
1000.0	10.0	15.7	23.0	24.3	25.5

Condition 1: Non-swelling time., MMT 5wt%, 6500 rpm, 1 min

Condition 2: Pre-swelling time (8 days), MMT 5wt%, 6500 rpm, 1 min

Condition 3: Pre-swelling time (10 days), MMT 5wt%, 13500 rpm, 1 min

Condition 4: Pre-swelling time (10 days), MMT 5wt%, 13500 rpm, 4 min

Condition 5: Pre-swelling time (10 days), MMT 5wt%, 13500 rpm, 10 min

Appendix B

d-spacing calculation

The d-spacing of MMT in MC/MMT nanocomposite films were calculated by Bragg's law equation as shown below.

$$n\lambda = 2d\sin\theta$$

where n = integer

λ = wavelength, 1.541 $^{\circ}$ A

d = d-spacing of organoclays interlaminar

θ = diffraction angle

MMT powder was measured diffraction angle by XRD. The value of 2θ is 6.7 angle which we can calculate d-spacing of powder showing as follow.

$$(1)(1.541) = 2d \sin (6.7)$$

$$d = 13.2^{\circ}\text{A}$$

$$d = 1.3 \text{ nm}$$

สถาบันวิทยบริการ
จุฬาลงกรณ์มหาวิทยาลัย

Appendix C

Tensile properties of MC nanocomposite and crosslinked Films

Appendix C-1 Tensile properties of MC nanocomposite films.

MMT Content (phr)	Tensile modulus (GPa)	Tensile strength (MPa)	Elongation at Break (%)
0	1.99 ± 0.06	67.76 ± 1.30	22.48 ± 0.27
1	2.15 ± 0.10	69.00 ± 2.30	22.27 ± 0.50
2	2.34 ± 0.03	77.54 ± 0.81	21.67 ± 0.21
3	2.52 ± 0.07	83.88 ± 1.43	21.19 ± 0.30
5	2.75 ± 0.13	85.13 ± 2.70	20.99 ± 0.47
10	3.29 ± 0.06	92.16 ± 1.05	18.92 ± 0.25

Appendix C-2 Tensile properties of MC crosslinked films.

GA Content (wt%)	Tensile modulus (GPa)	Tensile strength (MPa)	Elongation at Break (%)
0.0	1.99 ± 0.06	67.76 ± 1.30	22.48 ± 0.27
0.5	2.01 ± 0.02	64.25 ± 2.45	21.91 ± 0.18
1.5	2.17 ± 0.02	63.02 ± 3.15	17.08 ± 0.11
3.0	2.51 ± 0.15	64.64 ± 2.82	14.06 ± 2.01
4.5	2.98 ± 0.05	69.52 ± 1.84	14.95 ± 0.67
6.0	2.70 ± 0.09	67.75 ± 2.39	9.53 ± 0.59
12.0	2.48 ± 0.13	66.35 ± 3.23	2.94 ± 0.55

Appendix D

Net CO₂ evaluation of MC nanocomposites and crosslinked films

Specimens	Net CO ₂ evaluation							
	0 week		2 weeks		4 weeks		6 weeks	
	Area (GC)	CO ₂ (mmol) ×10 ⁻⁴	Area (GC)	CO ₂ (mmol) ×10 ⁻⁴	Area (GC)	CO ₂ (mmol) ×10 ⁻⁴	Area (GC)	CO ₂ (mmol) ×10 ⁻⁴
Blank	7434	0.7	53500	9.6	33751	5.2	47922	7.8
Nanocomposite films (weight ratio of MC/MMT)								
100:0	46405	8.0	246000	52.6	270000	58.0	334000	67.4
100:1	50581	9.0	187000	39.4	118000	24.0	132000	25.3
100:3	51207	9.1	198000	41.9	211000	44.8	223000	44.3
100:5	52430	9.4	117000	23.8	96332	18.8	122000	23.3
100:10	44250	7.3	185000	39.0	168000	35.2	188000	37.0
Crosslinked films (wt% of GA contents)								
0.5	29519	4.3	70453	13.4	37509	6.1	56071	95.2
1.5	18231	1.7	54930	10.0	34412	5.4	46398	75.0
3.0	7803	0.5	103000	20.7	99193	19.9	126000	24.0
4.5	39737	6.6	74898	14.4	54539	9.9	74882	13.4
6.0	6762	0.8	83406	16.3	64527	12.1	10114	0.5

Appendix E

Calibration curves

This appendix showed the calibration curves for calculation of CO₂ concentration. The test method is based on the determination of the net CO₂ evolution, the main product of the biodegradation reaction evolved from the mixture compost minus the CO₂ evolved from the unamended compost (blank).

The calibration curve is shown in Figures C.1, which exhibits the relationship between ml of area under the gas chromatography (GC) curve (x-axis) and CO₂ gas component (y-axis).

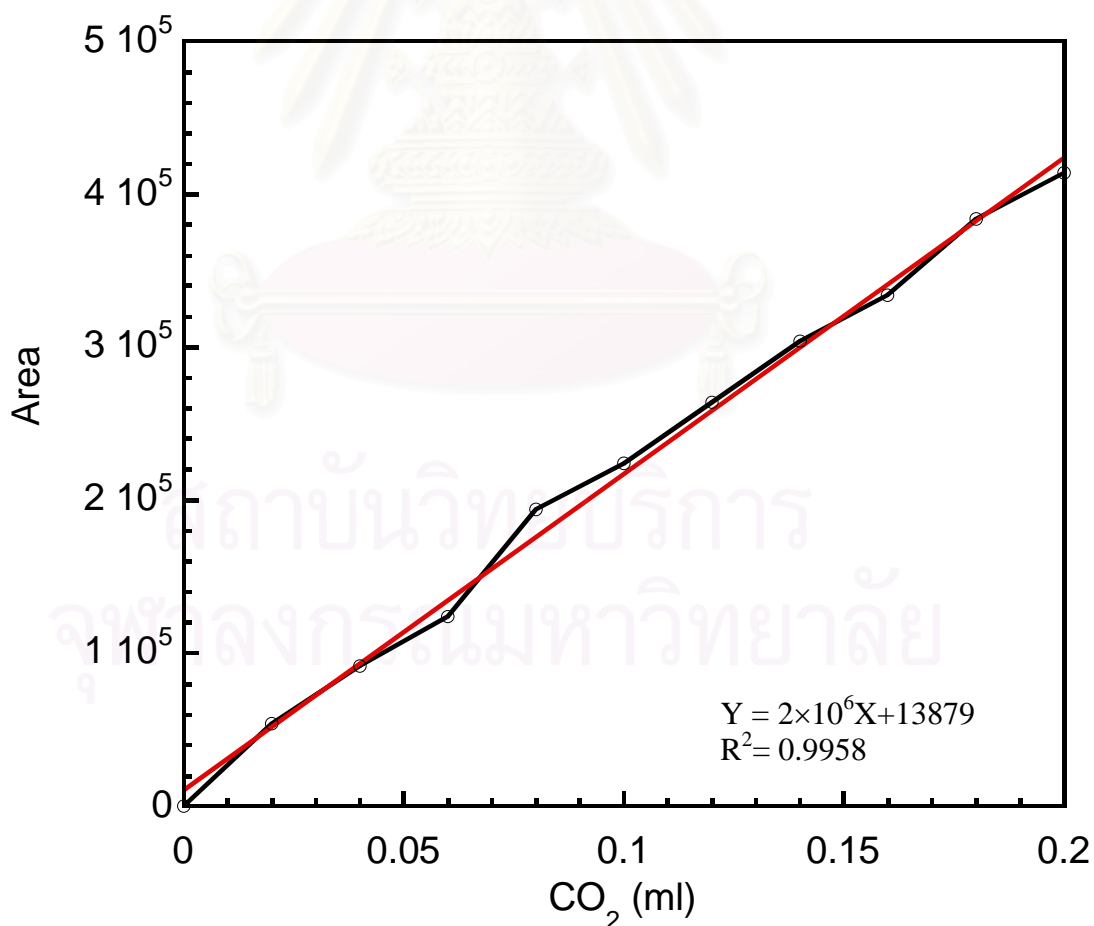


Figure C.1 The calibration curve of carbon dioxide.

Appendix F

Comparison on properties of nanocomposites and crosslinked MC

Properties	Pure MC	Nanocomposite Film (MMT 10 phr)		Crosslinked Film (4.5wt%)	
		Absolute Value	Relative Value*(%)	Absolute Value	Relative Value*(%)
T _g (°C), (tanδ)	190	194	+2	219	+15
Tensile modulus (GPa)	2.0	3.3	+65	2.9	+45
Tensile strength (MPa)	68	92	+35	70	+3
Elongation at break (%)	22.5	18.9	-16	14.9	-34
Moisture absorption (%)	133	108	-19	113	-15
Water absorption	Soluble	Swelled		Insoluble	
CO ₂ (mmol)×10 ⁻⁴ , at 6 weeks	67.4	37.0	-45	13.4	-80

*Comparison with pure MC

สถาบันวิทยบริการ
จุฬาลงกรณ์มหาวิทยาลัย

VITA

Miss Sorada Jingjid was born in Nakornsritammarat, Thailand on August 11, 1982. She completed senior high school at Demonstration School of Thepsatri Rajabhat University Lopburi, Thailand in 2000 and received Bachelor degree from the Department of Chemical Engineering, Faculty of Engineering, Srinakharinwirot University, Thailand in 2004. She continued her study for Master degree at Department of Chemical Engineering, Faculty of Engineering, Chulalongkorn University Bangkok, Thailand.

Some part of this work was selected for oral presentation in The Fourth Thailand Materials Science and Technology Conference to be held during March, 2006 to April 1, 2006 at Thailand Science Park Convention Center in conjunction with NSTDA Annual Meeting 2006.



สถาบันวิทยบริการ
จุฬาลงกรณ์มหาวิทยาลัย